

MODIFICATION OF SURFACES USING POLYMERS TOWARDS
PREPARATION OF FUNCTIONAL COATINGS

A THESIS SUBMITTED TO
THE GRADUATE SCHOOL OF NATURAL AND APPLIED SCIENCES
OF
MIDDLE EAST TECHNICAL UNIVERSITY

BY

İPEK TERZİOĞLU

IN PARTIAL FULFILLMENT OF THE REQUIREMENTS
FOR
THE DEGREE OF MASTER OF SCIENCE
IN
POLYMER SCIENCE AND TECHNOLOGY

DECEMBER 2024

Approval of the thesis:

**MODIFICATION OF SURFACES USING POLYMERS TOWARDS
PREPARATION OF FUNCTIONAL COATINGS**

submitted by **İPEK TERZİOĞLU** in partial fulfillment of the requirements for the degree of Master of Science in Polymer Science and Technology, **Middle East Technical University** by,

Prof. Dr. Naci Emre Altun
Dean, **Graduate School of Natural and Applied Sciences** _____

Prof. Dr. Necati Özkan
Head of the Department, **Polymer Science and Technology** _____

Prof. Dr. İrem Erel Göktepe
Supervisor, **Polymer Science and Technology, METU** _____

Prof. Dr. Sreeparna Banerjee
Co-Supervisor, **Biology, METU** _____

Examining Committee Members:

Prof. Dr. Ayşen Yılmaz
Chemistry, METU _____

Prof. Dr. İrem Erel Göktepe
Polymer Science and Technology, METU _____

Prof. Dr. Sreeparna Banerjee
Biology, METU _____

Prof. Dr. Ali Çırpan
Chemistry, METU _____

Assist. Prof. Dr. Gökçe Çalış İsmetoğlu
Chemistry, Gazi University _____

Date: 06.12.2024

I hereby declare that all information in this document has been obtained and presented in accordance with academic rules and ethical conduct. I also declare that, as required by these rules and conduct, I have fully cited and referenced all material and results that are not original to this work.

Name Last Name: İpek Terziođlu

Signature:

ABSTRACT

MODIFICATION OF SURFACES USING POLYMERS TOWARDS PREPARATION OF FUNCTIONAL COATINGS

Terzioğlu, İpek
Master of Science, Polymer Science and Technology
Supervisor: Prof. Dr. İrem Erel Göktepe
Co-Supervisor: Prof. Dr. Sreeparna Banerjee

December 2024, 101 pages

In this thesis study, self-polymerization of dopamine (DOP) in the presence of tannic acid (TA) was examined in 0.05 M Tris HCl buffer at pH 8.5 and 25 °C. Single- and multi-layer films of co-deposited polydopamine (PDA) and TA (PDATA) were prepared. The properties of PDATA films such as thickness, wettability, morphology and stability were compared with PDA films. PDA films exhibited higher thickness and rougher surfaces. TA provided control on the size of PDA particles and surface roughness of the films. Drying between each layer deposition and extended polymerization time reduced thickness for both PDA and PDATA films.

Additionally, layer-by-layer (LbL) assembly of PDATA and PDA was examined using branched polyethyleneimine (BPEI), TA, and poly(vinyl caprolactam) (PVCL). Electrostatic interactions were mainly responsible for LbL assembly with BPEI. The main driving force for TA and PVCL-based multilayers was hydrogen bonding. PDATA provided higher thickness than PDA based films when co-assembled with BPEI or PVCL. In contrast, it provided lower thickness when LbL

deposited with TA. PDA-based multilayers resulted in greater roughness due to formation of larger particles during polymerization. PDATA/TA films provided the roughest multilayer films among PDATA films, while PDATA/PVCL multilayers displayed smoothest surfaces. PVCL-based multilayers showed the lowest wettability, while multilayers with TA exhibited the highest wettability among all films. BPEI-based multilayers provided the highest stability in PBS at pH 7.4/37 °C. PVCL-based multilayers presented greater stability than TA containing films.

This thesis presents a comparative study of PDATA and PDA-based multilayers, generating fundamental information for optimization of PDA-based coatings.

Keywords: Polydopamine, Tannic acid, Layer-by-layer, Surface Modification

ÖZ

FONKSİYONEL KAPLAMALARIN HAZIRLANMASINA YÖNELİK YÜZEYLERİN POLİMERLER KULLANILARAK MODİFİKASYONU

Terzioğlu, İpek
Yüksek Lisans, Polimer Bilim ve Teknolojisi
Tez Yöneticisi: Prof. Dr. İrem Erel Göktepe
Ortak Tez Yöneticisi: Prof. Dr. Sreeparna Banerjee

Aralık 2024, 101 sayfa

Bu tez çalışmasında, dopaminin (DOP), tanik asit (TA) varlığında pH 8.5 ve 25 °C'deki 0.05 M Tris HCl tampon çözeltisinde kendi kendine polimerleşmesi incelendi. Birlikte kaplanan polidopamin (PDA) ve tanik asit filmlerinin (PDATA) tek ve çok-katmanlı örnekleri hazırlandı. PDATA filmlerinin kalınlık, ıslanabilirlik, morfoloji ve stabilite gibi özellikleri PDA filmleriyle karşılaştırıldı. PDA filmleri daha kalın ve daha pürüzlü yüzeyler sergiledi. TA, PDA parçacıkların boyutunda ve film yüzeyinin pürüzlülüğünde kontrol sağladı. Artan polimerleşme süresi ve her katman birikimi sonrasında kurutma işlemi uygulanması hem PDA hem de PDATA filmlerinin kalınlıklarının düşmesine neden oldu.

PDATA ve PDA'nın katman-katman (LbL) kendiliğinden yapılanması dallanmış polietilenimin (BPEI), TA ve poli(vinil kaprolaktam) (PVCL) kullanarak da incelendi. BPEI ile LbL yapılanmada elektrostatik etkileşimler başlıca rol oynarken, TA ve PVCL içeren çok-katmanlı filmlerde hidrojen bağları ana itici güç oldu. PDATA, BPEI veya PVCL ile LbL biriktirildiğinde PDA bazlı filmlere kıyasla yüksek kalınlık sağladı. Buna karşın, TA ile LbL birikimi yapıldığında daha düşük kalınlık sağladı. PDA esaslı çok-katmanlı filmlerin, polimerleşme sırasında daha

büyük partiküllerin oluşumu nedeniyle daha pürüzlü olduğu gözlemlendi. PDATA/TA filmleri, PDATA filmleri arasında en pürüzlü çok-katmanlı filmleri sağlarken, PDATA/PVCL çok-katmanlı filmleri en pürüzsüz yüzeyleri sergiledi. PVCL içeren çok-katmanlı filmler en düşük ıslanabilirliği gösterirken, TA içeren çok-katmanlı filmler tüm filmler arasında en yüksek ıslanabilirliğe sahip oldu. BPEI içeren çok-katmanlı filmler, pH 7.4/37 °C'deki fosfat tampon salin çözeltisi içerisinde en yüksek stabiliteyi sağladı. PVCL içeren çok-katmanlı filmler, TA içeren filmlerden daha yüksek kararlılık göstermiştir.

Bu tez, PDATA ve PDA tabanlı çok-katmanlı filmlerin karşılaştırmalı bir çalışmasını sunarak, PDA esaslı filmlerin optimizasyonu için temel bilgi üretmiştir.

Anahtar Kelimeler: Polidopamin, Tanik Asit, Katman-katman kendiliğinden yapılanma, Yüzey Modifikasyonu

To my beloved family and dearest husband

ACKNOWLEDGMENTS

I would like to express my appreciation to my supervisor Prof. Dr. İrem Erel Göktepe for her guidance, advice, encouragements and insight throughout the research. During my master's journey, her guidance in conducting research, integrating diverse perspectives with focused work, and developing strong time management skills deepened my passion for research.

I would like to extend my gratitude to my co-supervisor Prof. Dr. Sreeparna Banerjee for her esteemed support.

Special thanks to all the members of Erel research group, especially Çağrı Turan, Dilara Gündoğdu, Cemre Alemdar, Tuna Gökçe and Doğa Postacı for being such good friends and labmates. I appreciate all brainstorming, and endless laughter every day. Also, many thanks to my wedding witness, Gamze Yılmaz, my ex-roommate, Mine Kocatuş, and my travel buddy, Alara Özdemir, for always being there.

Thanks to Caner Yalçın for his assistance with Atomic Force Microscopy.

I also would like to thank my beloved family for their strong belief in me. I am lucky to have them for their unconditional love and respect all the time. With the support they have given since my childhood, they raised a self-supporting woman who always strives to do more and nourish her soul. I am so confident about they will be always there for my next journeys with pride.

Lastly, I appreciate to have my darling husband, my other half, Rahman who endlessly supports me emotionally. Many thanks for being such a great, patient and fun life-partner and the one that's always there. I am grateful for making the situation enjoyable even as we hit the road together for my experiments late at night. Thank you for always believing that I can achieve more and pushing me forward. I am so excited to explore future adventures together.

This thesis study has been financially supported by METU Scientific Research Projects (BAP-103-2023-11355).

TABLE OF CONTENTS

ABSTRACT.....	v
ÖZ.....	vii
ACKNOWLEDGMENTS.....	x
TABLE OF CONTENTS.....	xi
LIST OF TABLES.....	xiii
LIST OF FIGURES.....	xiv
LIST OF SCHEMES.....	xvii
LIST OF ABBREVIATIONS.....	xviii
CHAPTERS	
1 INTRODUCTION.....	1
1.1 Dopamine and Polydopamine.....	1
1.2 Polymerization Mechanism of Dopamine.....	2
1.2.1 Polymeric Models of PDA.....	3
1.2.2 Physical Models of PDA.....	4
1.2.3 Trimer-based Models of PDA.....	5
1.3 Preparation of PDA-based Surfaces.....	8
1.3.1 Mechanism of PDA Deposition at the Surface.....	8
1.3.2 The Factors Affecting the DOP Polymerization and Properties of PDA.....	10
1.4 Antimicrobial Properties of PDA.....	11
1.5 Applications of PDA Coatings.....	15
1.6 Tannic Acid.....	18

1.6.1	Applications of TA Coatings	21
1.7	Co-deposition of PDA and TA	23
1.8	Layer-by-Layer (LbL) Assembly	25
1.9	Aim of Thesis	30
2	EXPERIMENTAL	31
2.1	Materials	31
2.2	Instrumentation	32
2.3	PDATA- and PDA-Based Coatings	33
2.3.1	Preparation of Substrates	33
2.3.2	Co-deposition of PDA and TA	34
2.3.3	LbL Deposition of PDATA and PDA Films	35
2.3.4	Stability of PDATA and PDA Films	35
2.3.5	LbL Deposition of PDATA and PDA with Cationic, Anionic, Neutral Counterparts	36
3	RESULTS AND DISCUSSION	37
3.1	Co-deposition of PDA and TA	37
3.2	One-time versus LbL Deposition of PDATA and PDA	44
3.3	LbL Deposition of PDATA and PDA Using Cationic, Anionic and Neutral Polymers	52
3.3.2	Wettability of PDATA and PDA based multilayers	62
3.3.3	Stability of PDATA and PDA Containing Multilayers	64
4	CONCLUSION	71
	REFERENCES	75

LIST OF TABLES

TABLES

Table 1. Chemical structure of substances.	31
--	----

LIST OF FIGURES

FIGURES

Figure 1. Chemical structures of A) dopamine and B) polydopamine.	2
Figure 2. Polymeric structural models for polydopamine (Modified from [24], Hemmatpour et al., Nature Communications (2023)).	3
Figure 3. Physical structural models for polydopamine (Modified from [24], Hemmatpour et al., Nature Communications (2023)).	5
Figure 4. Trimer-based models for polydopamine (Modified from [24], Hemmatpour et al., Nature Communications (2023)).	6
Figure 5. Proposed covalent and physical pathways of polydopamine (Modified from [21], Hong et al., Sci. Adv. (2018)).	7
Figure 6. Schematic representation of PDA aggregation and deposition. Red cross describes no deposition of large PDA nanoparticles onto surfaces (Modified from [36], Zhang et. al. ACS Appl. Mater. Interfaces (2017)).	9
Figure 7. The relationship between initial dopamine concentration and deposition and/or aggregation rate (Modified from [30], Ding et. al. Langmuir (2014)).	10
Figure 8. ROS generation and scavenging mechanism of PDA (Modified from [55], H. Liu et al. Acta Biomaterialia 88 (2019)).	14
Figure 9. Chemical structure of TA.	19
Figure 10. Illustration of A) fabrication of LbL method, B) LbL-coated polyelectrolyte films.	26
Figure 11. A) Oxidation of TA (left), polymerization of DOP (right) and the possible interactions (Micheal Addition and Schiff Base reactions, π - π stacking, hydrogen bonding) between oxidized TA and PDA (below). B) Thickness comparison of 0.5 mg/mL PDATA and PDA films after 4 and 16-hours deposition. C) Hydrodynamic size of 0.5 mg/mL PDATA particles after 4 hours. D) AFM 2D (left) and 3D (right) height images (10×10 μ m scan size) of 1-layer PDATA and PDA films. E) Thickness comparison of 0.5 mg/mL and 1 mg/mL PDATA deposition after 4 and 16 hours. F)	

Hydrodynamic size of 1 mg/mL PDATA particles (right) and hydrodynamic size of 0.5 mg/mL PDATA particles after 2, 4 and 6 hours (left). 43

Figure 12. A) Thickness of 0.5 mg/mL PDATA/PDATA surfaces (□ refers 4x4h refreshed deposition, ○ refers 1x16h one-time deposition, and △ refers 4x4h unrefreshed deposition (data obtained for each 4h)) (left) and the evolution of hydrodynamic size distribution of PDATA particles as a function of time at 4- and 16 hours (right). B) Thickness of 0.5 mg/mL PDA/PDA surfaces (□ refers 4x4h refreshed deposition, ○ refers 1x16h one-time deposition, and △ refers 4x4h unrefreshed deposition (data obtained for each 4h)). C) Evolution of normalized absorbance as a function of time for A) 4x4h (refreshed) PDATA (left) and PDA films (right); B) 1x16h (one-time) PDATA (left) and PDA films (right); C) 4x4h (unrefreshed) PDATA (left) and PDA (right) films. Insets show the absorbance spectra of the films before and after 2 hours and 24 hours exposure to PBS at pH 7.4 and 37°C. Multilayers were constructed onto quartz slides. D) AFM 2D (left) and 3D height (right) images (10x10 μm scan size) of 4-layers of PDATA and PDA films. E) Comparison of PDATA and PDA wettability properties based on deposition conditions. F) Absorbance spectra of TA at pH 5.5, pH 7.4 and pH 8.5. 51

Figure 13. The LbL growth profile of A) PDATA/BPEI and PDA/BPEI surfaces, B) PDATA/TA and PDA/TA surfaces, inset: The effect of dissolution of TA in 0.05 M Tris Buffer and 0.01 M Tris Buffer on the growth of PDATA/TA films, C) PDATA/PVCL and PDA/PVCL surfaces. 57

Figure 14. 3D AFM images of (10×10 μm scan size, Zmax = 900 nm) A) PDATA/BPEI (left) and PDA/BPEI (right), B) PDATA/TA (left) and PDA/TA (right), C) PDATA/PVCL (left) and PDA/PVCL (right)). 59

Figure 15. Maximum height (Sz) (right) and Maximum peak height (Sp) (left) of PDATA- and PDA- based multilayers (10×10 μm scan size). 60

Figure 16. AFM 2D and 3D height images (extracted 2×2 μm scan size from 10×10 μm, Zmax = 900 nm) of A) relatively rough region of PDATA/BPEI (left) and relatively smooth region of PDATA/BPEI (right), B) relatively rough region of PDATA/TA (left) and relatively smooth region of PDATA/TA (right), C) relatively

rough region of PDATA/PVCL (left) and relatively smooth region of PDATA/PVCL (right)..... 61

Figure 17. AFM 2D and 3D height images (extracted 2×2 μm scan size from 10×10 μm, Zmax = 900 nm for PDATA and PDA films) of A) relatively rough region of PDA/BPEI (left) and relatively smooth region of PDA/BPEI (right), B) relatively rough region of PDA/TA (left) and relatively smooth region of PDA/TA (right), C) relatively rough region of PDA/PVCL (left) and relatively smooth region of PDA/PVCL (right)..... 61

Figure 18. Evolution of contact angle for 7- and 13-layer A) PDATA/BPEI and PDA/BPEI, B) PDATA/TA and PDA/TA, C) PDATA/PVCL and PDA/PVCL films. 64

Figure 19. Evolution of normalized absorbance as a function of time for 7-layer A) PDATA/BPEI (left) and PDA/BPEI films (right); B) PDATA/TA (left) and PDA/TA films (right); C) PDATA/PVCL (left) and PDA/PVCL films (right). Insets show the absorbance spectra of the films before and after 2 hours and 24 hours exposure to PBS at pH 7.4 and 37 °C. Multilayers were constructed onto quartz slides..... 69

LIST OF SCHEMES

SCHEMES

Scheme 1. The mechanism of H ₂ O ₂ generation during polymerization of dopamine. (Modified from [54], Lee et al. Journal of Catalysis (2022)).	13
Scheme 2. Illustration of LbL assembly of PDATA and PDA using BPEI, TA and PVCL.	53

LIST OF ABBREVIATIONS

ABBREVIATIONS

AgNPs	Silver nanoparticles
AMPs	Antimicrobial peptides
ALG	Alginate
CHI	Chitosan
CMC	Carboxymethyl cellulose
DHI	5,6-dihydroxyindole
DOP	Dopamine
DOX	Doxorubicin
FAS	Fatty acid synthase
FTIR	Fourier-transform infrared spectroscopy
HA-DN	Dopamine-modified hyaluronic acid
HPLC	High-performance liquid chromatography
HDPE	High-density poly(ethylene)
HRP	Horseradish peroxidase
HTACC	N-[(2-hydroxy-3-trimethyl ammonium)propyl]chitosan chloride
IPCN	Interconnected porous carbon nanosheet
LbL	Layer-by-layer
NIR	Near-infrared
NMR	Nuclear Magnetic Resonance

PA	Polyamide
PAA	Poly(acrylic acid)
PAH	Poly(allylamine hydrochloride)
PBS	Phosphate-buffered saline
PDA	Poly(dopamine)
PDADMAC	Poly(diallyldimethylammonium chloride)
PEG-FA	Poly(ethyleneglycol)-folic acid
PET	Poly(ethylene terephthalate)
PSS	Poly(sodium 4-styrene sulfonate)
PVAM	Polyvinylamine (PVAM)
RI	Refractive index
ROS	Reactive oxygen species
RO	Reverse osmosis
SEM	Scanning electron microscopy
TA	Tannic acid
TFC	Thin-film composite (TFC)
TMSNs	Templated mesoporous silica
Tris HCl	Tris(hydroxymethyl)aminomethane-hydrochloride
UV-Vis	Ultraviolet-visible
QACs	Quaternary ammonium compounds

CHAPTER 1

INTRODUCTION

1.1 Dopamine and Polydopamine

Dopamine (DOP) is known as a biological neurotransmitter found in living organisms (Fig. 1A). It plays a significant role in the treatment of the symptoms of Parkinson's disease, schizophrenia, and attention-deficit/hyperactivity disorder [1]. DOP, derived from mussel adhesive proteins, has attracted attention due to its self-polymerization ability in the presence of oxidizing agents (such as air, oxygen, ammonium persulfate, sodium periodate etc.) at alkaline conditions [2]. Polydopamine (PDA, Fig. 1B), synthetic analogue of naturally occurring melanin (eumelanin), is also defined as a mussel-inspired material endowing strong wet adhesion, independent of the substrate type [3]. The use of PDA has become one of the most effective ways for surface modification due to its single-step surface chemistry, simplicity, significantly improved stability [4], controllable thickness [5] and adjustable properties [6]. The potential use of PDA has been shown in a wide range of applications such as modification of biomaterials [7], therapeutics [8], catalysts [9], and sensing applications [10] have been observed. PDA is classified as catecholamine, and PDA chains have imine, indole, amine, catechol and carbonyl moieties [11]. The diverse functional groups in the chemical structure provides PDA various properties such as radical scavenging, photothermal conversion, biocompatibility and UV-shielding [12,13]. Similar to many polyphenols, catechol moieties of PDA allow chelation of ions through metal coordination bonds [14]. In addition, primary amino and catechol groups are capable of participating in Michael addition and/or Schiff base reactions which allow the further modification of PDA films [15]. Antibacterial property with PDA coatings can be achieved through different mechanisms: i) covalent incorporation of antibacterial agents through

catechol and/or amino moieties [16], contact-killing behavior through protonation of primary amino groups [17] and/or reactive oxygen species (ROS) generation [18]. Apart from antibacterial property, the indole structures of PDA contribute to photothermal conversion characteristics in a broad absorption spectrum and enhance electrochemical properties through formation of planar conjugated and donor-acceptor structures [19,20]. Properties of polydopamine films can be controlled by tuning polymerization conditions. However, the exact polymerization mechanism is still controversial. Some studies in the literature have proposed different mechanisms to explain polymerization of dopamine.

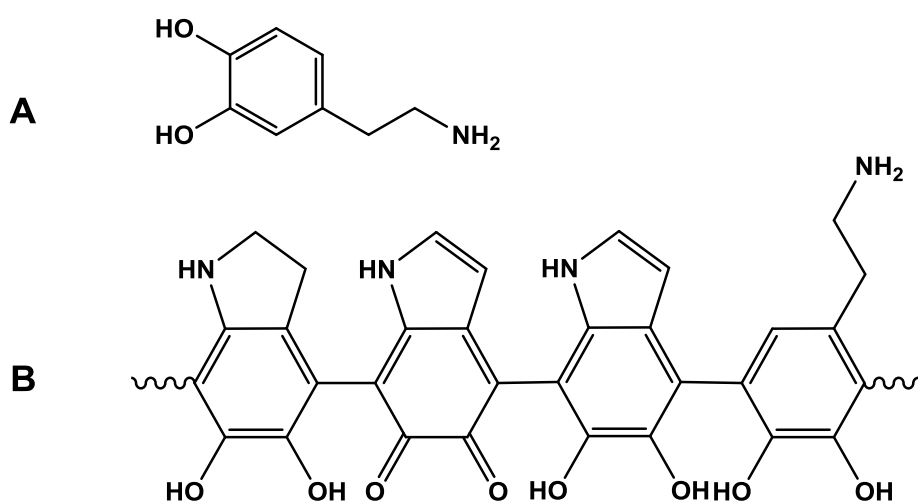


Figure 1. Chemical structures of A) dopamine and B) polydopamine.

1.2 Polymerization Mechanism of Dopamine

The first stages of dopamine polymerization which involve oxidation, intermolecular cyclization, and isomerization reactions, have been recognized in many studies [21–23]. However, further steps for the PDA formation are still a matter of discussion and explained with different potential structures of PDA. These structures are classified into three main sections: polymeric, physical and trimer-based models [24].

1.2.1 Polymeric Models of PDA

There are two different mechanisms for the polymeric model of PDA: i) the “Eumelanin model,” in which 5,6-dihydroxyindole (DHI) unit is regarded as the major component of PDA and PDA formation is resembled to the synthetic pathway of melanin pigments in living organisms (Fig. 2A) [2], and (ii) the “open-chain poly(catechol/quinone) model,” which defines PDA as linear chains of catecholamines bonded by biphenyl-type bonds (Fig. 2B) [25]. In addition to these two models, Della Vecchia et al. proposed the presence of pyrrole dicarboxylic acid moieties due to partial degradation of DHI and covalent incorporation of tris(hydroxymethyl)aminomethane (Tris) into PDA structure during the polymerization (Fig. 2C) [26]. Liebscher et. al claimed the covalent coupling between eumelanin-like polymer chains composed of DHI units with different degrees of saturation and open-chain dopamine units during the formation of PDA (Fig. 2D) [27]. Also, Delparastan et al. proved the covalent binding of PDA subunits during the formation of high molecular weight chains [22].

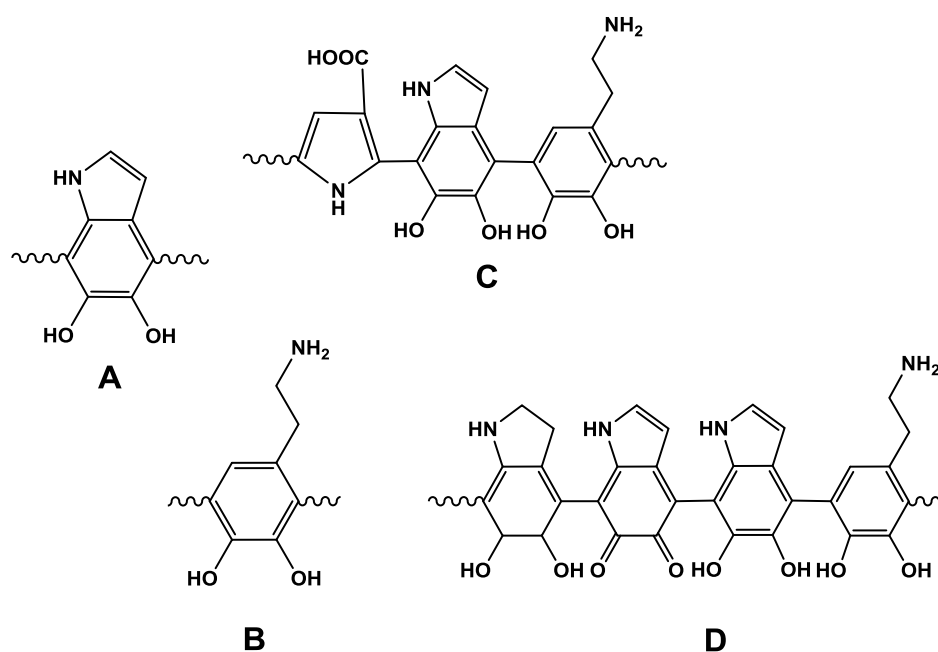


Figure 2. Polymeric structural models for polydopamine (Modified from [24], Hemmatpour et al., Nature Communications (2023)).

1.2.2 Physical Models of PDA

Some studies suggested that supramolecular structure of PDA was formed through physical interactions. For example, Hong et al. highlighted the presence of self-assembled physical trimers and (dopamine)₂/DHI, stabilized through van der Waals forces and hydrogen bonds (Fig. 3A). The co-contribution of (dopamine)₂/DHI to the covalently PDA formation was proposed after characterization of the physical complex using high-performance liquid chromatography (HPLC) and nuclear magnetic resonance (NMR) spectroscopy [23]. Dreyer et al. described PDA as a supramolecular aggregate consisting of DHI and its quinone derivatives which associate through hydrogen bonding, π - π , and charge transfer interactions using solid-state spectroscopy (Fig. 3B) [28]. This model was supported by Chan et. al who demonstrated non-covalently bound supramolecular aggregates of dopamine and the cyclized intermediate dopaminedochrome as the main building blocks of PDA through mass spectrometry and isotope-labeling studies (Fig. 3C) [29]. Recently, Hong et al. proposed cation- π association between protonated amines of uncyclized DOP/dopaminequinone and π -system indole groups of DHI and their subsequent oligomers in addition to the above-mentioned physical interactions in the formation of PDA [21]. Nowadays, PDA formation has been explained through non-covalent interactions of oligomers, particularly trimers which formed by covalent coupling oxidation reactions.

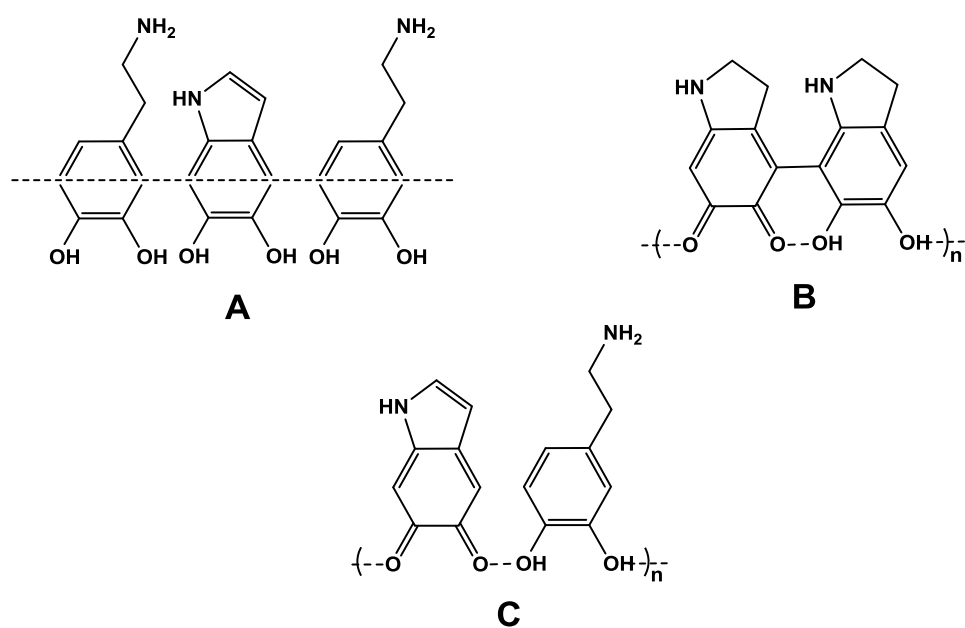


Figure 3. Physical structural models for polydopamine (Modified from [24], Hemmatpour et al., Nature Communications (2023)).

1.2.3 Trimer-based Models of PDA

Ding et al. supported trimer-based formation of PDA using high-resolution mass spectrometry. They demonstrated the formation of a covalently bonded trimer which was composed of (DHI)₂/pyrrole dicarboxylic acid, followed by self-assembly of the trimers to form the supramolecular structure of PDA (Fig. 4A) [30]. In contrast to the formation of DHI-based oligomers, Alfieri et al. proposed another model for the PDA formation which was based on polycyclic systems with chain breakage through quinone-amine conjugation (Fig. 4B) [31]. Besides, Lyu et al. suggested a molecular structure primarily composed of complex formation among dopaminechrome and dopamine units using mass spectrometry to define PDA formation (Fig. 4C) [32,33]. In summary, a clear and cohesive PDA mechanism has not been established yet (Fig. 5). It is crucial to investigate the functional groups that are generated and how they evolve during dopamine polymerization to enhance the comprehension of the PDA formation mechanism.

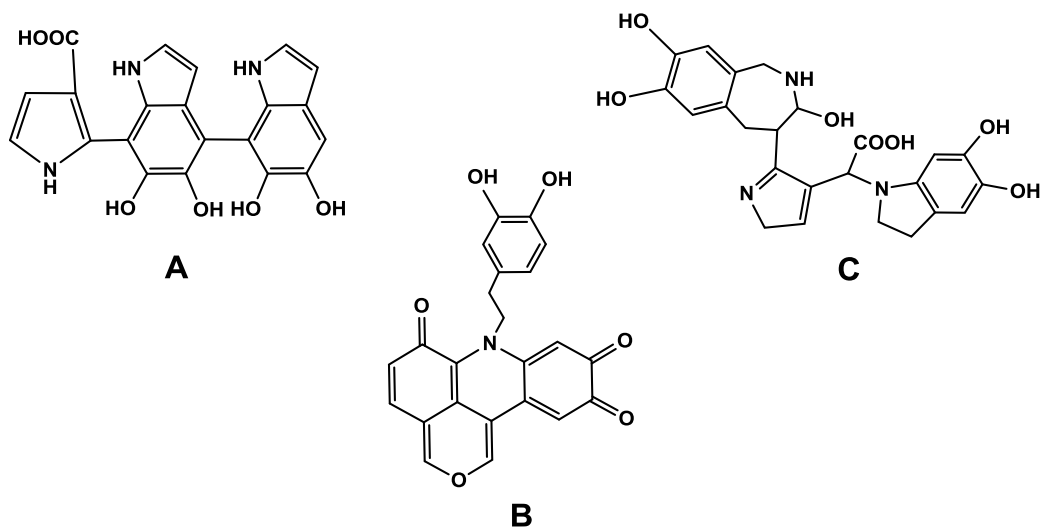


Figure 4. Trimer-based models for polydopamine (Modified from [24], Hemmatpour et al., Nature Communications (2023)).

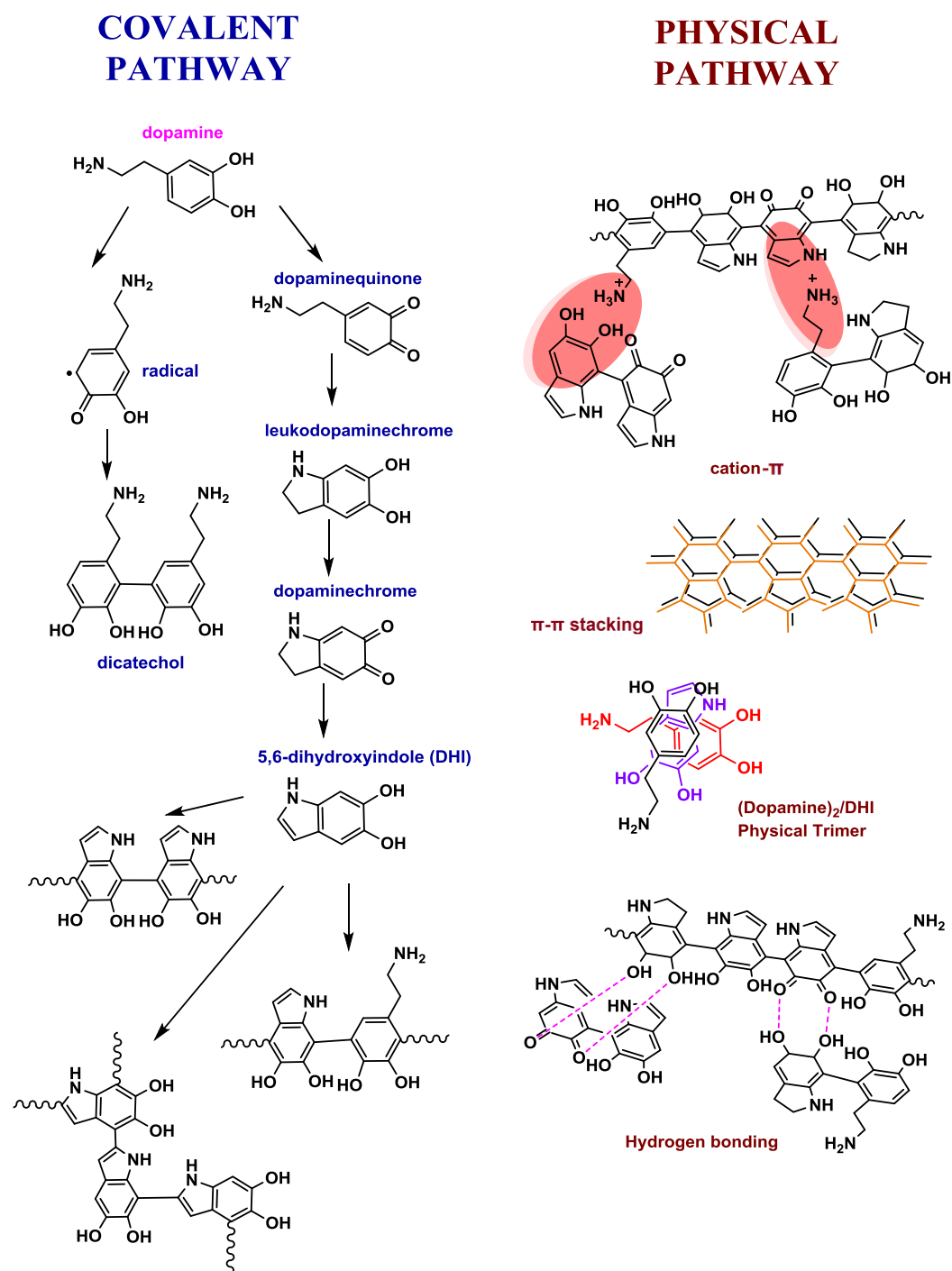


Figure 5. Proposed covalent and physical pathways of polydopamine (Modified from [21], Hong et al., Sci. Adv. (2018)).

1.3 Preparation of PDA-based Surfaces

PDA has received significant attention due to its ability to adhere to nearly any surface, thus offers a straightforward method for creating multifunctional coatings. An adherent PDA layer at a surface can be obtained by immersing a substrate in the dopamine polymerization solution for a certain period [3].

1.3.1 Mechanism of PDA Deposition at the Surface

Delparastan et al. explained the formation of PDA films through adsorption of small oligomers at the solid–liquid interface, followed by polymerization for the formation of higher molecular weight PDA chains [22]. In parallel to this study, Bernsmann et al. suggested that dopamine monomers and small oligomers adsorbed at the surface of a substrate and polymerized similarly to that described for the solution case. They claimed that the polymerization of DOP was initiated by the formation of dopamine-semiquinone radicals, followed by formation of oligomers, high-molecular-weight polymer, PDA nanoaggregates and eventually deposition of a continuous PDA film at the surface. They also mentioned that monomers, nanoaggregates (2-20 nm) and some larger PDA particles (20-50 nm) in the polymerization solution can also be incorporated into the deposited PDA layer through covalent bonding, π - π stacking, and non-covalent interactions during the deposition. Therefore, the thickness of a PDA layer increases gradually with polymerization time [34]. Large PDA particles and their aggregates were found to not adhere to the substrate since they were readily washed off when the substrate was rinsed with deionized water following the coating process (Fig. 6) [35].

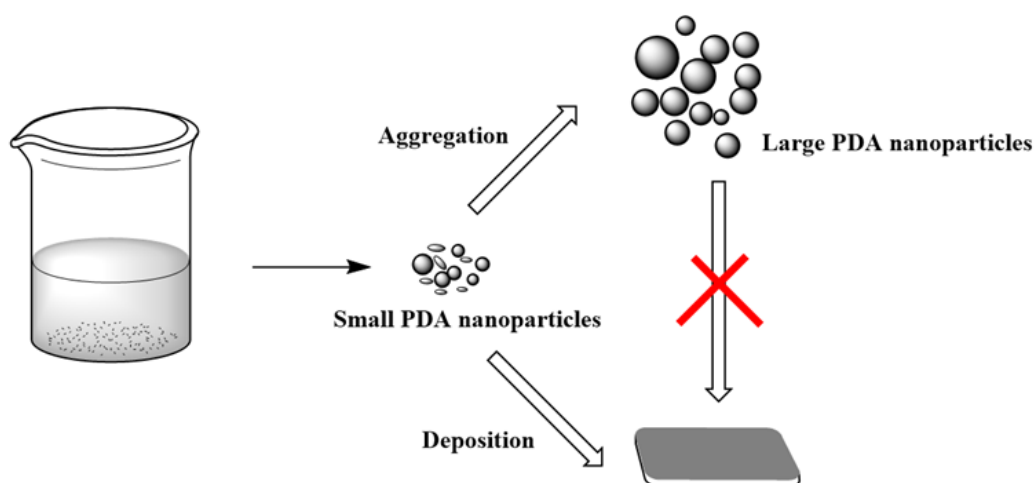


Figure 6. Schematic representation of PDA aggregation and deposition. Red cross describes no deposition of large PDA nanoparticles onto surfaces (Modified from [36], Zhang et. al. ACS Appl. Mater. Interfaces (2017)).

In accordance with this mechanism, Ding et al. proposed that deposition and aggregation were two competing processes during the formation of a PDA layer. They examined this hypothesis by following the film formation through polymerization at 2 different dopamine concentration ranges, i.e. 0.25-1.0 g/L and 1.0-4.0 g/L. In the former case, the increase in initial dopamine concentration was found to increase the deposition rate of PDA at the surface, while a decrease in the aggregation rate in solution was suggested due to the relatively large mean free path between dopamine and/or DHI units (Condition I). In the latter case, the mean free path between dopamine and/or DHI units significantly diminished, leading to accelerated aggregation rate in solution when compared to the deposition rate at the substrate (Condition II) (Fig. 7). They reported a remarkable decrease in PDA thickness and roughness in the case of higher initial dopamine concentration [30].

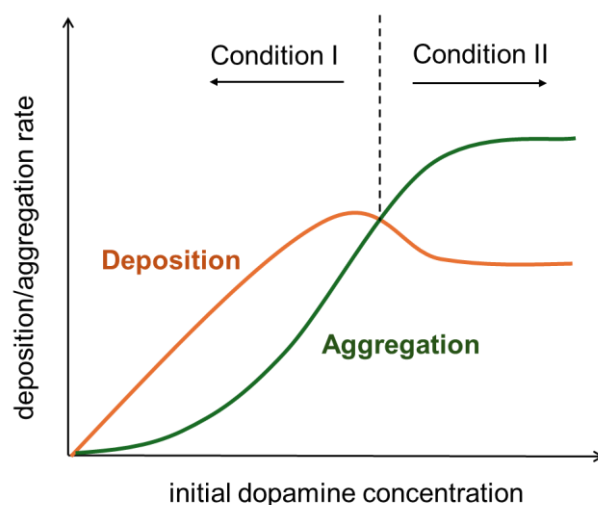


Figure 7. The relationship between initial dopamine concentration and deposition and/or aggregation rate (Modified from [30], Ding et. al. Langmuir (2014)).

Many studies reported on the interactions between the PDA layer and the surfaces as follows: 1) covalent interactions through Michael addition and/or Schiff base *via* amino and catechol groups, 2) non-covalent interactions such as π - π stacking, cation- π and hydrogen bonding interactions, 4) electrostatic interactions, 5) chelation with metal ions [37]. The main advantages of PDA coatings can be mentioned as follows: i) strong adhesion to substrates with long-term stability [38], ii) acting as a reductant to introduce metallic nanoparticles without need of additional reducing agents [39], iii) mild and non-destructive reaction/coating conditions, and iv) further surface functionalization through catechol and amino groups [40].

1.3.2 The Factors Affecting the DOP Polymerization and Properties of PDA

Alkaline pH range was found to be crucial for the self-polymerization of DOP under autoxidation conditions where air is used as oxidizing agent. Ball et. al reported that the polymerization rate decreased at low pH, while increased as a function of pH up to pH 10 [41]. PDA coatings were found to disintegrate beyond pH 10 and Hong et al. correlated this fact with the deprotonation of amino groups, leading to the

destruction of cation - π interactions which initially played a role in the deposition of PDA chains [21]. Teunissen et al. reported successful PDA formation in neutral and/or acidic environments through polymerization in the presence of various oxidants, such as sodium periodate (NaIO_4) [42]. In addition to pH, increasing temperature was found to increase the rate of polymerization through promoting PDA oxidation [43]. Increasing temperature and extended polymerization time were also found to enhance PDA deposition at the surface [35]. The type of buffer also influenced the PDA deposition. For example, Vecchia et al. performed the polymerization of DOP in different buffers, including Tris, phosphate, and bicarbonate and demonstrated that the morphology, thickness, and particle size of PDA coatings were affected by the type of buffer. They reported that tris buffer covalently incorporated into the PDA through a nucleophilic attack by ammonia in the Tris structure and led to the formation of smaller PDA particles [44]. Conversely, amine-free organic and/or inorganic buffers could be used as alternatives to avoid Tris incorporation; however, co-deposition of PDA aggregations were found to be inevitable [45]. The requirement for the presence of oxygen in dopamine polymerization was also considered by Lee et al., showing a reduced PDA deposition rate when oxygen was partially removed [2]. Kim et al. reported significantly accelerated PDA deposition and highly smooth surfaces with improved homogeneity when pure oxygen was used instead of air [46]. As mentioned earlier in Section 1.3.1, initial dopamine concentration is also critical in polymerization of DOP and formation of PDA films since it controls the two competing processes, i.e. aggregation versus deposition.

1.4 Antimicrobial Properties of PDA

PDA is notable for the antibacterial effects against several microorganisms such as *E.coli*, *S. aureus*, *P. aeruginosa* and *MRSA* through different mechanisms [3,47]. These antibacterial mechanisms of PDA can be grouped in four main parts:

i) contact-killing: the bacterial cell membrane can be destroyed *via* PDA through the electrostatic interaction and the chelation of proteins/ions.

ii) generation of ROS: PDA is able to produce ROS due to the existence of the high amount of catechol moieties which results in transferring electrons through isomerism of phenolic quinone. These catechol moieties also provide chelation of ions leading to destruction of the bacterial cell wall [3].

iii) good photothermal conversion capability: the conjugated structure of indole-5,6-quinone and the electron donor–acceptor structures between 5,6-dihydroxyindole synergistically causes a wide range of light absorption and enables PDA as photothermal therapeutic agent and damages and/or destruct the cell membrane [48].

iv) chemical modification of PDA: chlorinating PDA to form N-halamine can endow strong antibacterial properties owing to the destructive action of halogen ions [3].

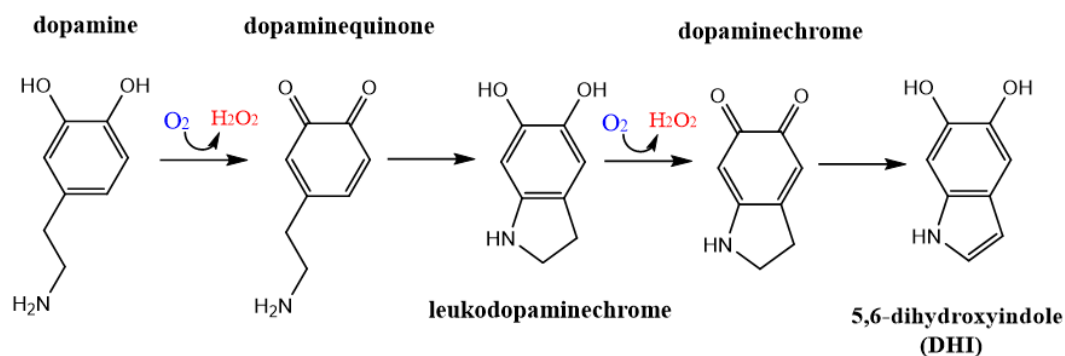
1.4.1 Contact-Killing Mechanism of PDA

The contact killing property emerges from catechol moieties and protonated amino groups of PDA. The antibacterial mechanism through catechol groups is similar to that provided by some natural polyphenols such as tannic acid [49]. The ability of catechol groups to chelate with the metal ions that are needed for the vital activity of bacteria disturbs the physiological metabolism of bacteria, followed by the disruption of the cell membrane [50]. Additionally, the protonated amine moieties of PDA lead to lysis of the bacteria and the exudation of cell contents when PDA contacts with the cell wall of bacteria [3].

1.4.2 Generation of ROS Mechanism of PDA

As mentioned before, the polymerization mechanism of PDA is still under discussion. However, it is known that during the polymerization of PDA, ROS is generated. The produced ROS throughout polymerization is referred to as hydrogen

peroxide (H_2O_2) and superoxide anions ($\text{O}_2^{\bullet-}$). Lee and his co-workers indicated that the catechol group in dopamine was known as the active site for oxygen (O_2) reduction [51]. They explained the mechanism of oxidation of dopamine and production of $\text{O}_2^{\bullet-}$ and H_2O_2 in the following way: During dopamine oxidation, one-electron oxygen reduction reaction (ORR) takes place, involving the dehydrogenation of dopamine's catechol group. This results in the formation of a superoxide anion radical ($\text{O}_2^{\bullet-}$) and dopamine o-semiquinone radical [52]. As dopamine undergoes further oxidation, the generated superoxide anion radical is subsequently converted into H_2O_2 via another reduction step [53]. The oxidized catechol units are restored to their active catechol state after the amine group undergoes cyclization, forming the dopaminechrome structure. This process leads to the generation of another H_2O_2 molecule through a second ORR step, followed by the creation of DHI [53]. Furthermore, no significant decomposition of H_2O_2 was observed in the presence of dopamine or DHI, confirming that the produced H_2O_2 remains unaffected during the oxidation process. The mechanism of H_2O_2 generation can be found in Scheme 1.



Scheme 1. The mechanism of H_2O_2 generation during polymerization of dopamine. (Modified from [54], Lee et al. Journal of Catalysis (2022)).

Note that PDA exhibits both ROS (H_2O_2) production and scavenging behaviour. PDA tends to produce H_2O_2 in the presence of electron donors such as oxygen; however, PDA is able to scavenge and quench the radicals in the case of free radical donor. The electron transfer mechanism between PDA and oxygen is challenging to explain due to co-existence of three distinct species of PDA: the relatively stable

oxidized quinone (Q), the reduced catechol (QH₂), and the less stable semi-quinone radical intermediate (Q•). The findings indicated ROS may be generated during both the oxidation of QH₂ to Q• and the subsequent conversion of Q• to Q. (Fig.8) However, it is not clear yet which one it originates from, since the studies haven't distinguished these two oxidative processes [55]. The produced H₂O₂ is considered to be responsible for the antibacterial effect due to its potential for destruction of the inner cell membrane and the cell wall of bacteria, leading to leak out of the proteins in the cells and causing the death of bacteria [3,48].

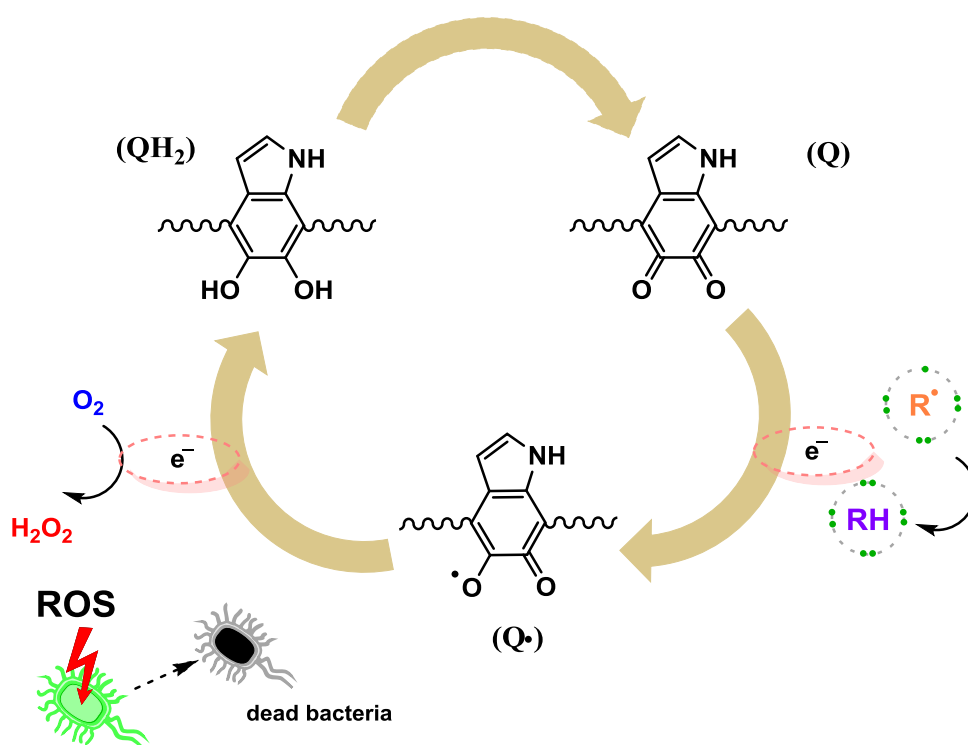


Figure 8. ROS generation and scavenging mechanism of PDA (Modified from [55], H. Liu et al. Acta Biomaterialia 88 (2019)).

There are many studies which discussed the increasing production of H₂O₂ during the DOP polymerization. For instance, Li et al. found that horseradish peroxidase (HRP) significantly accelerated polymerization, boosting the rate by nearly 100 times [56]. HRP has been extensively used in the oxidative polymerization of phenolic compounds in the presence of H₂O₂ [57]. They mentioned that HRP's activity relied on forming a complex with H₂O₂, which was effective on oxidizing

various substances, such as phenols or nitrates. Of note, the precise mechanism behind these reactions has not been clarified yet. Authors compared HRP-catalyzed and autooxidised dopamine polymerization (where O₂ acts as oxidant) rates. When HRP and low-concentration H₂O₂ (typical for HRP-catalyzed reactions) were added, the solution rapidly turned brown-black in 48 seconds. On the other hand, polymerization of DOP was slow in the presence of O₂ even after 4 hours [56]. Additionally, Du and colleagues presented the light-triggered dopamine polymerization using ultraviolet (UV) light to generate ROS *in situ*, which acted as oxidants of PDA polymerization. They demonstrated that UV irradiation could accelerate dopamine polymerization under acidic, basic, and neutral conditions by producing ROS. This method involved over an hour of UV light exposure at a controlled intensity (260 nm, 7.5 mW cm⁻²). To confirm that UV light could initiate dopamine polymerization, the UV-Vis spectra of dopamine solutions (2 mg/mL) were recorded following UV irradiation. The experiment was conducted with Tris buffer solutions at pH 8.5 (commonly used for PDA coatings) and pH 7.0 (where dopamine polymerization typically proceeds slower). At pH 7.0, the solutions turned dark yellow after 2 hours of UV exposure, while non-irradiated solutions showed almost no visible change. The observed increase in polymerization rate under UV light can be attributed to ROS, which may be generated even from small amounts of O₂. To verify UV-triggered dopamine polymerization is an oxidation-driven process, 2 mg/mL of ascorbic acid (vitamin C, ROS scavenger) was added to the dopamine solution to prevent ROS formation during UV irradiation. No polymerization was observed after 2 hours of UV exposure, either at pH 7.0 or pH 8.5, indicating that UV-triggered dopamine polymerization relies on dopamine oxidation induced by ROS [58].

1.5 Applications of PDA Coatings

The potential use of PDA coatings has been demonstrated for many different applications such as water treatments, preparation of vanadium redox flow batteries,

antibacterial surfaces and sensing [59]. For instance, Ouyang et al. demonstrated the preparation of protein-imprinted PDA nanowires with good monodispersity. In this study, PDA film formation was performed through DOP polymerization onto protein-immobilized anodic alumina oxide nanomold. By the removal of the template and immobilized protein, a PDA cavity structure was obtained which provided amino and hydroxyl groups, capable of participating in π - π interactions. These features enabled PDA cavity to present selectivity for some template proteins, specifically bovine and human hemoglobin for rebinding to the template [60]. Additionally, PDA coatings have also been suggested to modify the surface of nanofibrous scaffolds for vascular tissue engineering and bone biosubstitutes for bone tissue engineering applications [61,62]. Besides, PDA has garnered significant attention in the preparation of hydrogels. For instance, Suneetha et al. prepared a multifunctional hydrogel using PDA, sodium alginate and polyacrylamide. They showed that PDA enhanced the adhesion strength of the hydrogel due to π - π or cation- π interactions between the free catechol groups of PDA and the amine or thiol groups on the skin tissue. High swelling, good adhesion between the cells and hydrogels, relatively short blood clotting time and higher platelet adhesion were also attributed to the presence of PDA in the hydrogels [63]. PDA is also used as a capping layer in the preparation of drug carrier systems. For instance, Lyng et al. adsorbed fluorescent liposomes onto PLL precoated glass slides and deposited PDA as a capping layer to enhance their interaction with myoblast cells [64]. Cheng et al. modified mesoporous silica nanoparticles with PDA and functionalized them using poly(ethyleneglycol)-folic acid (PEG-FA). They reported pH-dependent and sustained release of doxorubicin (DOX) from the particles through *in vivo* and *in vitro* experiments. The pH-dependent release was attributed to the pH-responsive property of PDA at acidic pH, and sustained release was correlated with the blocking of the pores of mesoporous silica nanoparticles by PDA. Of note, rapid drug release was observed with non-modified particles due to improved solubility of DOX in acidic environment [65]. As it was discussed before, PDA is well-known for its antibacterial and antifungal effects against various microorganisms. In the literature,

there are few studies on contact-killing properties of PDA. Iqbal et al. investigated the antimicrobial property of PDA coatings against *E. coli* through self-polymerization of DOP onto *E. coli* cells. They confirmed the PDA coating on *E. coli* cells via Fourier-transform infrared spectroscopy (FTIR) and reported a uniform PDA coating with 120 nm thickness which was shown by Scanning electron microscopy (SEM). The deformation and damage of the bacterial cells during polymerization was demonstrated by capillary electrophoresis Ultraviolet-visible (UV-Vis) spectroscopy. In this study, such possibilities for the antibacterial mechanism of PDA were suggested as follows: i) the formation of a PDA layer over the cell resulted in collisions between the cells and the settling PDA particles. ii) PDA-coated *E. coli* cells would not have enough space for it to grow and multiply as they embedded and permanently trapped in PDA over time. iii) Amine groups of PDA on the outer membrane may show antimicrobial activity with the similar mechanism of quaternary amine compounds v) Interaction between charged PDA and cells resulted in bending or stretching forces on *E. coli* cells which may damage them [17]. In a study of Su et al., it had been developed that roughened PDA (rPDA) coatings via a shaking-assisted method that significantly enhanced antibacterial activity against both *Gram-positive* and *Gram-negative bacteria* through contact-killing mechanism, even without use of external antibacterial agents [66]. Furthermore, Patel et al. showed that PDA coatings prepared using different buffers can manipulate antibacterial properties by controlling the functional groups present in the coatings. They discussed that PDA coatings prepared with Tris and sodium hydroxide exhibited greater antibacterial activity due to higher amount of hydroxyl moieties on the surface than those fabricated with sodium bicarbonate and phosphate-buffered saline (PBS). Although the antibacterial mechanism of Tris and sodium hydroxide-based PDA films hasn't explored yet, they suggested that negatively charged *E. coli* was repelled by nucleophilic -OH groups on the surfaces [67]. In another study, a reverse osmosis (RO) membrane was coated with PDA. pH-dependent antibacterial activity of PDA was examined against *E. coli* and the contact-killing based bactericidal effect of PDA-coated RO membrane was attributed

to the existence of protonated amine groups of PDA [68]. Chien et al. demonstrated enhanced antibacterial efficacy of PDA coating through *N*-Halamine functionalization, wherein the amino groups of PDA are chlorinated. They reported significant antibacterial activity against *S. aureus* and *E. coli* within a short contact time compared to PDA coating and emphasized the regenerable nature of the *N*-Halamine structure through repeated rechlorination cycles [16]. Song et al. prepared antibacterial PDA-ferrocene functionalized TiO₂ nanorods which were designed as implants, capable of combating bacterial infections and inhibiting biofilm formation. They explained the antibacterial mechanism of PDA in two potential mechanisms: i) generation of intermediate H₂O₂ and ii) induction of significant photothermal effect through the dissipation of near-infrared (NIR) radiation, both contributing to bacterial cell damage and/or destruction. The antibacterial effect was further enhanced by the incorporation of ferrocene, converting H₂O₂ into highly toxic ·OH radicals, enabling localized and rapid antibacterial treatment. Surprisingly, they also reported that the photothermal effect accelerated ·OH generation with increasing temperature, highlighting the synergistic potential of the system [69].

1.6 Tannic Acid

Tannic acid (TA) is a natural polyphenol which is extracted from different plants such as Chinese galls, tara pods, sumac leaves and *Quercus infectoria* [70]. It has commonly been used over the past decade in different biomedical applications due to its antibacterial, antioxidant, antiviral, antifungal and anticancer activities. In addition to these, TA is commonly preferred for the preparation of thin film coatings and nanoparticles. As a natural crosslinking agent, TA is preferred as a building block in the preparation of synthetic and natural hydrogels [71]. In Figure 9, the chemical structure of TA can be found.

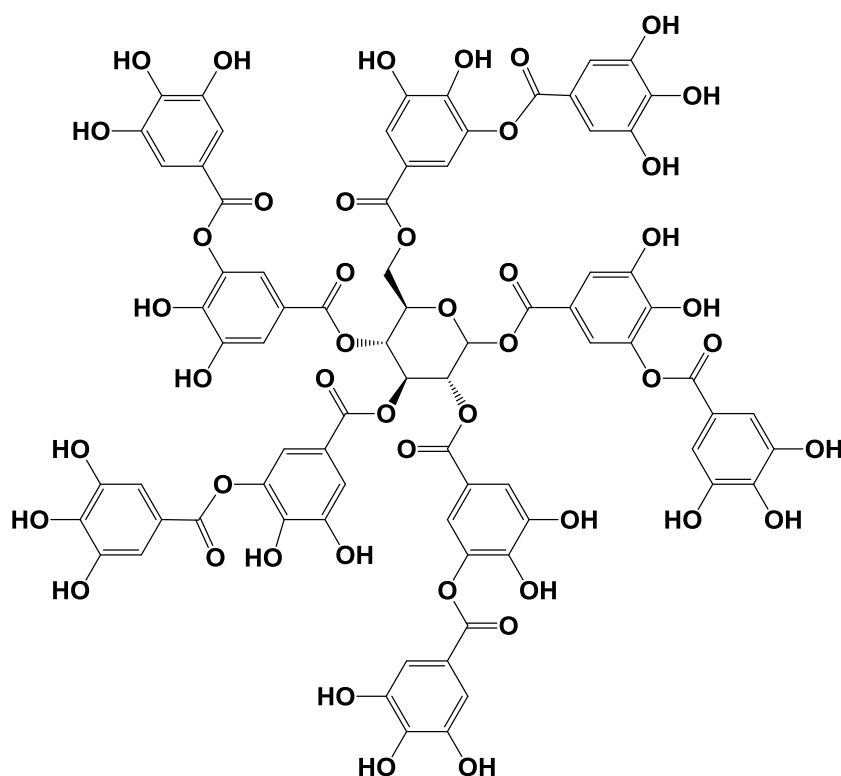


Figure 9. Chemical structure of TA.

In general, antioxidants have gained attention due to their ability to reduce oxidative stress by neutralizing unstable oxygen radicals. Oxidative stress results from an imbalance in the cell's normal redox state, leading to the production of ROS like superoxide radicals, hydroxyl radicals, and hydrogen peroxide. ROS can damage cellular components such as proteins and DNA, trigger inflammation, and even cell death [72]. TA, as an antioxidant, has been shown to counteract the formation of hydroxyl radicals and exhibit strong scavenging abilities for superoxide anions and hydrogen peroxide. However, TA has also prooxidant properties. It binds copper ions in chromatin and damages DNA [73]. The ability of TA functioning as an antioxidant or prooxidant depends on its concentration. At lower concentrations, TA exhibits beneficial antioxidant effects, but at higher concentrations, it shifts to prooxidant behaviour. While the antioxidant properties of TA provide reducing oxidative stress, its prooxidant characteristics such as stimulating oxidative stress and the chelation with metal ions play a crucial role in enhancing its antibacterial and anticancer activities [74].

TA also shows antiviral and antifungal properties. It has been reported to inhibit several viruses, including influenza, SARS-CoV, herpes simplex virus (HSV), hepatitis C, Zika virus, and HIV. The antiviral effect of TA was ascribed to its ability to preventing of receptor binding of viruses and inhibiting neuraminidase enzyme that enabling the spread of infection [75]. For example, TA blocks viral binding in norovirus and inhibits the entry of hepatitis C and Zika virus into host cells [76].

TA is also known for its potential in anticancer studies. TA has been shown to have tumor-inhibiting behavior in animal models, such as reducing skin tumor progression and inhibition of liver mutagenesis. TA was found to trigger apoptosis in various cancer cell lines, such as prostate, breast, liver, colon, and glioma cancers, through its ability to generate reactive oxygen species (ROS) at higher concentrations which disrupted cancer cell metabolism and inhibited fatty acid synthase (FAS), a crucial enzyme overexpressed in many cancers [77,78]. The exact anticancer mechanism of TA has still not been clarified in the literature. Yet, several proposed actions of TA including its antioxidant and prooxidant activities, the inhibition of cancer cell signaling and cell cycle progression have considered as possible pathways [71].

Although TA has been used in traditional medicine in early times for purposes like oral hygiene, its potential as an antibacterial agent has recently been recognized [79]. The antibacterial activity of TA was shown against *S. aureus*, a Gram-positive bacteria responsible for various infections such as skin infections, pneumonia, and toxic shock syndrome [80]. TA was also found effective against other Gram-positive bacteria such as *Bacillus subtilis*, *Enterococcus faecalis*, and Gram-negative bacteria such as *Pseudomonas aeruginosa*, and *Pectobacterium chrysanthami* [81–83]. Inhibition of gram-negative *E.coli* biofilm formation by TA was reported [84]. However, TA has been reported to be more effective against Gram-positive bacteria such as *S. aureus* than Gram-negative bacteria such as *E. coli.*, *K. pneumoniae* and *Salmonella* [85]. Lower antibacterial activity against Gram-negative bacteria was mostly attributed to the lipopolysaccharide in the outer membrane of Gram-negative bacteria which makes reaching of antibacterial

materials to the peptidoglycan layer of the bacteria difficult. Of note, Gram-positive bacteria don't possess lipopolysaccharides [86]. Since Gram-negative bacteria are reported as more harmful and cause serious diseases, understanding their interaction with TA is crucial. The antimicrobial efficacy of TA is influenced by various factors, including its concentration, pH, temperature, and the medium of application [87].

Although the exact antibacterial mechanism of TA has not been fully understood yet, three primary mechanisms are suggested: i) binding to bacterial enzymes and substrates, ii) inhibiting nutrient absorption, and iii) penetrating bacterial cell membranes [88,89]. The interaction with the membrane involves hydrogen bonding between TA's hydroxyl groups and bacterial membrane proteins [90], leading to altered membrane permeability, osmotic imbalances, disruption of the cell metabolism, and eventually cell destruction [88]. TA also inhibits the uptake of sugars and amino acids, limiting bacterial growth [91]. Additionally, the ability of TA for chelating metal ions, such as iron, which is essential for metabolic process of bacteria, can provide inhibition of bacterial growth [92].

1.6.1 Applications of TA Coatings

The pK_a of phenolic hydroxyl groups of TA ranges from 2.5 to 8.5 depending on the tannin source, allowing it to function as a weak acid [93]. This makes TA a useful building block in LbL deposition, where it can interact with neutral and positively charged materials through hydrogen bonds, electrostatic interactions, covalent bonding, hydrophobic interactions, and metal-polyphenol complexes [94–96]. Multilayers prepared with TA can deliver various substances in a controlled manner due to their pH-responsive dissolution properties [94]. For instance, Zhuk et al. demonstrated preparation of electrostatic LbL films composed of TA and various antibiotics with antibacterial activity against *S. epidermidis*, *S. aureus* and *E. coli*. They reported bacteria-triggered drug release through dissolution of multilayers at local acidic environment in the existence of bacteria. The disruption of multilayers was explained by the change in the charge balance within the multilayers upon

protonation of TA with decreasing pH [97]. Iqbal et. al prepared TA/collagen layer-by-layer films and reported antibacterial activity against *S. aureus* through TA release. They investigated the effect of type of buffer (acetate versus citrate buffers) that was used in the self-assembly on the morphology and antibacterial properties of TA/collagen LbL films. Citrate buffer provided stronger TA/collagen interactions and higher amount of TA release due to immobilization of excess TA by citrate ions through electrostatic interactions. Furthermore, granular topography of multilayers resulted in higher specific surface, inducing the local release of TA at a concentration above MIC when multilayers dissolved upon exposure to PBS [98]. The differences in the cell wall structures between Gram-positive and Gram-negative bacteria require the development of antibacterial coatings capable of collapsing their cell membranes upon contact. Silięka et al. prepared TA-modified colorless polycarbonate surfaces and investigated their antibacterial activity. They reported strong antibacterial activity against *P. aeruginosa* and *S. aureus* through contact killing mechanism just after three hours of exposure [99]. Singhal et al. presented a nanocomposite based on graphene nanoplatelets, TA, and silver (Ag) nanoparticles -also known for its strong antibacterial properties- and their epoxy-based coatings. They explained the excellent antibacterial and antibiofilm activities of the nanocomposites by the synergistic effect of all the ingredients. It was claimed that while the hydrophobic characteristics of graphene nanoplatelets and epoxy prevented the adhesion of bacteria, TA and Ag nanoparticles took part in the killing of bacteria through contact with bacteria. The existence of TA was believed to provide more binding sites for Ag nanoparticles and different possible antibacterial mechanisms such as inhibition of key enzymes for the synthesis of bacterial fatty acids, destroy of the cell wall of bacteria and decrease the levels of the biofilm [100]. Besides, TA coatings can be used for the preparation of antiviral surfaces. For instance, Haapakoski et al. prepared TA-immobilized cellulose-based paperboards by covalent conjugation of chitosan. They investigated the antiviral efficacy against coxsackievirus B3 (CVB3) and human coronavirus OC43 (HCoV-OC43) and remarkable antiviral activity of TA was reported even at low amounts and in noticeably short incubation time on top

of the samples [101]. Furthermore, tumor-inhibiting behavior of TA makes it suitable for use in anticancer studies. Tan et al. coated TA onto Ti surfaces with varying thicknesses using low-energy electron beam deposition to fabricate implants inhibiting bone tumors. They investigated kinetics of TA release and reported correlation between the increase in thickness of TA films and the elevated release of TA. Their findings demonstrated that TA films provided long-term inhibition of both the activity and migration of bone tumor cells through sustained release [102]. Furthermore, TA can be preferred for the preparation of functionalized surfaces with antioxidant effects. Yang et al. constructed a bioinspired TA/lysozyme LbL film through H-bonding and electrostatic interactions between the layers. In this study, the preparation of multifunctional multilayers was aimed where lysozyme and TA provided antibacterial properties, while TA also contributed with its antioxidant properties. The TA/lysozyme coating demonstrated strong ROS scavenging through the conversion of phenol moieties of TA to quinone groups in a ROS environment and enhanced bacterial killing against *S. aureus*, *Micrococcus lysodeikticus*, and *E. coli* by damaging the bacterial cell membranes. Although, the antibacterial activity of lysozyme was reported to diminish when LbL-assembled with oppositely charged polyelectrolytes, such an effect was not observed in the study of Yang et al [103].

1.7 Co-deposition of PDA and TA

Recently, some studies reported that under alkaline conditions, the catechol and amino groups of DOP could covalently react with quinone groups of TA through Michael addition/Schiff base reactions. For instance, Yang et al. modified the surface of a hydrophobic PVDF membrane through polymerization of DOP in the presence of TA and compared the hydrophilicity, infiltration capacity and antifouling properties of the membrane with that of an unmodified membrane. They observed an outstanding oil-repellent capability together with a benign protein interception performance, but importantly a more uniform PDA coating was achieved when DOP was polymerized in the presence of TA [104]. In another study, Xie et al.

demonstrated a straightforward and adaptable method for fabricating anti-fouling RO membranes. They deposited a PDATA interlayer onto RO membrane, followed by adsorption of Fe^{3+} -PhA through complexation between Fe^{3+} ions and TA. This modification significantly enhanced the membrane's hydrophilicity, wettability, and anti-fouling performance [105]. Zhang et al. deposited PDATA onto Ti substrate and incorporated Ag ions into PDATA through complexation with phenolic hydroxyl groups of TA. The resulting surfaces showed enhanced hydrophilicity, good cytocompatibility, and effective antibacterial activity against Gram-negative *E. coli*, holding promise for modifying the surface of Ti implants [106]. Lee et al. also showed that PDA and TA co-deposition can be used for creating high-performance electrochemical capacitors. In their study, a polydopamine coating was initially applied, followed by the deposition of Fe^{3+} ions and TA using a LbL process on interconnected porous carbon nanosheet (IPCN) electrodes. After deposition of the polydopamine coating, the specific capacitance was found to increase by ~40% as compared to that of an unmodified IPCN electrode. The increase in capacitance was attributed to the redox-active catechol groups of polydopamine, which induced a pseudocapacitance mechanism that enhanced charge storage capacity through surface redox reactions. The electrodes coated with both polydopamine and multilayers of Fe^{3+} and tannic acid exhibited an additional increase in the capacitance, which is ~83% higher than that of the unmodified IPCN electrode. This was explained by the additional redox moieties introduced by tannic acid. Additionally, the strong interactions between Fe^{3+} ions and catechol groups led to enhanced capacitance retention, even after 1,000 cycles. The mussel-inspired surface modification of IPCN electrodes shown in this study holds potential for the development of new pseudocapacitive electrode materials with outstanding performance [107]. Gao et al. functionalized TA-templated mesoporous silica nanoparticles (TMSNs) with DOP using a straightforward biomimetic coating approach to create a novel sorbent for the removal of Cu^{2+} from aqueous solutions. The factors which affect their sorption capacity, such as contact time, initial pH, K^+ and Na^+ concentrations, co-existing polyvalent metal ions, and adsorption-

desorption cycles, were examined. They found that DOP-TMSNs achieved a maximum adsorption capacity for Cu^{2+} at pH 5.5. Furthermore, K^+ and Na^+ concentrations had minimal impact on the sorption process, and the adsorption capacity remained at 89.2% after four cycles of reuse. These findings indicate that DOP-TMSNs were highly effective sorbents for Cu^{2+} removal [108]. Finally, PDA and TA co-deposition was also used for the development of a thin-film composite (TFC) membrane, consisting of a novel high-density polyethylene (HDPE) support, a polydopamine (PDA)/TA- Fe^{+3} interlayer, and a polyamide (PA) topmost layer. The resulting TFC membrane exhibited excellent dye rejection capabilities, outstanding solvent resistance in harsh environments, and a good methanol flux in SRNF applications [109].

1.8 Layer-by-Layer (LbL) Assembly

Layer-by-layer (LbL) deposition is a straightforward and adaptable technique for creating complex films with distinct structural and physicochemical properties. These multilayer films are also ideal for controlled release of active substances from surfaces. LbL technique relies on deposition of interacting polymers onto a surface. In the literature, multilayers are mostly prepared by the common following driving forces: hydrogen bonding, electrostatic interactions, metal ligand coordination bonding, charge-transfer interactions [110]. The simplicity, affordability, and ease of controlling film properties during self-assembly and/or post-assembly can be mentioned as advantages of LbL method [111]. This method allows the use of a variety of charged species ranging from viruses to macromolecules [112]. By adjusting the assembly conditions, LbL ensures consistency in film composition, structure, thickness, and mechanical properties [113]. In Fig. 10, illustration of LbL self-assembly process can be found.

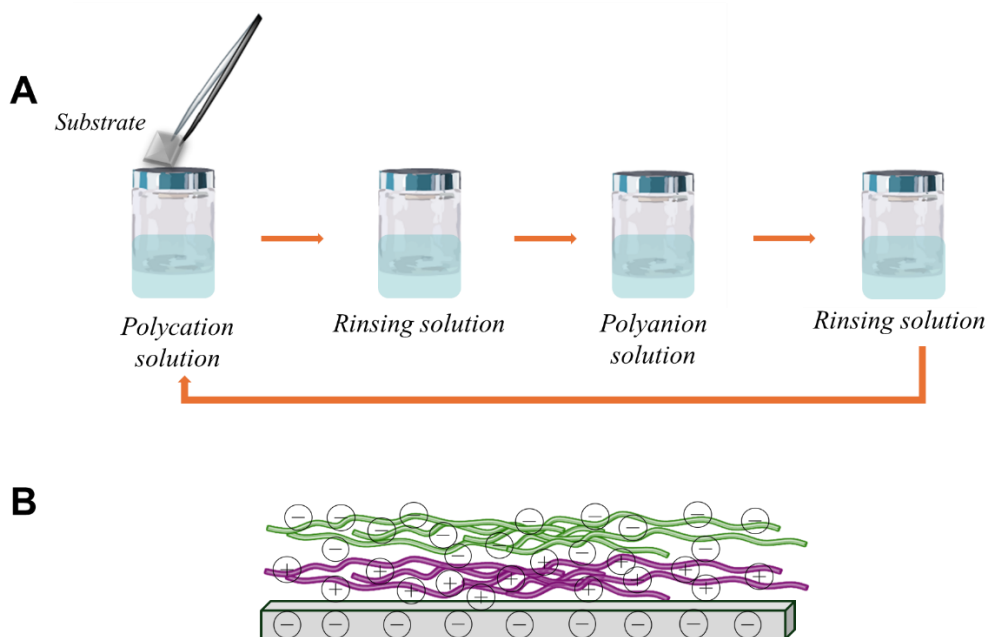


Figure 10. Illustration of A) fabrication of LbL method, B) LbL-coated polyelectrolyte films.

Multilayers have drawn attention for preparation of antimicrobial surfaces, including contact-killing, antifouling, and biocide-releasing surfaces. The majority of the contact-killing surfaces including quaternary ammonium compounds (QACs), antimicrobial peptides (AMPs), and polycations [114,115]. The widely accepted contact-killing mechanisms can be explained as follows: (i) positively charged quaternary amine (N^+) of QACs alters the critical ionic balance (such as Na^+ , K^+ , Mg^{2+} , Ca^{2+}) of bacterial cell and disrupts the membrane by interacting with the negatively charged bacterial cell membrane, (ii) increased hydrophobicity of the QACs with longer alkyl chain enhances their ability to penetrate the bacterial cell membrane, and (iii) AMPs targets bypassing the bacterial wall to reach intracellular components, interacts with negatively charged bacterial membranes through their hydrophobic and positively charged amino acid residues by displacing calcium and magnesium ions bound to the microorganism's polysaccharides, and damages the membrane and DNA [114].

Contact-killing surfaces prepared through LbL-assembly have been reported in many studies. For instance, in a study conducted by Illergard et al, multilayers prepared with cationic polyvinylamine (PVAM) and poly(acrylic acid) (PAA) on fiber were characterized with respect to antibacterial properties in two different perspectives: i) the evaluation of the reduction of bacteria and ii) determination of leaching possibility and the effect of leaching on the antibacterial activity. They demonstrated successful inhibition of the growth of *E. coli* owing to high positive charges on the surface without any polymer leaching, suggesting that the fibers operated through a contact-killing antibacterial mechanism [116]. Furthermore, Rubner et al. adjusted the assembly and post-assembly conditions of polyelectrolyte multilayers poly(sodium 4-styrene sulfonate) (PSS)/poly(allylamine hydrochloride) (PAH) by varying pH to impart mobile cationic charges on the surface. Multilayers were prepared at high pH and subsequently immersed into low pH solutions. A reversible pH-dependent swelling transition behaviour of multilayers was demonstrated. Protonation of uncharged amines provided sufficient positive charges, which induced cell death and provided antimicrobial activity against *S. epidermidis* and *E. coli*, with switchable functionality based on pH conditions [117]. In another study conducted by Gomes and et al., cotton samples were LbL-modified using chitosan (CHI) and alginate (ALG) to produce an antibacterial wound dressing. CHI/ALG multilayers were highlighted with antibacterial functionality assessed against *S. aureus* and *K. pneumoniae*. This activity was attributed to bacteriostatic properties of multilayers due to the high number of side amine groups of CHI with high deacetylation degree (80%) [118]. Furthermore, in a study of Graisuwan et al., N-[(2-hydroxy-3-trimethyl ammonium)propyl]chitosan chloride (HTACC), a quaternary ammonium compound, was synthesized and LbL-assembled with PAA on a plasma-treated poly(ethylene terephthalate) (PET) substrate. The inclusion of HTACC improved the antibacterial properties of the modified PET against *E. coli* and *S. aureus* [119]. Zhang et al. reported improved hydrophilicity of different surfaces by LbL depositing PVAM (positive charge due its rich free amino group within the polymer chain) and dopamine-modified hyaluronic acid (HA-DN,

negative charged) through both electrostatic interactions and covalent bonds. The growth of *E. coli* and *S. aureus* was notably inhibited, and bacterial growth was almost suppressed as the layer number increased g [120].

In addition to these, LbL-technique is widely used for preparation of antifouling surfaces [121,122]. Antifouling property of a surface can be defined as the prevention of organisms from attaching to surfaces [123]. The phenomenon of antifouling is commonly recognized by two widely accepted concepts: surface hydration and steric hindrance effects [124]. For example, Schmolke and colleagues assembled poly(diallyldimethylammonium chloride) (PDADMAC)/poly(acrylic acid) (PAA), and poly(allylamine hydrochloride) (PAH)/PAA multilayers on PDMS substrates using LbL technique. These films reduced the attachment and adhesion strength of *S. cerevisiae*. The authors reported superior performance for PDADMAC/PAA films compared to PAH/PAA multilayers due to their significantly higher swelling behaviour in a salt-rich aqueous environment, which reduced the adhesion between the cells of the hydrophobic *S. cerevisiae* and surface. In fact, adding a layer of pegylated PAA (PAA-g-PEG) to these PEMs further reduced the microbial adhesion by up to two orders of magnitude due to the antifouling characteristic of PEG [125]. Xie et al. developed an antifouling and bactericidal polymeric membrane through LbL deposition of zwitterionic sulfobetane-grafted PEI polymer (PEI-g-SBMA) and oxidized sodium alginate. The resulting surface demonstrated excellent resistance to bacterial adhesion. Furthermore, silver nanoparticles (AgNPs), known for their broad-spectrum bactericidal properties, were anchored on the surface through the chelation Ag^+ ions by PEI-SBMA, resulting in bactericidal characteristic of membrane [126]. In a study by Park et al., a polyethylene terephthalate (PET) substrate, commonly used in orthodontic appliances, was treated with oxygen plasma to activate the surface, followed by LbL deposition of carboxymethyl cellulose (CMC) and chitosan *via* electrostatic interactions. Furthermore, the modified PET, which displayed excellent chemical and physical stability, was found to be superhydrophilic through the crosslinking between CMC and chitosan and prevented bacterial adhesion, reducing

bacteria by up to 75% ratio [127]. Furthermore, in two studies of Yinn and coworkers, silicon substrates were modified using polyacrylic acid as the polyanion (PAA) and *N,N*-dodecyl,methyl-polyethylenimine as the polycation to form LbL-multilayer films. After modification, the surfaces demonstrated strong antifouling properties. In addition, antimicrobial activity could also be introduced when the topmost layer was *N,N*-dodecyl,methyl-polyethylenimine. They reported that antifouling performance could be improved by placing the polyanions as the outermost layer [128].

LbL method allows incorporation of bactericidal components into multilayer films to prepare antimicrobial coatings. These components can be released into the surrounding. For example, antibiotics can be incorporated into LbL assemblies and released from films to combat bacteria. In a study of Chuang et al., gentamicin, a positively charged antibiotic, was alternately deposited with biocompatible polyanionic hyaluronic acid and a hydrolytically degradable poly(β -amino ester) to form LbL thin films. The controlled release of gentamicin from multilayers was provided *via* hydrolytic degradation of poly(β -amino ester). The disassembly of the film and gentamicin diffusion showed effective bactericidal activity against *S. aureus* [129]. Similarly, vancomycin and metronidazole antibiotics were incorporated into different LbL-assembled films, targeting *S. aureus* [130] and *Porphyromonas gingivalis* [131], respectively. In a study of Schmidt et al., gentamicin was LbL-assembled with negatively charged Prussian blue nanoparticles to achieve more precise control over antibiotic release. Upon applying a small anodic electric potential, the Prussian blue nanoparticles were oxidized from negatively charged to neutral, triggering the release of gentamicin to kill *S. aureus* [132]. Also, immobilizing bacteriophages that are viruses targeting *Gram-positive* and *Gram-negative* bacteria on surfaces are widely used for the preparation of antimicrobial coatings especially in food applications [133]. Tidim et al., prepared ultra-thin multilayer films and embedded bacteriophages into the film. Such films were found to show antibacterial activity against *Salmonella Enteritidis* highlighting the potential of the LbL films as an antibacterial coating for food packaging applications.

The antibacterial activity was more pronounced at neutral pH (7.0), but no activity was observed in acidic conditions. Additionally, they wrapped *Salmonella Enteritidis*-contaminated chicken with aluminum foil coated with phage-loaded chitosan/alginate multilayers and reported significant decrease in the number of bacterial colonies on the meat [134].

1.9 Aim of Thesis

As discussed in detail in Sections 1.4 and 1.6, both PDA and TA exhibit significant potential for biomedical applications such as preparation of antibacterial surfaces and drug-delivery platforms for cancer therapy. Inspired by these features, the main aim of this thesis study was to conduct a comparative study to reveal the differences in the surface properties of multilayers based on PDATA and PDA. In this context, the following sub-aims can be listed:

i) optimization of the conditions such as concentration and polymerization time for the self-polymerization of DOP and deposition of PDA at the surface in the presence and absence of TA.

ii) preparation of single- and multi-layer films composed solely of PDATA and PDA and comparison of their surface properties with respect to thickness, wettability, morphology, and stability using techniques such as ellipsometry, UV-Vis spectroscopy, contact angle measurements, and atomic force microscopy.

iii) LbL self-assembly of PDATA and PDA using various counterparts such as positively charged BPEI, negatively charged TA and electrically neutral PVCL to understand the effect of interlayer association on the surface properties such as thickness, morphology, wettability and stability.

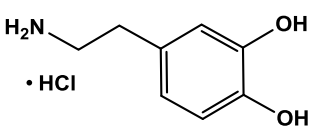
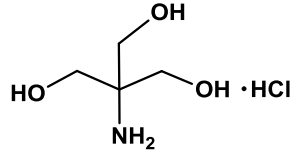
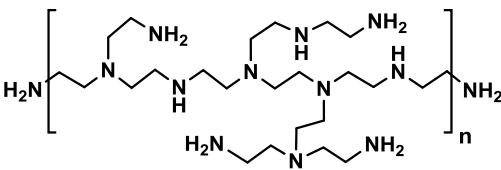
CHAPTER 2

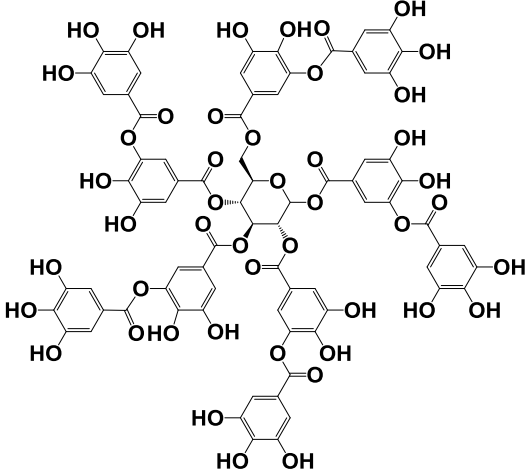
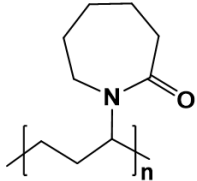
EXPERIMENTAL

2.1 Materials

Branched poly(ethylene imine) (BPEI, 25,000 g/mol), dopamine hydrochloride (DOP, 189.64 g/mol), phosphate buffer saline (PBS) tablets and Hellmanex III were purchased from Sigma Aldrich. Tannic acid (powder) (1701.20 g/mol) and sodium dihydrogen phosphate dihydrate ($\text{NaH}_2\text{PO}_4 \cdot 2\text{H}_2\text{O}$) were purchased from Merck Chemicals. Poly(N-Vinyl caprolactam) (PVCL, 1300 g/mol) was obtained from Polymer Source Inc. Tris(hydroxymethyl)aminomethane-hydrochloride (Tris HCl, 157.60 g/mol) buffer was purchased from Serva Electrophoresis GmbH. Sulfuric acid (95%-98%) was purchased from Tekkim Kimya. Deionized (DI) water was purified by Milli-Q system (Millipore) at 18.2 M Ω .

Table 1. Chemical structure of substances.

DOP	
Tris HCl	
BPEI	

TA	
PVCL	

2.2 Instrumentation

The dry thicknesses of the films were measured by using an Optosense (OPT-S6000, USA) Spectroscopic Ellipsometer, operating within a wavelength range of 400 nm to 1000 nm at a 65° incident angle. Thickness measurements were performed at three randomly selected places at the surface of the sample. Average thickness values were calculated and presented with standard deviations.

Hydrodynamic size measurements of PDATA and PDA particles were performed through DLS technique using a ZetaSizer Nano-ZS (Malvern Instruments Ltd., U.K.) at a scattering angle of 173° (backscatter) and 633 nm HeNe laser based. The reference material was selected as polystyrene latex with the refractive index (RI) of 1.590. The dispersant was chosen as water with the refractive index 1.330 and 0.872 cP viscosity. The hydrodynamic size was obtained by cumulative analysis of the autocorrelation data. The initial concentrations of DOP and/or TA were 0.5 mg/mL. The measurements were carried out in plastic cuvettes at 25 °C. For all measurements, three independent measurements were performed with 8 sub-runs.

Zeta-potential of PDATA and PDA particles were measured using a ZetaSizer Nano-ZS Instrument (Malvern Instruments Ltd., U.K.). Zeta-potentials values were obtained from electrophoretic mobility values using the Smoluchowski approximation. The averages of three independent measurements, each consisting of 100 sub-runs, were reported.

The absorbance spectra of the films were recorded using a HITACHI U-2800 A spectrophotometer before and after exposure to PBS.

Static contact angle measurements were carried out using an Attension Theta Lite optical tensiometer. Approximately 1.5 μ L droplet of DI water was dropped onto multilayers constructed onto glass slides (2.5 cm x 2.5 cm). Measurements were repeated eight times. For each measurement, ten independent measurements were recorded.

AFM images of multilayers were recorded using an Ambient AFM/Magnetic Force Microscope (MFM) (Nanomagnetics Instruments, Türkiye) in tapping mode with Si cantilevers. Multilayer films were deposited onto 1.0 cm x 1.0 cm glass slides. Images with 10 x 10 μ m and 2 x 2 μ m scan sizes were recorded. Gwyddion software (version 2.66) was used for analysis of AFM images.

2.3 PDATA- and PDA-Based Coatings

2.3.1 Preparation of Substrates

Silicon wafers were cut into 1 cm x 1 cm pieces. They were immersed into acetone for 10 minutes which was preheated to 52 °C. Then, they were dipped into methanol for 5 minutes. The wafers were rinsed with DI water and dried under nitrogen flow. Afterwards, they were immersed into concentrated sulfuric acid for 85 minutes and rinsed with DI water. The wafers were then immersed into 0.25 M NaOH solution for 10 minutes, followed by rinsing with DI water and drying under nitrogen flow.

Glass substrates were cut into 2.5 cm x 2.5 cm pieces for contact angle measurements and 1 cm x 1 cm for AFM measurements. They were treated with concentrated sulfuric acid for 85 minutes and rinsed with DI water. The glass substrates were immersed in 0.25 M NaOH solution for 10 minutes. After 10 minutes, all substrates are taken from the base and put into the DI water. The substrates were then rinsed with DI water and dried under nitrogen flow.

Quartz slides (2.5 cm x 2.5 cm) were initially treated with a 1% (v/v) Hellmanex III solution for 30 minutes. Later, the slides were rinsed with DI water and dried under nitrogen flow. The cleaned quartz substrates were subjected to ethanol for 10 minutes and subsequently immersed in concentrated sulfuric acid for 85 minutes. After acid treatment, the substrates were rinsed with DI water and dried under nitrogen flow. Finally, the quartz slides were immersed in a 0.25 M NaOH solution for 10 minutes, followed again by rinsing with DI water and drying under nitrogen flow.

2.3.2 Co-deposition of PDA and TA

2.5 mg of DOP and 2.5 mg of TA were weighed and dissolved in 5 mL of 0.05 M Tris-HCl buffer at pH 8.5 and 25 °C, under continuous stirring at 150 rpm. The initial concentrations were 0.5 mg/mL for both DOP and TA. A silicon wafer was dipped into this solution. The polymerization proceeded for either 4 hours or 16 hours. The film was rinsed in 5 mL of 0.05 M Tris HCl buffer for 5 minutes. For size and zeta potential measurements, 50 µL of samples were taken and diluted to 1 mL. To examine the effect of concentration on PDATA coatings, a similar experiment was performed at initial concentrations of 1.0 mg/mL for both DOP and TA. The film thickness was measured using ellipsometry technique. Control experiments were conducted with PDA in the absence of TA using the same procedures described above.

2.3.3 LbL Deposition of PDATA and PDA Films

4-layer PDATA films were prepared through the co-deposition of PDA and TA for 4 hours by refreshing the polymerization solutions (0.5 mg/mL initial concentration for both DOP and TA in 0.05 M Tris HCl buffer at pH 8.5 and 25 °C) after deposition of each layer. The films were rinsed for 5 minutes with 0.05 M Tris HCl buffer and film growth was followed by Ellipsometer. This way of film preparation was mentioned as “refreshed deposition”. If multilayer deposition was conducted by placing the substrate into the same polymerization solution, it was mentioned as “unrefreshed deposition”. Thickness measurements were performed using ellipsometry. As a control experiment, an additional PDATA film was prepared by continuous deposition of PDATA onto the wafer for 16 hours without external intervention. Such a film was mentioned as “one-time deposition”. All experiments were performed with DOP in the absence of TA to obtain PDA-based multilayers.

2.3.4 Stability of PDATA and PDA Films

PDATA and PDA multilayer films were deposited onto 2.5 x 2.5 cm quartz slides with previously described procedures in Section 2.3.3. Multilayer growth was followed using UV-Vis spectroscopy in the range of 200-800 nm. pH stability of multilayers was examined by exposing the films to phosphate buffer saline (PBS) at pH 7.4 and 37 °C and following the absorbance spectrum of the films as a function of time. Films were rinsed with 0.01 M phosphate buffer and dried under nitrogen flow prior to measurements. The absorbance spectra were recorded from three different regions on the substrate and presented with baseline correction.

2.3.5 LbL Deposition of PDATA and PDA with Cationic, Anionic, Neutral Counterparts

PDATA was self-assembled at the surface using either of the polymers as the counterpart: BPEI, TA and PVCL. 0.5 mg/mL of BPEI and 0.5 mg/mL of PVCL were dissolved overnight in 0.05 M Tris HCl buffer at 25 °C. 0.5 mg/mL of TA was freshly dissolved in 0.01 M Tris HCl buffer at 25 °C prior to use. PDATA layer was deposited through self-polymerization of DOP in the presence of TA at pH 8.5 and 25 °C for 4 hours, followed by rinsing using 0.05 M Tris HCl buffer at pH 8.5. BPEI, TA or PVCL was deposited at pH 5.5 for 15 minutes, followed by rinsing with either 0.05 M (for BPEI and PVCL) or 0.01 M (for TA) Tris HCl buffer. This cycle continued until the desired number of layers were deposited at the surface. Same experiments were conducted with PDA.

CHAPTER 3

RESULTS AND DISCUSSION

3.1 Co-deposition of PDA and TA

Polymerization of DOP starts with oxidation of DOP to DOP-quinone, followed by an “early” intercyclization reaction *via* 1,4 Michael-type addition forming leukodopaminechrome which can be reversibly oxidized to dopaminechrome. Dopaminechrome is intramolecularly rearranged to produce 5,6-dihydroxyindole (DHI). Further oxidation of DHI forms 5,6-indolequinone and branching reactions take place between these two products at different positions. The following steps concern diverse dimerization reactions with multiple products such as DHI-DHI dimer, DHI-DHI-DOP trimer, DHI-DOP dimer. The development of self-assembled larger oligomers occurs through reverse dismutation reaction between catechol and o-quinone [135]. Recent studies have shown that the degree of oligomerization was limited. Physical interactions between these low molecular weight oligomers through cation- π , hydrogen bonding, π - π stacking interactions were suggested to be responsible in the formation of a PDA layer. PDA also exists in the “spherical micro-/nanoparticle” form due to rapid aggregation of small oligomer chains which evolve into larger structures in a relatively homogeneous manner [44].

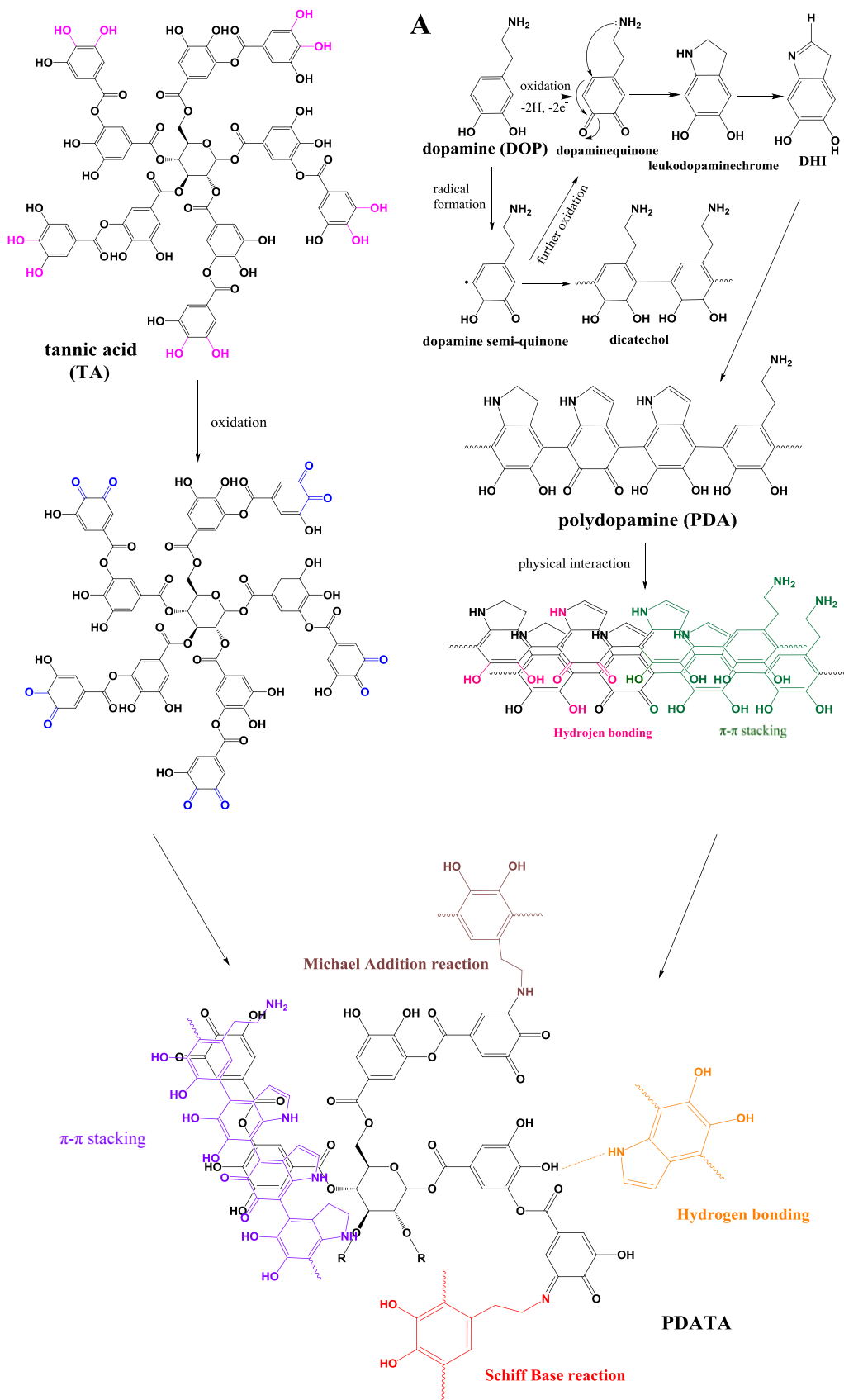
The co-deposition of PDA and TA has been discussed in a few studies. The phenolic hydroxyl moieties of TA can be partially oxidized into quinone moieties under alkaline conditions and interact with PDA chains through Michael addition and Schiff base reactions between amino groups of PDA and quinone groups of TA [104]. In addition, hydrogen bonding and π - π stacking interactions between PDA and TA have been also suggested as the driving forces for the formation of a PDATA layer [136]. The covalent and physical interactions between PDA and TA are illustrated in Fig. 11A.

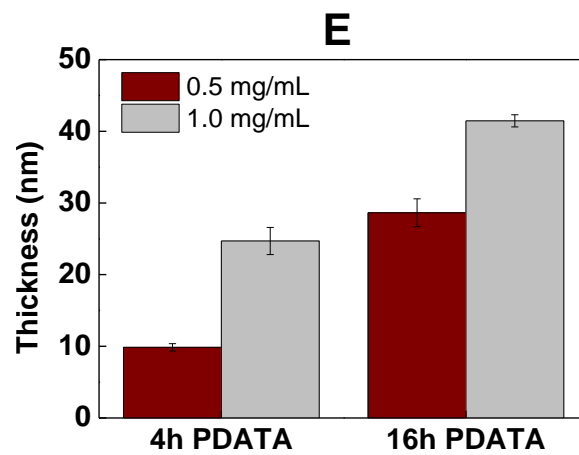
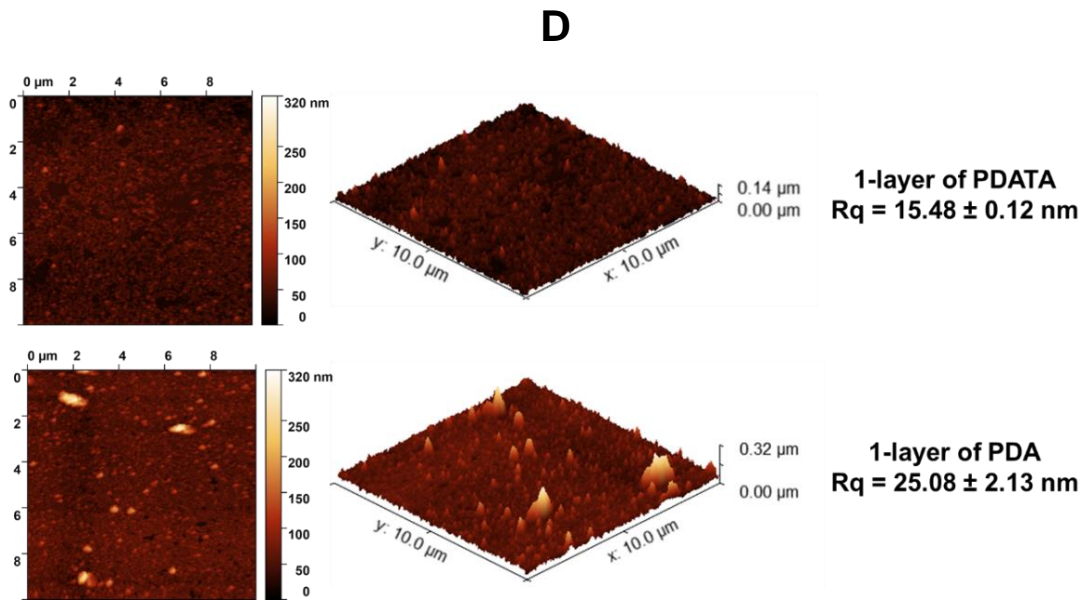
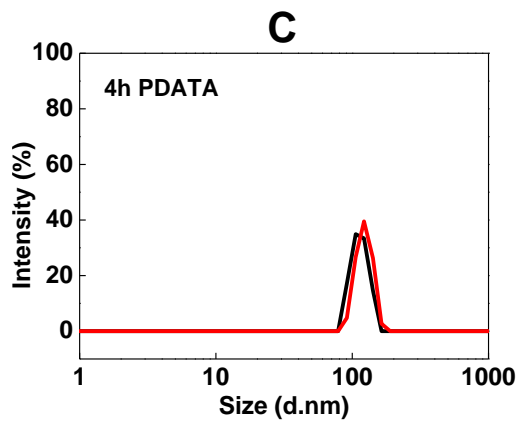
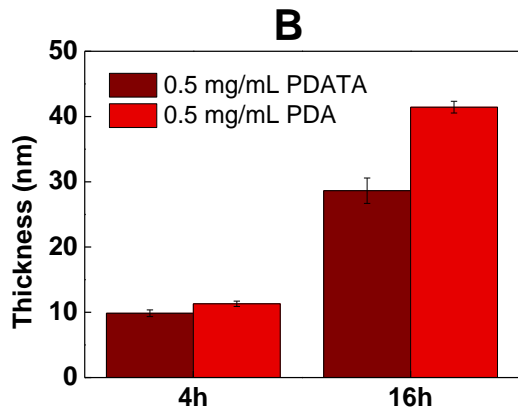
In this study, DOP and TA were dissolved together in a buffer solution at pH 8.5. Each had an initial concentration of 0.5 mg/mL. A silicon wafer was immersed into this polymerization solution and co-deposition of a layer composed of PDA and TA was followed through ellipsometric dry thickness measurements (Fig.11B, left). For comparison, PDA deposition (in the absence of TA) was performed under identical conditions (Fig.11B, right). Note that each deposition was performed in a different polymerization solution to provide precise time control and eliminate the effect of drying on film deposition and thickness. Deposition of PDATA and PDA onto silicon wafer was provided through hydrogen bonding between SiO₂ and phenolic hydroxyl groups of PDA and TA, and electrostatic interactions between ionized silanol groups (pK_a for surface SiOH groups: 6.8 [137]) and protonated amino groups of PDA. Of note, it has been reported that PDA exhibits characteristic feature of mussel adhesive proteins due to co-existence of catechol and amine functional groups and its adhesion did not depend on the type of substrate [45].

The thickness of a PDATA film was comparable to that of a PDA film after 4 hours of polymerization. The thickness increased with increasing deposition time for both PDATA and PDA films. Increasing thickness values with respect to deposition time has been reported for PDA films and correlated with chain-to-chain deposition of PDA through cation- π interactions between aromatic rings and protonated amino groups of PDA together with hydrogen bonding and π - π stacking interactions between PDA chains [21]. Similarly, aromatic rings and phenolic hydroxyl groups of TA could participate in the deposition of stacks composed of PDATA particles. The thickness difference between PDA and PDATA layers increased as the deposition time increased (16 hours). Considering increasing chain-to-chain deposition with time, the thickness difference became more remarkable as the number of PDATA and PDA layers increased in the stacks. The lower thickness of PDATA film was attributed to relatively low particle size of the aggregates when self-polymerization of DOP proceeded in the presence of TA. DLS analysis showed that polymerization of DOP in the presence of TA provided control in size of the particles. The size of PDATA particles was ~120 nm after 4 hours of polymerization,

while size measurements could not be performed for PDA due to precipitation of large particles and insufficient number of particles remained in the solution (Fig.11C). The decrease in the size of PDA particles in the presence of TA agrees well with the findings of Zhong and Jia in which size control was achieved through self-polymerization of dopamine in the presence of PEI. They demonstrated that hydrogen bonding between the amino groups of PEI and the amino/phenolic hydroxyl groups of PDA disrupted both intra- and intermolecular interactions, leading to a notable reduction in the size of PDA aggregates [138]. Apart from this, it has been suggested that PDATA exhibited more network-like structure due to its high molecular weight and more reactive nature of TA than DOP [104]. On the other hand, particle-bound feature was mentioned for the deposition of PDA [36]. In the light of these information, lower thickness of PDATA may also be correlated with more network-like structure of PDATA. In accordance with the difference in the film structures and thickness values, PDATA film had relatively smooth surface morphology with lower roughness values compared to PDA film (Fig.11D). The lower roughness possibly resulted from close packing of the smaller PDATA particles at the surface. Importantly, Xu and co-workers reported that relatively small PDA nanoparticles could deposit at the surface, while larger aggregates were prone to precipitate from the solution [36]. In summary, these results suggest that although PDA particles were larger and supposed to have lower tendency for deposition at the surface, the greater surface roughness of PDA film might have provided additional surface area and enhanced deposition of the subsequent PDA particles, marking for the greater thickness of PDA films [41]. Deposition of PDA in the form of nanoparticles and the resulting rough surfaces may limit the use of PDA coated surfaces for certain applications where smooth surfaces are required. Higher surface roughness of PDA coating poses challenges particularly in the functionalization of nanomaterial surfaces like particles, rods, and wires [139]. In this context, decreasing the roughness through co-deposition with TA while keeping the identity of PDA in the coating can be preferable for certain applications.

Lastly, the effect of concentration on the PDATA film thickness was examined. The thickness doubled for films with 4 hours of deposition when the concentration was increased by x2. On the other hand, the extent of increase was less for films with 16 hours of deposition at a similar concentration increase (Fig. 11E). DLS analysis of PDATA polymerization solution showed that particle size increased as the concentration of DOP and TA increased (Fig. 11F, right). This result agreed well with the literature reporting increased PDA particle size at increasing DOP concentrations [140]. Besides, particle size increased with increasing polymerization time (Fig. 11F, left) which is also consistent with the findings obtaining larger PDA particles with extended polymerization time [141]. The relatively low thickness increase over time in the concentrated solution was correlated with the formation of larger particles and their lower tendency for deposition at the surface [36]. In the rest of the experiments, co-deposition of PDA and TA was performed in a solution containing 0.5 mg/mL of DOP and TA to control the thickness and not to exceed the reliable range for ellipsometric measurements during LbL studies. Of note, it has been reported that initial DOP concentration also affected the relationship between the deposition and aggregation rate of PDA in the solution. 0.25 - 1.0 mg/mL initial concentration of DOP was reported to diminish the aggregation rate and enhanced deposition rate of PDA, whereas initial concentration between 1.0 - 4.0 mg/mL resulted in higher aggregation rate of PDA over deposition rate [30]. Our results are in good agreement with these findings where deposition, thus film thickness increased when the concentration increased from 0.5 mg/mL to 1.0 mg/mL.





F

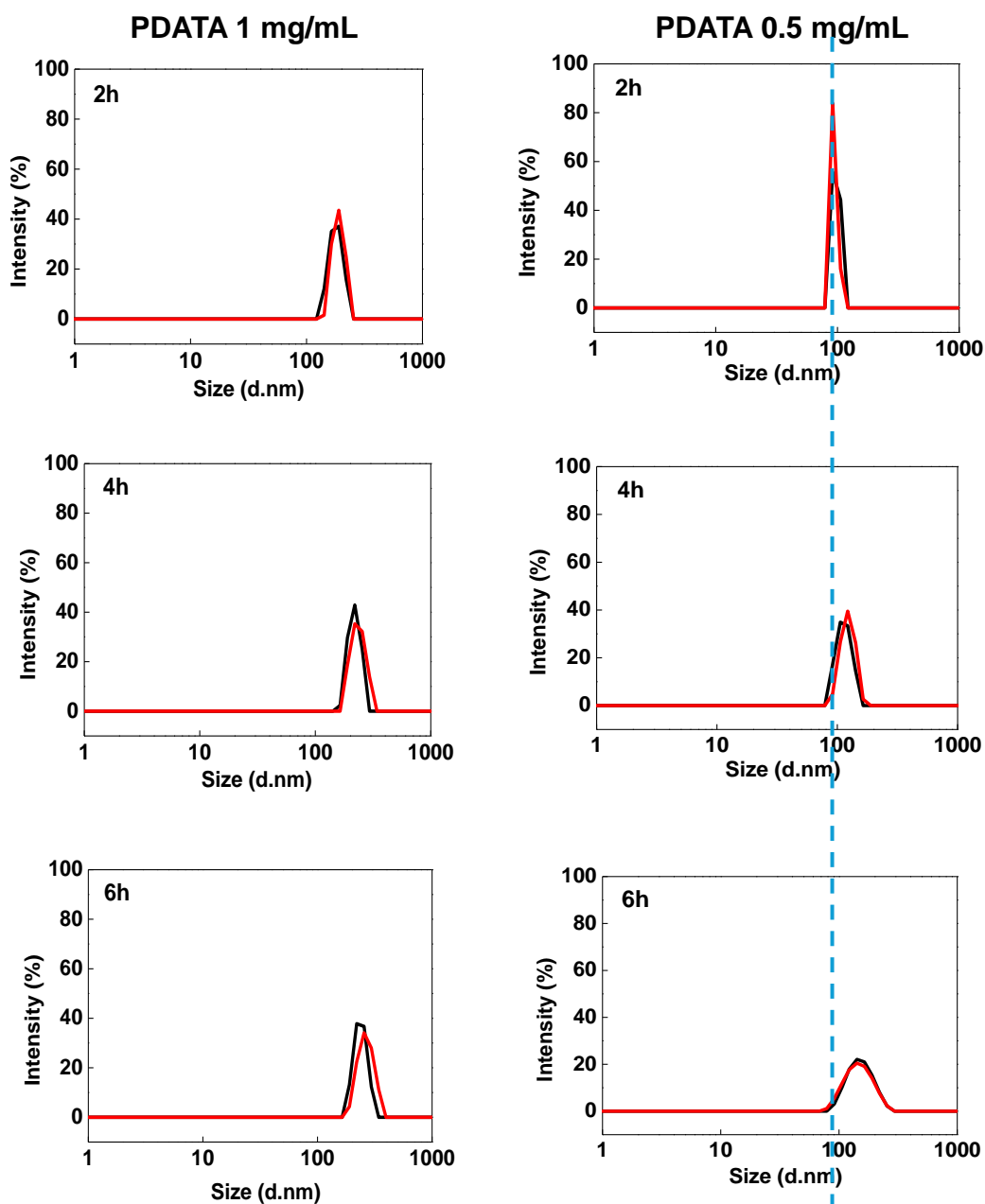


Figure 11. A) Oxidation of TA (left), polymerization of DOP (right) and the possible interactions (Micheal Addition and Schiff Base reactions, π - π stacking, hydrogen bonding) between oxidized TA and PDA (below). B) Thickness comparison of 0.5 mg/mL PDATA and PDA films after 4 and 16-hours deposition. C) Hydrodynamic

size of 0.5 mg/mL PDATA particles after 4 hours. D) AFM 2D (left) and 3D (right) height images ($10 \times 10 \mu\text{m}$ scan size) of 1-layer PDATA and PDA films. E) Thickness comparison of 0.5 mg/mL and 1 mg/mL PDATA deposition after 4 and 16 hours. F) Hydrodynamic size of 1 mg/mL PDATA particles (right) and hydrodynamic size of 0.5 mg/mL PDATA particles after 2, 4 and 6 hours (left).

3.2 One-time versus LbL Deposition of PDATA and PDA

Two different LbL assembly was performed. In the first one, each PDATA layer was deposited for 4 hours and DOP/TA containing polymerization solution (in 0.05 M Tris HCl buffer at pH 8.5 and 25 °C) was refreshed after deposition of each layer. The film is so called “4x4h PDATA” (refreshed). In the second one, polymerization solution was not refreshed, the substrate was removed from the polymerization solution every 4 hours, thickness measurement was performed, and the film was placed back in the same solution. The film is so called “4x4h PDATA (unrefreshed). For comparison, a PDATA film was prepared by continuous immersion of the substrate into DOP/TA polymerization solution. The film is so called “1x16h PDATA (one-time). The evolution of film thickness for LbL and one-time PDATA films are compared in Fig. 12A (left). 16 hours of continuous deposition and 4-layers of PDATA film with polymerization solution refreshed every layer provided similar film thickness. As mentioned in the previous section, particle size plays a critical role on the deposition of particles at the surface and smaller particles have greater tendency for deposition. Despite the increasing PDATA particle size with time (Fig. 12A, right) and an expectation for a lower film thickness with one-time deposition, the comparable thickness values can be explained by the effect of drying on LbL deposition and thickness of the films. The drying under nitrogen gas flow prior to ellipsometric thickness measurements after each layer deposition possibly induced a rearrangement of polymer chains at the surface, resulting in an ordering of polymer chains and flattening of the films. Such a smoothening possibly decreased the amount of deposition of the subsequent layer due to decrease in roughness and

surface area. The combinatorial effect of increasing particle size and drying is seen with 4-layers of PDATA film, prepared using unrefreshed polymerization solutions. The thickness obtained after each layer was lower than that with refreshed polymerization solutions, indicating the adverse effect of increasing particle size on deposition of PDATA at the surface.

Similar experiments were also performed with DOP in the absence of TA and the results showed a similar trend (Fig.12B). However, PDA films were always thicker than PDATA films regardless of the preparation method. As discussed above, the greater thickness values for PDA films were correlated with the larger particle size and nanoparticle-based deposition of PDA which provided greater surface roughness and additional surface area for enhanced deposition.

Although LbL and one-time films provided similar thickness values, the difference in surface roughness values was remarkable (Fig.12C). AFM imaging studies showed that LbL deposition (4-layer, each with 4 hours of deposition with refreshed solutions) resulted in greater surface roughness for both PDATA ($R_q = 30 \pm 2$ nm) and PDA ($R_q = 57 \pm 8$ nm) films compared to those obtained through one-time deposition (16 hours of continuous deposition, $R_q = 16 \pm 0.5$ nm and $R_q = 25 \pm 2$ for PDATA and PDA, respectively). The higher surface roughness with increasing layer number can be explained by the formation of an irregularly packed film composed of either PDA or PDATA and greater possibility for the deposition of subsequent PDA or PDATA layers on higher parts of the surface. This phenomenon was more remarkable for PDA films due to larger size and nanoparticle-bound deposition of PDA and relatively high surface roughness. Apart from this, free TA molecules, which did not participate in the formation of a PDATA layer, might have deposited onto the valleys, smoothing the film surface [142,143].

Wettability of PDATA and PDA surfaces was compared through contact angle measurements (Fig.12D). LbL (4-layer, each with 4 hours of deposition with refreshed solutions) and one-time (16 hours of continuous deposition) PDATA and PDA films had nearly zero apparent contact angle. The primary pre-requisite for a

surface to be called superhydrophilic (superwetting) is that water spreads on it completely (to a nearly zero apparent contact angle; $< 5-10^\circ$, not measurable accurately by optical systems) [144]. Water contact angle (WCA) values for 4-layers of PDATA and PDA, prepared using unrefreshed solutions, were $\sim 11^\circ$ and $\sim 9^\circ$, respectively. Considering the lower thickness values obtained with unrefreshed polymerization solutions and the contact angle of bare glass surface ($\sim 19^\circ$), this slight decrease in the wettability of surfaces might result from inefficient coating of the glass substrate. The wettability of surfaces is mainly determined by the surface functional groups, micro/nano topological structure and roughness of the surface [145]. The effects of micro/nano topological structure and surface roughness on wettability are associated with each other and are described using different models. Micro/nano-cavities are defined as possible penetration sides for water in Wenzel model, thus wettability was found to increase with increasing surface roughness for hydrophilic surfaces. On the other hand, the opposite is observed with hydrophobic surfaces: WCA increases with increasing surface roughness. Wenzel also explains large contact angle hysteresis, in other words, the difference between advancing and receding contact angles, due to the complete permeation of water into the cavities, resulting “sticky” behavior [146]. Cassie-Baxter wettability model suggests trapping of air within micro/nano-cavities, providing the droplets to sit on “air cushions” [147]. In this way, the contact area between the water and the surface decreases, leading to higher WCA in the presence of higher fractions of air. In summary, the Wenzel model describes surfaces exhibiting weak hydrophobicity, whereas the Cassie–Baxter model characterizes surfaces with strong hydrophobicity [148].

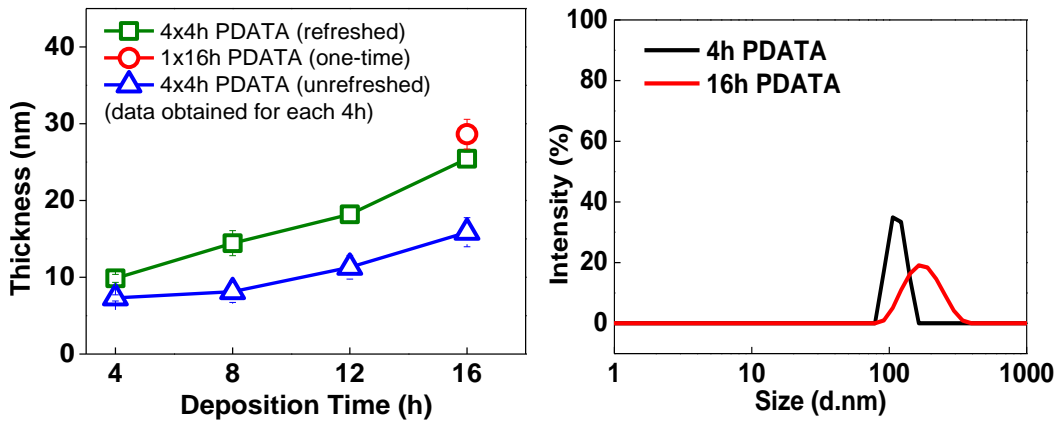
In general, PDA coating introduces hydrophilicity to hydrophobic surfaces [35]. In a study conducted by Li et. al, PDA and PDA-antibiotic complexes were prepared in the presence of NaIO_4 as the oxidant and LbL deposited (4-layers by refreshing each layer in every 20 minutes) onto hydrophilic Si substrates. The surfaces were found to be hydrophilic starting from the first layer. This was attributed to large numbers of hydrophilic groups such as amine groups and phenolic hydroxyl groups of PDA

and contribution of carboxyl groups which were formed as a result of oxidation of o-quinone to carboxyl by NaIO_4 under acidic conditions. Furthermore, they found that the surfaces turned into superhydrophilic with a growing number of layers. This increase in hydrophilicity was attributed to the increased density of the deposited nanoparticles with increasing layer number, and eventually forming a micro/nano topological structure to enhance penetration of water [145]. In the light of this study, the hydrophilic characteristic of PDA and PDATA multilayers can be ascribed to the functional groups on the surfaces such as hydroxyl, quinone carbonyl and amine moieties as well as increased deposition of particles with increasing deposition time and/or layer number, resulting in enhanced penetration of water [149].

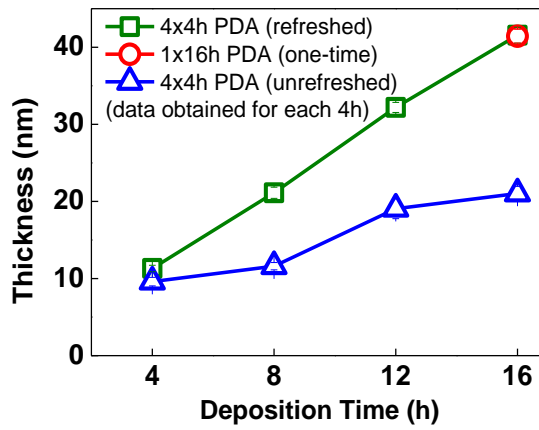
Stability of single- and multi- PDA and PDATA films was examined in PBS at pH 7.4 and 37 °C to simulate physiological conditions. For this purpose, multilayers were coated onto quartz surfaces and the evolutions of absorbance of multilayer films were followed as a function of time using UV-Visible Spectroscopy (Fig.12E). It was reported that dopamine displays a peak at 220 nm due to π - π^* interactions [150] and another peak at 280 nm which indicates L_a and L_b coincident transition of the catechol groups [151]. Unlike DOP, PDA coating has been reported to exhibit a weaker absorbance peak at 280 nm because of the oxidation of catechol moieties to quinone together with a broad absorption across 200-800 nm wavelength range [47,150]. The absorption spectrum of TA exhibits two peaks at 214 and 280 nm at acidic pH when TA exists in the neutral form [93]. When pH is increased, the intensities of the peaks at 214 and 280 nm decreases and two new additional peaks at 245 nm and 320 nm are observed due to ionization and/or oxidation of the phenolic hydroxyl groups of TA [152,153]. Although there were no distinct peaks in the spectra of the films, the stability of multilayers in PBS at pH 7.4 and 37 °C was examined by following the absorbance of the films at both 280 nm and 320. The decrease in the absorbance of the films was accepted as an indication of the loss of polymers from the surface.

In general, all types of PDATA films displayed low stability in PBS at pH 7.4 and 37 °C. Specifically, one-time coated PDATA film was found to be less stable (~86% loss) than 4x4h coated film prepared with refreshed polymerization solution (~61% loss) (Fig. 12E, left). Relatively low stability of one-time coated films compared to 4x4h coated PDATA film with refreshed polymerization solution may be attributed to increasing particle size with time which made it difficult to stack particles side-by-side and on top of each other at the surface, resulting in lower extent of association among the layers and decreased stability. The relatively low stability of 4x4h coated film prepared with unrefreshed polymerization solution (~73% loss) supported the speculation based on the adverse effect of increasing particle size on the stability of the films. On the other hand, PDA films prepared under similar conditions exhibited greater stability than PDATA films (Fig.12E, right). Notably, ~30% loss was recorded for PDA film prepared by 4x4h refreshed polymerization solution which was half of % loss recorded for PDATA film. pK_a values of PDA is correlated to its quinone-imine form ($pK_{a,1} = 6.3$) and dimerization of catechol groups ($pK_{a,2} = 9.4$, $pK_{a,3} = 10.6$, $pK_{a,4} = 11.7$ and $pK_{a,5} = 12.8$) [154]. pK_a values of TA are $pK_{a,1} = 6.5$ and $pK_{a,2} = 8.0$ [111,155]. pK_a of phenolic hydroxyl groups of TA is lower than catechol groups of PDA. Therefore, the amount of negative charge within the multilayers was expected to be greater for PDATA films at pH 7.4. The excess negative charge might have decreased the stability of the films due to electrostatic repulsion among the layers. In addition, considering greater number of phenolic hydroxyl groups in PDATA films, the extent of dynamic switching between quinone and phenolic hydroxyl groups might have been greater for PDATA than PDA and played a critical role on the disassembly of the films due to partial disruption of hydrogen bonds when the pH was decreased from 8.5 to 7.4. Of note, hydrogen accepting feature of quinones was reported to be greater than hydroxyl groups [156]. The pH-dependent change in absorption spectrum of TA is presented in Fig.12F.

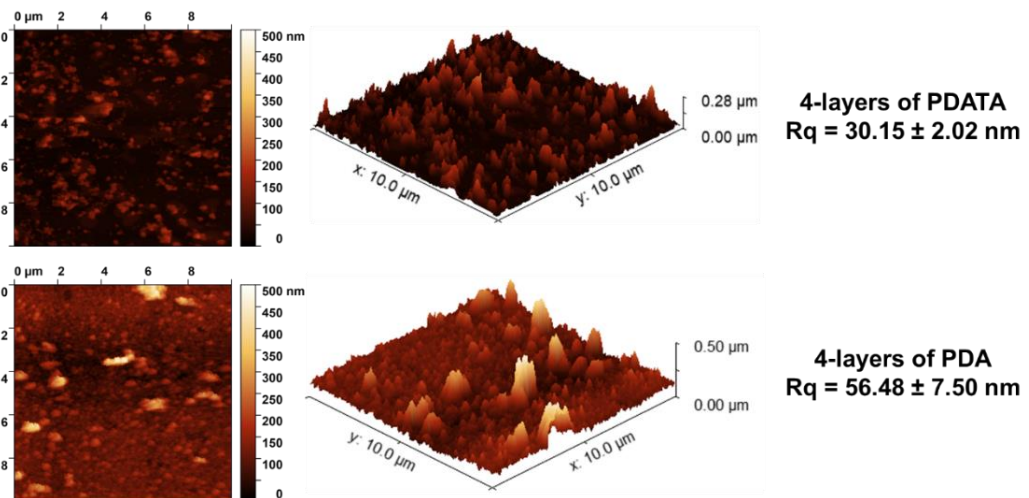
A



B



C



D

4x4h (refreshed) deposition

WCA < 5°



WCA < 5°



1x16h (one-time) deposition

WCA < 5°

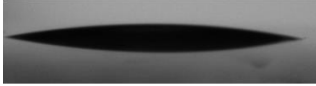


WCA < 5°



4x4h (unrefreshed) deposition

WCA ~ 9°



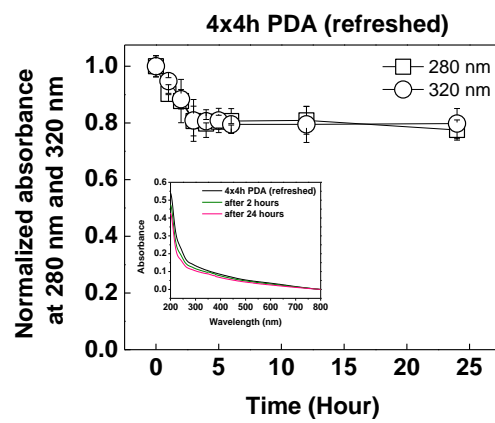
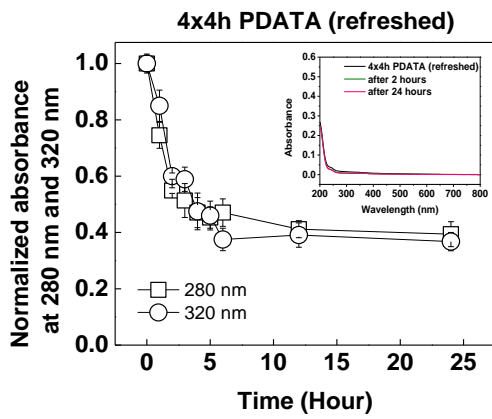
WCA ~ 11°

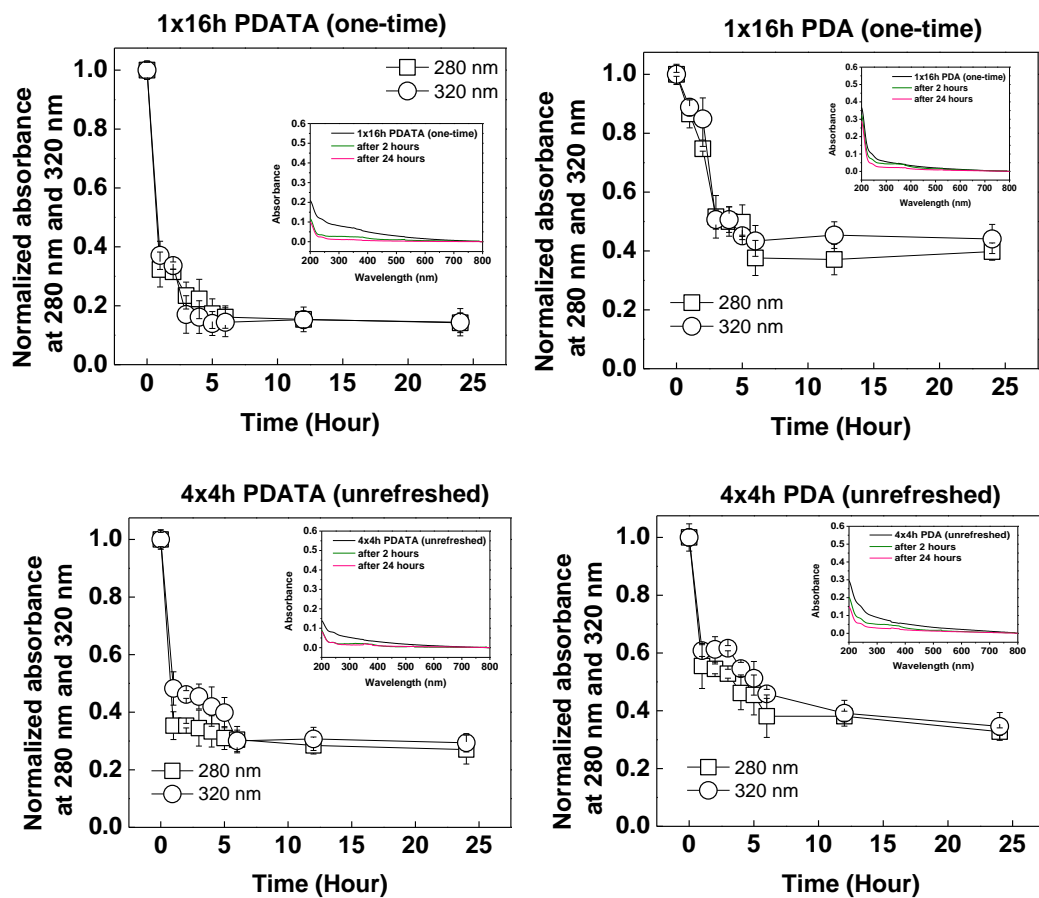


PDATA deposition

PDA deposition

E





F

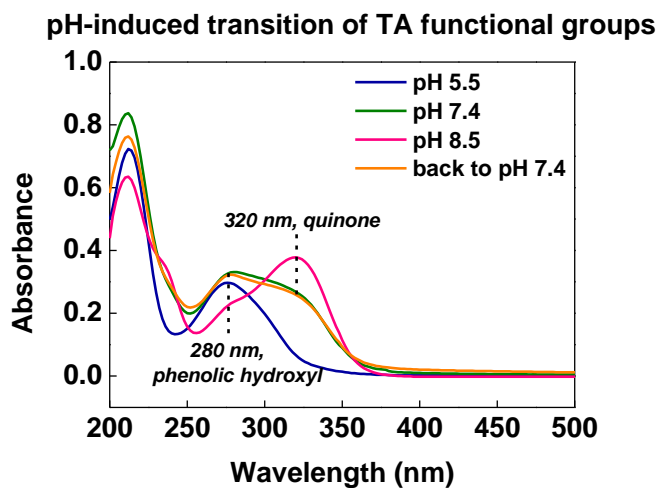
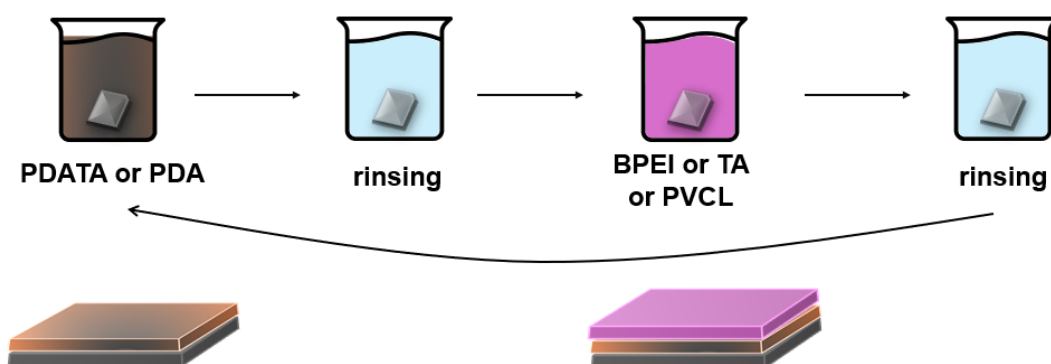


Figure 12. A) Thickness of 0.5 mg/mL PDATA/PDATA surfaces (□ refers 4x4h refreshed deposition, ○ refers 1x16h one-time deposition, and △ refers 4x4h

unrefreshed deposition (data obtained for each 4h)) (left) and the evolution of hydrodynamic size distribution of PDATA particles as a function of time at 4- and 16 hours (right). B) Thickness of 0.5 mg/mL PDA/PDA surfaces (□ refers 4x4h refreshed deposition, ○ refers 1x16h one-time deposition, and △ refers 4x4h unrefreshed deposition (data obtained for each 4h)). C) Evolution of normalized absorbance as a function of time for A) 4x4h (refreshed) PDATA (left) and PDA films (right); B) 1x16h (one-time) PDATA (left) and PDA films (right); C) 4x4h (unrefreshed) PDATA (left) and PDA (right) films. Insets show the absorbance spectra of the films before and after 2 hours and 24 hours exposure to PBS at pH 7.4 and 37 °C. Multilayers were constructed onto quartz slides. D) AFM 2D (left) and 3D height (right) images (10x10 μm scan size) of 4-layers of PDATA and PDA films. E) Comparison of PDATA and PDA wettability properties based on deposition conditions. F) Absorbance spectra of TA at pH 5.5, pH 7.4 and pH 8.5.

3.3 LbL Deposition of PDATA and PDA Using Cationic, Anionic and Neutral Polymers

The information generated with self-assembly of PDATA and PDA particles was taken as a basis to examine co-assembly of the particles with either amine-rich BPEI, hydroxyl-rich TA and amide-rich PVCL as the cationic, anionic and neutral counterparts, respectively (Scheme 2). Considering the relatively high thickness and stability of 4x4h (refreshed) films, PDATA and PDA layers were assembled by 4 hours of polymerization using fresh solutions. All multilayers had either PDATA or PDA as the topmost layer. The resulting films were compared with respect to thickness, wettability and surface morphology.



Scheme 2. Illustration of LbL assembly of PDATA and PDA using BPEI, TA and PVCL.

PDATA/BPEI and PDA/BPEI multilayers

PDATA and PDA layers were deposited at pH 8.5 through self-polymerization of DOP/TA and DOP, respectively. The pK_a values of dopamine were reported as $pK_{a,1} = 9.05$, $pK_{a,2} = 12.07$ for phenolic hydroxyl groups and $pK_{a,3} = 10.58$ for amine moieties [157]. It must be borne in mind that the assigned pK_a values of PDA is correlated to its quinone-imine form ($pK_{a,1} = 6.3$) and dimerization of catechol groups ($pK_{a,2} = 9.4$, $pK_{a,3} = 10.6$, $pK_{a,4} = 11.7$ and $pK_{a,5} = 12.8$) [154]. PDA demonstrates a "zwitterionic" nature, characterized by an isoelectric point within the pH range of 4–4.5 [158]. The pH-dependent behaviour arises from the change in the charge densities associated with the amine and phenolic hydroxyl groups. Specifically, at pH values above the isoelectric point ($pH > 4$), the PDA films and/or nanoparticles acquire a net negative charge, whereas at pH values below the isoelectric point, they are positively charged. In this study, the zeta potentials of PDATA and PDA were determined by DLS after 4 hours of polymerization at pH 8.5 in 0.05 M Tris buffer, yielding approximately -31 mV and -27 mV values, respectively. These results agree with previously reported zeta potential values for PDA in Tris buffer at pH 8.5 [159]. The pK_a values of BPEI have been reported as $pK_{a,1} = 9.4-9.64$, $pK_{a,2} = 6.8-8.6$ and $pK_{a,3} = 4.4-5$ for tertiary, secondary and primary amino groups, respectively [160,161]. BPEI was deposited at pH 5.5 for 15 minutes where amino groups were protonated. Ionization of phenolic hydroxyl groups of

PDATA and PDA were expected to enhance in the presence of BPEI within the multilayers [162]. Thus, the main driving force for LbL growth of PDATA/BPEI and PDA/BPEI was electrostatic interactions between protonated amino groups of BPEI and phenolate groups of PDATA and PDA. Hydrogen bonding interactions between amino groups of BPEI and phenolic hydroxyl groups of PDATA and PDA as well as amino groups of BPEI and quinone carbonyl of PDA or PDATA might have also contributed to the multilayer growth.

Both PDATA/BPEI and PDA/BPEI exhibited non-linear growth (Fig.13A). The increase in film thickness upon PDATA or PDA deposition was followed by a decrease or insignificant change in thickness upon deposition of BPEI layers for both films. Polyelectrolyte multilayers possess “stripping” behavior when one of the building blocks has a relatively low molecular weight [163]. Few studies reported on the molecular weight of PDA. Low-molecular-weight PDA ranging between 550 and 2450 g/mol was obtained at short polymerization times (5 min to 2 hours) [164–166], while relatively high-molecular-weight PDA with average molecular weight of 11,200 g/mol was obtained with 16 hours of polymerization [22]. In this study, polymerization of DOP/TA or DOP was maintained for 4 hours, thus they were expected to be low molecular weight. While BPEI with relatively high molecular weight (25,000 g/mol) deposited at the surface, PDATA or PDA might have partially desorbed from the surface, forming water-soluble complexes with BPEI. As a result, a decrease or insignificant change in thickness was observed upon deposition of each BPEI layer. Apart from these, PDA coatings were reported to dissolve at strongly acidic and alkaline conditions due to electrostatic repulsion between protonated amino groups of PDA at acidic pH and deprotonated catechol groups of PDA at basic pH [165]. Indeed, Yang et al. showed that peeling of PDA layer occurred not only in strongly acidic and alkaline conditions, but also within the pH range of 4-7, although at smaller amounts. The detachment was reported to be approximately 15% at ~ pH 5 and remained nearly constant from pH 5 to pH 7 [167]. In the light of these studies, the decrease or insignificant change in thickness upon deposition of BPEI at pH 5.5 may also be correlated with the slight detachment of PDATA or PDA layers.

Despite the higher thickness obtained with one-time or LbL type PDA films (Sections 3.2), the thickness of PDATA/BPEI multilayers (54 nm) was higher than PDA/BPEI film (45 nm) at similar layer numbers. The higher thickness for PDATA/BPEI may be attributed to the presence of TA in PDATA layers which provided more interaction sites (additional phenolic hydroxyl and quinone carbonyl moieties from TA) for association with BPEI. Of note, it is also possible that free TA might have remained at the surfaces and promoted deposition of BPEI at the surface.

PDATA/TA and PDA/TA multilayers

PDATA/TA and PDA/TA and films were assembled through LbL deposition of PDATA and PDA layers at pH 8.5 and TA layers at pH 5.5. Similar to LbL using BPEI, both PDA/TA and PDATA/TA exhibited zig-zag growth with a thickness decrease after every TA layer deposition and increase after PDATA and PDA layer deposition (Fig.13B). It must be borne in mind that pK_a values of TA are $pK_{a,1} = 6.5$ and $pK_{a,2} = 8.0$ [111,155]. As mentioned earlier, ionization of polyacids was found to enhance in the presence of polycations within the multilayers [162]. Therefore, phenolic hydroxyl groups of TA were expected to be partially deprotonated at the deposition pH of 5.5. The main driving force for LbL growth of PDATA/TA and PDA/TA was hydrogen bonding interactions between quinone carbonyl, hydroxyl and amino groups of PDATA or PDA and hydroxyl and quinone carbonyl groups of TA. Note that, although PDA carries net negative charge at $pH > 4$, the presence of protonated amino groups in PDA cannot be ignored [68]. Therefore, electrostatic interactions between amine groups of PDATA and PDA and phenolate groups of TA might have played a role in the multilayer growth. Besides, π - π stacking interactions between TA and PDA or PDATA might have also taken place within PDATA/TA and PDA/TA multilayers. Unlike multilayers with BPEI, PDA/TA films were thicker (55 nm) than PDATA/TA multilayers (45 nm). The higher amount of negative charge in PDATA layers might have decreased the amount of TA deposition due to electrostatic repulsion between the like charges. It is worth to mention that different from multilayers co-assembled with BPEI, LbL growth couldn't be achieved when

TA was dissolved in 0.05 M Tris HCl at pH 5.5. For this reason, TA was dissolved in 0.01 M Tris HCl buffer for LbL self-assembly (inset, Fig. 13B). It was reported that buffer concentrations participate in the optimization of LbL self-assembly where critical factors are controlled such as the degree of polyelectrolyte ionization, the length scale of electrostatic shielding, and the kinetics of self-assembly [168]. In this case, two possibilities might be relevant for the inhibition of LbL growth in 0.05 M Tris HCl: 1) higher concentration of salt ions might have significantly screened the electrostatic charges of TA [169] which reduced the electrostatic association between amino groups of PDATA and phenolate groups of TA [170,171]; 2) enhanced ionization of phenolic hydroxyl groups of TA as well as previously adsorbed PDA in the presence of salt cations might have prevented formation of hydrogen bonds between TA and PDATA [172]. In addition, this excess negative charge might have led to electrostatic repulsion between PDATA and TA and limited their association at the surface.

PDA/PVCL and PDATA/PVCL multilayers

Similar to self-assembly with BPEI and TA, PDATA and PDA layers were constructed at pH 8.5, while PVCL deposition was performed at pH 5.5. The driving force for multilayer preparation with neutral polymer PVCL was hydrogen bonding interactions among hydrogen accepting carbonyl groups of PVCL and phenolic hydroxyl and/or amine groups of PDATA or PDA. Similar to BPEI containing multilayers, PDATA/PVCL films were slightly thicker (58 nm) than PDA/PVCL (52 nm) films (Fig.13C). Based on these results, it is suggested that additional phenolic hydroxyl groups of TA in a PDATA layer promoted deposition of the PVCL layer. It is important to mention that different from self-assembly using BPEI or TA, PDATA/PVCL films grew linearly until 7th layer and then displayed a stair-like growth at increasing layer numbers. The lack of dissolution of PDATA layer by PVCL at low layer numbers can be explained by the relatively low molecular weight (1300 g/mol) and non-charged (neutral) nature of PVCL which made it less effective in solubilization of PDATA layers. However, as chain coiling increases and layers became more diffusive, the extent of association among the layers possibly

decreased, facilitating the chain solubilization by PVCL. The decrease in ordering and enhanced interpenetration among the layers with increasing layer number in hydrogen-bonded driven LbL films has been reported by Kharlampieva et. al. They claimed that loss of ordering was likely due to increased chain entropy causing greater chain coiling at larger distance from the substrate [173]. In contrast to PDATA/PVCL multilayers, linear growth wasn't observed for PDA/PVCL films. This may be attributed to the presence of TA in PDATA/PVCL films which might have provided stronger association with PVCL at the surface.

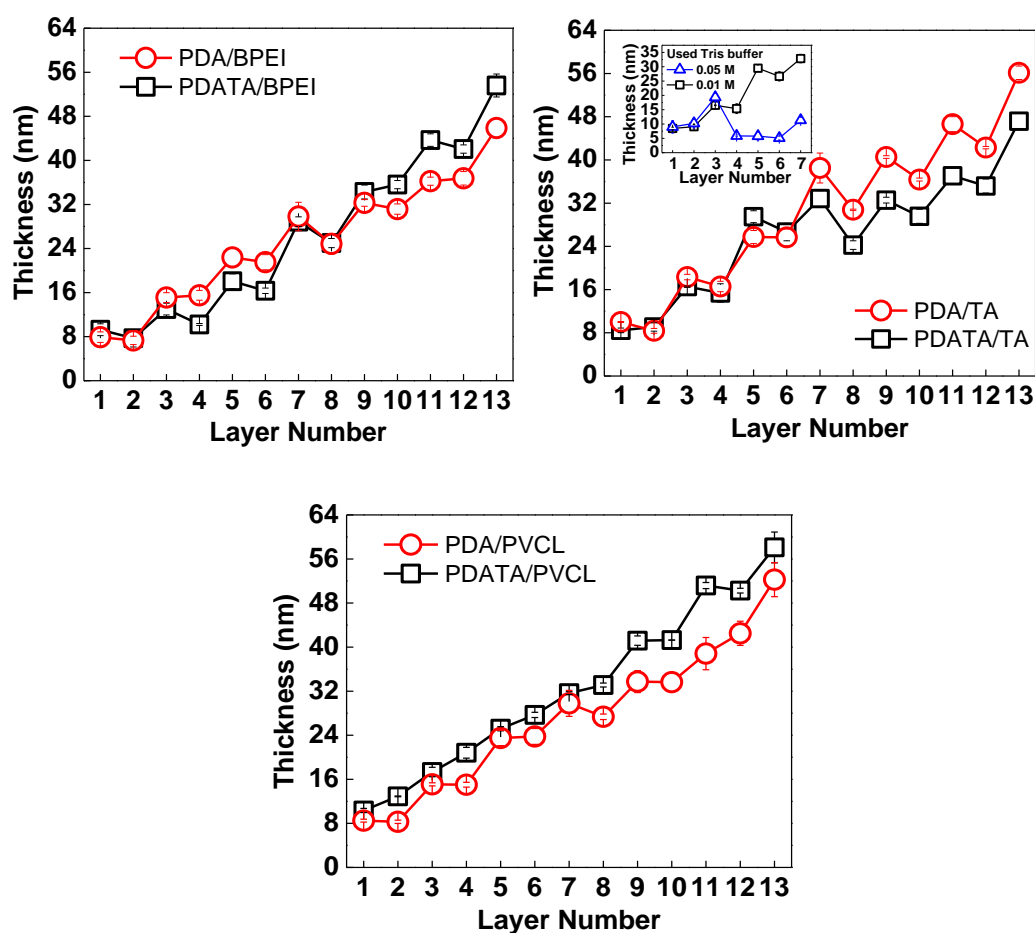


Figure 13. The LbL growth profile of A) PDATA/BPEI and PDA/BPEI surfaces, B) PDATA/TA and PDA/TA surfaces, inset: The effect of dissolution of TA in 0.05 M Tris Buffer and 0.01 M Tris Buffer on the growth of PDATA/TA films, C) PDATA/PVCL and PDA/PVCL surfaces.

3.3.1 Surface Morphology of Multilayers

As discussed earlier for 1-layer and LbL films consisted solely of PDATA and PDA, the surface roughness of PDA containing films was always higher than PDATA films due to larger size and nanoparticle-bound deposition of PDA compared to PDATA with lower particle size and more network-like structure. In accordance with these results, PDATA multilayer films exhibited relatively low surface roughness compared to PDA multilayers regardless of the counterpart, i.e. BPEI, TA and PVCL (Fig.14). Among PDATA films, the highest roughness was obtained with co-assembly using TA. The greater roughness of PDATA/TA films can be explained with the tendency of TA molecules towards self-association both in solution and at the surface, resulting in deposition in the form of aggregates. This anticipated effect of self-association of TA molecules on the roughness was not observed for PDA/TA films possibly due to lower amount of TA in PDA/TA films. Among PDA multilayers, co-assembly with PVCL displayed the highest surface roughness. The association among PVCL and PDA was based on solely hydrogen bonding interactions, while both electrostatic and hydrogen bonding interactions were present among the layers in PDA/BPEI and PDA/TA films. On the contrary, PDATA/PVCL displayed the lowest surface roughness compared to those co-assembled with BPEI and TA. The strong association between PVCL and TA [94] might have formed an intense film structure with relatively smooth surface morphology. Note that, the average Rq values were provided from three different images with 10 μm x 10 μm scan size.

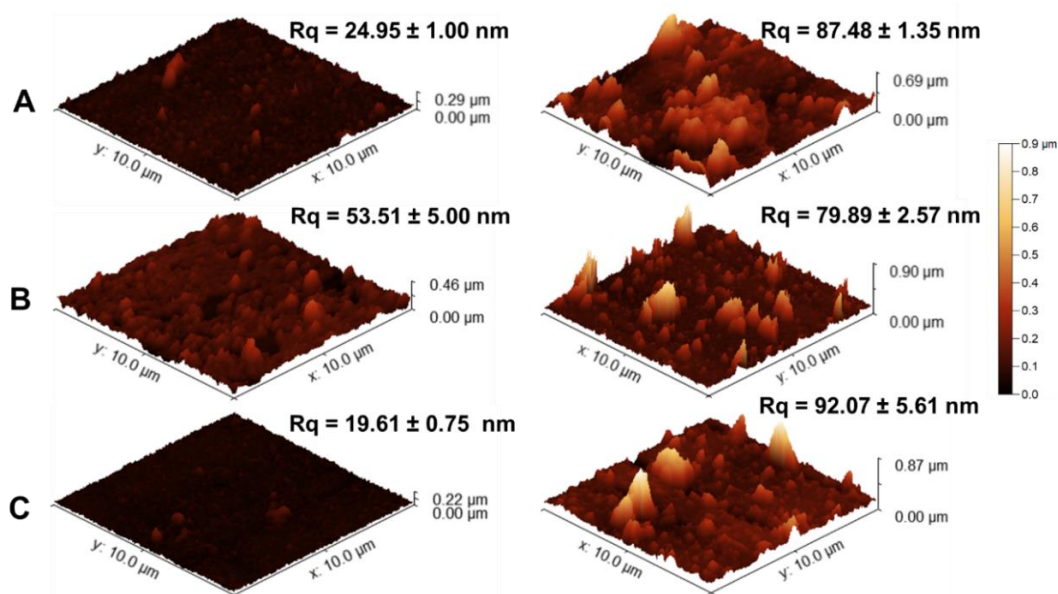


Figure 14. 3D AFM images of (10×10 μm scan size, Zmax = 900 nm) A) PDATA/BPEI (left) and PDA/BPEI (right), B) PDATA/TA (left) and PDA/TA (right), C) PDATA/PVCL (left) and PDA/PVCL (right)).

The maximum peak height (S_p) represents the maximum height of the peak within the measured area and maximum height (S_z) is defined as the summation of the maximum peak height and the maximum valley depth within the measured area. Figure 15 demonstrates S_z and S_p of PDATA and PDA films. PDA films revealed higher maximum peak height compared to PDATA films. This result agreed well with the larger PDA particles obtained in the absence of TA. Conversely, significantly lower maximum peak height observed in PDATA films was due to smaller particle size obtained in the presence of TA during polymerization. It is worth noting that, S_p and S_z were represented as average values obtained from three different images, each with 10 μm x 10 μm scan size.

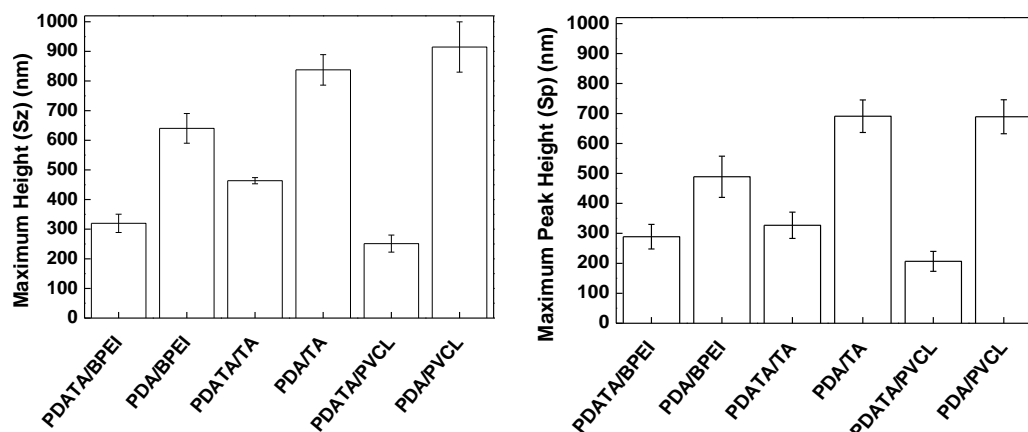


Figure 15. Maximum height (Sz) (right) and Maximum peak height (Sp) (left) of PDATA- and PDA- based multilayers ($10 \times 10 \mu\text{m}$ scan size).

Both PDATA and PDA films exhibited regions populated by large aggregates on their surfaces, which significantly affected their roughness values. However, it is important to mention that the roughness varied significantly from one region to another in the same film. In general, PDATA films contained aggregates with height, ranging between $\sim 100 - 180$ nm in the smoother regions, while aggregates as high as $\sim 270 - 400$ nm were detected in the rougher parts of the same films. The difference in the height of the aggregates was more remarkable for PDA films in which the height of the aggregates ranged between $\sim 170 - 210$ nm and $\sim 210 - 700$ nm in the rough and smooth regions, respectively. Accordingly, the roughness varied between $13-68$ nm and $25-140$ nm for PDATA and PDA multilayers, respectively. Fig. 16 and Fig. 17 present the zoomed-in regions ($2 \times 2 \mu\text{m}$) of $10 \times 10 \mu\text{m}$ images (already presented in Fig. 14) belonging to various PDATA- and PDA-based films, respectively, to reveal the significant variations in the roughness.

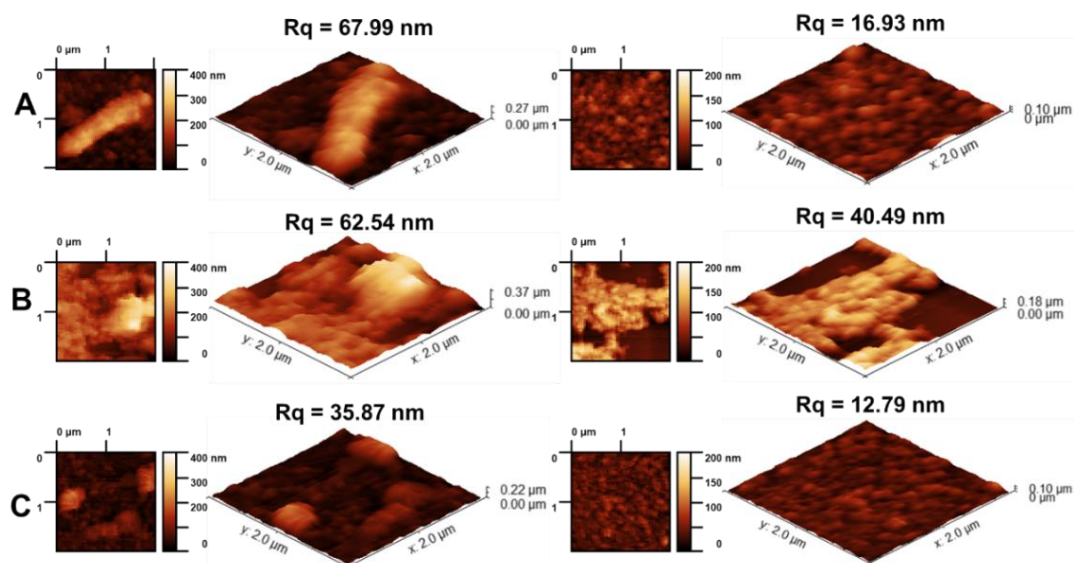


Figure 16. AFM 2D and 3D height images (extracted $2 \times 2 \mu\text{m}$ scan size from $10 \times 10 \mu\text{m}$, $Z_{\text{max}} = 900 \text{ nm}$) of A) relatively rough region of PDATA/BPEI (left) and relatively smooth region of PDATA/BPEI (right), B) relatively rough region of PDATA/TA (left) and relatively smooth region of PDATA/TA (right), C) relatively rough region of PDATA/PVCL (left) and relatively smooth region of PDATA/PVCL (right)

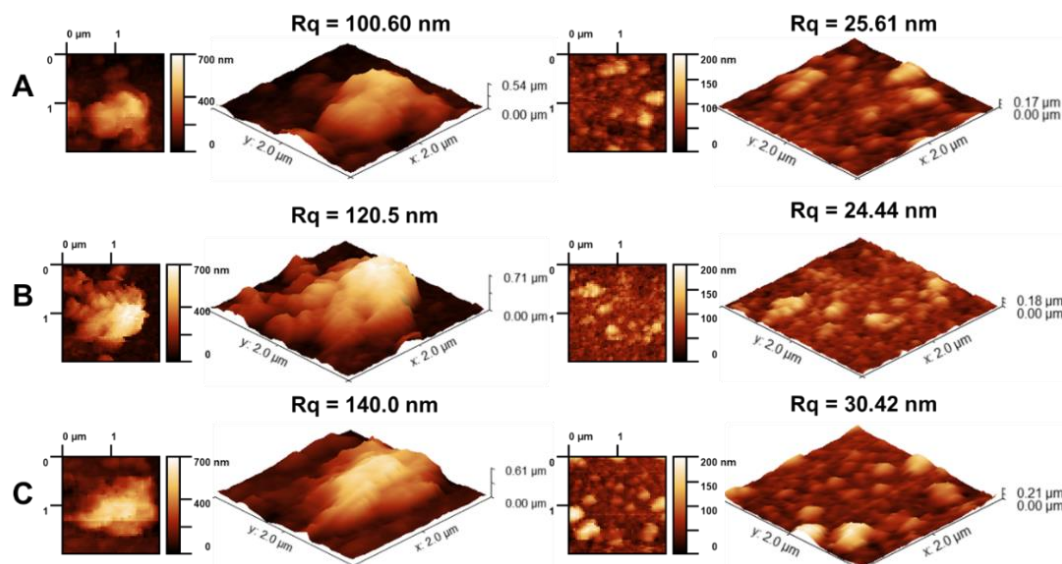


Figure 17. AFM 2D and 3D height images (extracted $2 \times 2 \mu\text{m}$ scan size from $10 \times 10 \mu\text{m}$, $Z_{\text{max}} = 900 \text{ nm}$ for PDATA and PDA films) of A) relatively rough region of

PDA/BPEI (left) and relatively smooth region of PDA/BPEI (right), B) relatively rough region of PDA/TA (left) and relatively smooth region of PDA/TA (right), C) relatively rough region of PDA/PVCL (left) and relatively smooth region of PDA/PVCL (right).

3.3.2 Wettability of PDATA and PDA based multilayers

The surface wettability is mainly determined by the chemical composition and morphology of the topmost layer [145]. The evolution of contact angle with respect to layer number is presented in Figure 18 for PDATA and PDA, self-assembled using either BPEI, TA or PVCL. All multilayers contained either PDATA or PDA as the topmost layer. The lowest wettability was obtained with PVCL containing multilayers which were constructed mainly through hydrogen bonding interactions as the primary driving force. In contrast to positively charged BPEI and partially negatively charged TA, PVCL existed in the neutral form at the self-assembly conditions and was expected to adopt coiled and loopy conformation due to lack of electrostatic repulsion between the repeating units and intramolecular interactions in the same chain. It has been reported that interdiffusion within the multilayers was higher for polymers with coiled and loopy conformation. For this reason, the contribution of previous PVCL layer to the surface and wettability should be greater compared to multilayers with BPEI and TA as the polymer counterpart.

Apart from these, the effect of surface functional groups on wettability might be discussed. While PVCL provided amide groups, BPEI and TA contributed with amino and hydroxyl groups to the multilayers, respectively. As mentioned above, PVCL existed in the neutral form at the self-assembly conditions. Wettability is affected by the ionization of functional groups which lead to the change in free-energy of solid-liquid interface [174]. The findings demonstrated a decrease in contact angle and the attainment of a more hydrophilic surface when the carboxylic acid groups deprotonate at high pH and amine groups protonate at low pH [175]. This increase in wettability was attributed to enhanced energy of adhesion between

the surface and water [176]. In the light of this information, the lower wettability of PVCL based multilayers could be attributed to their non-charged form. The increasing contact angle values with increasing layer number can be explained by the enhanced interpenetration between the layers as moved farther from the substrate and greater contribution of PVCL to the topmost layer. Although the wettability of PDATA/PVCL and PDA/PVCL was comparable for 7-layer films, the difference in contact angle values between PDATA/PVCL and PDA/PVCL increased for 13-layer films. This can be explained with the stronger association between PVCL and PDATA due to greater number of hydrogen donating hydroxyl groups, resulting in lower extent of interdiffusion between the layers. As mentioned earlier in Section 3.1, the stronger association among PDATA films might have resulted from smaller particle size and dense packing of the particles side-by-side and on top of each other within the film.

In the case of BPEI containing LbL films, the wettability of PDATA/BPEI films were not affected by the layer number in the films. On the other hand, similar to PVCL containing multilayers, wettability decreased with increasing layer number for PDA/BPEI films. This difference in the behavior of the films was attributed to greater electrostatic association between PDATA and BPEI and relatively low interdiffusion between the layers because of not only greater number of phenolic hydroxyl groups in PDATA but also enhanced ionization of phenolic hydroxyl groups of TA compared to that of PDA. It must be borne in mind that, as mentioned in Section 3.3, pK_a values of phenolic hydroxyl groups of TA are lower than those of PDA. Note that, when 7-layer PDATA/BPEI and PDA/BPEI films were compared, the wettability was found to be higher for PDA/BPEI films. The greater electrostatic association between BPEI and PDATA possibly left lower number of free phenolic hydroxyl groups at the topmost PDATA layer, leading to an increase in the contact angle value. On the other hand, greater interdiffusion between PDA and BPEI and greater contribution of BPEI chains to the topmost PDA layer resulted in a decrease in wettability due to the lower wettability characteristic of amino groups compared to hydroxyl groups [177].

Among all types of films, co-assembly with TA provided the highest wettability for both PDATA and PDA containing films due to hydroxyl rich TA. For PDATA/TA films, the contact angle values did not change as a function of layer number, indicating lower interdiffusion among the layers possibly due to highly rigid nature of TA. For example, WCA of a single-layer PDATA obtained after 4 hours of polymerization was recorded as 9° and WCAs of 7- and 13-layers of PDATA/TA films were 11.4° and 11.1°, respectively.

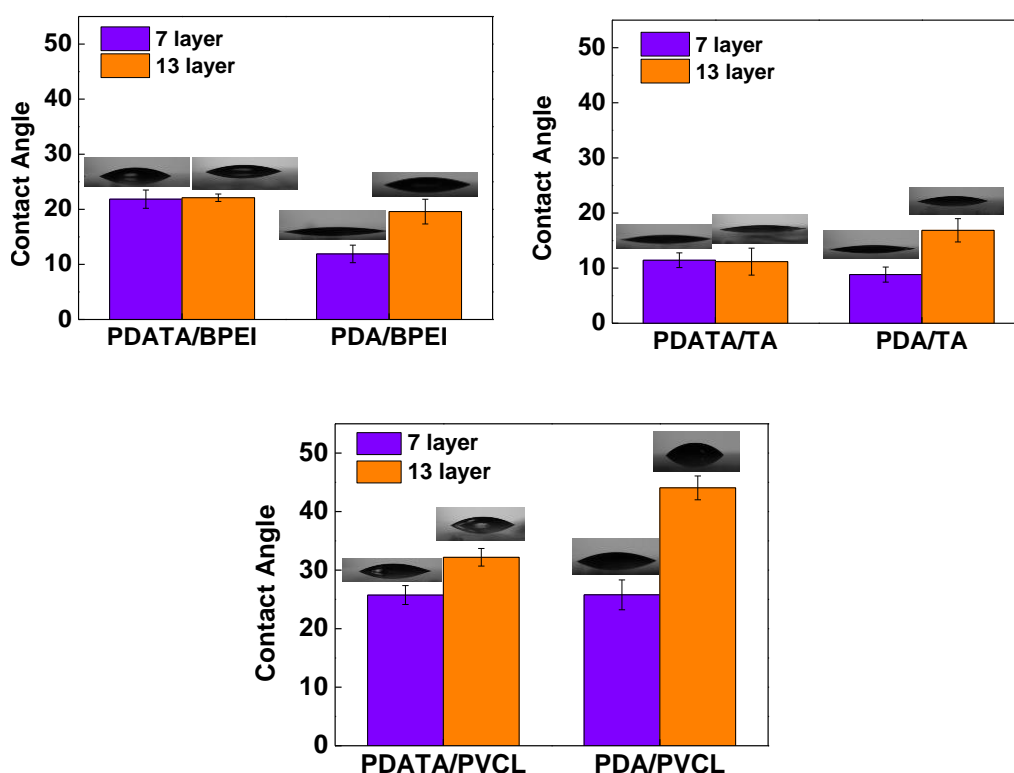


Figure 18. Evolution of contact angle for 7- and 13-layer A) PDATA/BPEI and PDA/BPEI, B) PDATA/TA and PDA/TA, C) PDATA/PVCL and PDA/PVCL films.

3.3.3 Stability of PDATA and PDA Containing Multilayers

In this section, the stability of 7-layer PDATA and PDA films which were co-assembled with either BPEI, TA or PVCL was examined in PBS at pH 7.4 and 37 °C to simulate physiological conditions. For this purpose, multilayers were

constructed onto quartz surfaces and the evolution of absorbance of multilayers films was followed as a function of time using UV-Visible Spectroscopy.

PDATA/BPEI and PDA/BPEI Films

The absorption peaks of DOP, PDA and TA were discussed in detail in Section 3.1. Briefly, dopamine reveals two peaks at 220 nm [150] and at 280 nm [151], whereas PDA coating displays a broad absorption across 200-800 nm wavelength range [47,150]. TA exhibits two peaks at 214 and 280 nm at acidic pH [93] and the intensities of the peaks at 214 and 280 nm decreases and two new additional peaks at 245 nm and 320 nm are observed when pH is increased [152,153]. Of note, BPEI does not have an absorption peak in the UV-Vis range. Different from PDA/BPEI films with a small peak at 280 nm and a broad absorption between 200-800 nm, PDATA/BPEI films made the peak at 320 nm more distinct due to greater number of ionized/oxidized phenolic hydroxyl groups in the film. The stability was examined by following the absorbance at both 280 nm and 320 nm for PDATA/BPEI (Fig. 19A, left) and PDA/BPEI (Fig. 19A, right) multilayers. The decrease in the absorbance of the films indicated loss of polymers from the surface. The evolution of the normalized absorbance of the peaks at 280 nm and 320 nm were very similar for PDA/BPEI films and indicated ~25% loss from the surface after 24 hours of immersion in PBS. For, PDATA/BPEI films, the peaks at 280 nm and 320 nm showed ~20% and ~30% decrease in absorbance after 24 hours. The loss from the multilayers was mainly attributed to salt-induced disruption of electrostatic association between BPEI and PDA or BPEI and PDATA layers upon exposure to PBS. Of note, the stability was examined in PBS (a mixture of 0.002 M NaH₂PO₄, 0.008 M Na₂HPO₄, 0.0027 M KCl and 0.137 M NaCl) which contained higher amount of salt ions than Tris buffer used in self-assembly. Salt-induced disintegration of multilayers has been reported before. The dissolution of electrostatically bound multilayers was explained through charge screening by the salt ions, resulting in disruption of electrostatic interactions between the polyelectrolytes [178]. Similarly, the critical pH at which multilayers disintegrate was found to decrease in the presence of salt ions for hydrogen-bonded multilayers

[179]. In addition, disruption of electrostatic association among the layers due to protonation of amino groups of BPEI and phenolate groups of PDA at pH 7.4 might have induced a charge imbalance within the film and contributed to the loss from the surface. It must be borne in mind that last layers of the films were either PDATA or PDA and their depositions were performed at pH 8.5. Exposing multilayers to pH 7.4 enhanced protonation of amino groups in PDATA, PDA and BPEI layers as well as phenolate groups of TA.

When a comparison was made between PDATA/BPEI and PDA/BPEI films by taking the peak at 280 nm as a basis, the slightly greater stability (by ~5%) of PDATA films was attributed to the presence of TA which provided additional interaction sites for association with BPEI at the surface. On the other hand, the greater decrease in the absorbance of the peak at 320 nm was correlated with the loss of TA from the surface which physically incorporated into PDATA aggregates or deposited at the surface in the free form. Apart from this, the decrease in the absorbance of the peak at 320 nm might have also resulted from pH-induced dynamic switching between quinone and phenolic hydroxyl groups of TA through pH [180]. It was reported that the pyrogallol groups and catechol moieties of TA tended to ionize at neutral pH conditions, leading to dissociation of hydrogen bonds between TA and the hydrogen-accepting building blocks [95]. Therefore, decreasing pH from pH 8.5 (deposition pH of last PDATA layer) to 7.4 might have resulted in an increase in the number of phenolic hydroxyl groups and a decrease in the amount of quinone moieties, thus a decrease in the absorbance of the peak at 320 nm. Of note, the absorbance at 280 nm might have increased due to protonation of phenolic hydroxyl groups of PDA and TA with decreasing pH. Such an increase in the absorbance of the peak at 280 nm was ignored when normalized absorbance values were calculated.

PDATA/TA and PDA/TA Films

The lowest stability was obtained with films in which PDATA and PDA were co-assembled with TA (Fig.19B). Owing to the increase in the amount of TA in the multilayers, these films showed also a peak at 245 nm, correlated with the ionized

form of TA. For comparison with BPEI containing films, the peak at 280 nm was taken as a basis. Although PDATA/TA and PDA/TA films had the contribution of electrostatics in addition to the hydrogen bonding interactions between the layers, both multilayers showed lower stability compared to BPEI containing films. The majority of the loss occurred in the first hour and attributed to pH and salt-induced ionization of TA which not only disrupted the hydrogen bonding interactions between the layers but also created excess negative charge and electrostatic repulsion within the film, followed by dissolution of the layers. It must be borne in mind that in case of BPEI containing films, the excess negative charge created within the multilayers due to ionization of hydroxyl groups of PDA and phenolic hydroxyl groups of PDATA was compensated by the protonated amino groups of BPEI, thus multilayers displayed greater stability under similar conditions. Differently, PDATA/TA and PDA/TA films contained greater amount of TA and the positive charge provided by the amino groups of PDA was probably not enough to compensate the negative charge created within the multilayers.

PDATA/PVCL and PDA/PVCL Films

Self-assembly of both PDATA and PDA using PVCL yielded multilayers with lower stability at pH 7.4/37 °C conditions compared to BPEI containing multilayers (Fig.19C). The difference was due to contribution of both electrostatic and hydrogen bonding interactions to the association between PDATA/BPEI and PDA/BPEI multilayers, while PVCL based films were constructed solely through hydrogen bonding interactions. The dissolution of PDATA/PVCL and PDA/PVCL can be explained by the ionization of phenolic hydroxyl groups of PDATA and PDA and disruption of hydrogen bonding interactions among the layers. Of note, LbL deposition of PVCL was carried out at pH 5.5. Phenolic hydroxyl groups of PDA were expected to protonate at pH 5.5 and form hydrogen bonds with PVCL. Ionization of the phenolic hydroxyl groups enhanced in PBS at pH 7.4 due to not only pH increase but also relatively high salt concentration. Enhanced ionization of polyacids in the presence of salt ions has been reported [172]. Moreover, in contrast to BPEI containing films but similar to multilayers co-assembled with TA,

PDATA/PVCL films (~ 70% loss) exhibited lower stability than PDA/PVCL (~ 40% loss) films. This was due to higher pK_a values of phenolic hydroxyl groups of PDA than that of TA, providing greater extent of hydrogen bonding driven association with PVCL. Besides, it was reported that the presence of salt ions resulted in the weakening of hydrogen-bonds and induced microphase separation between the multilayers due to the ability of salts to change polymer solubility and hydration [181,182]. The higher stability of PVCL containing films compared to those co-assembled with TA can be explained by the strength of hydrogen bonds and relatively more hydrophobic nature of PVCL. Hydrogen bonding acceptor strengths of functional groups are evaluated through their hydrogen bond basicity (pK_{HB}). Groups with higher basicity generally exhibit stronger hydrogen bond acceptor characteristics and pK_{HB} increases in the following order: phenols < amine < amide < cyclic amide (lactam), indicating stronger hydrogen accepting capability for lactams [183,184]. The effect of strength of hydrogen bonding driven association to the film stability has been demonstrated [179]. Contribution of hydrophobicity to the stability of LbL films has also been reported. For example, Kharlampieva and Sukhishvili compared the stability of PMAA-based hydrogen bonded-multilayers prepared using PVCL and PVPON as the counterparts. PMAA/PVCL multilayers exhibited higher stability than PMAA/PVPON films due to enhanced hydrophobic interactions between PMAA and PVCL layers, arising from two additional methyl groups in the caprolactam ring of PVCL [179]. Lastly, as mentioned earlier, the greater decrease in the normalized absorbance at 320 nm can be attributed to either release of free TA molecules or switching from quinone to hydroxyl groups with decreasing pH.

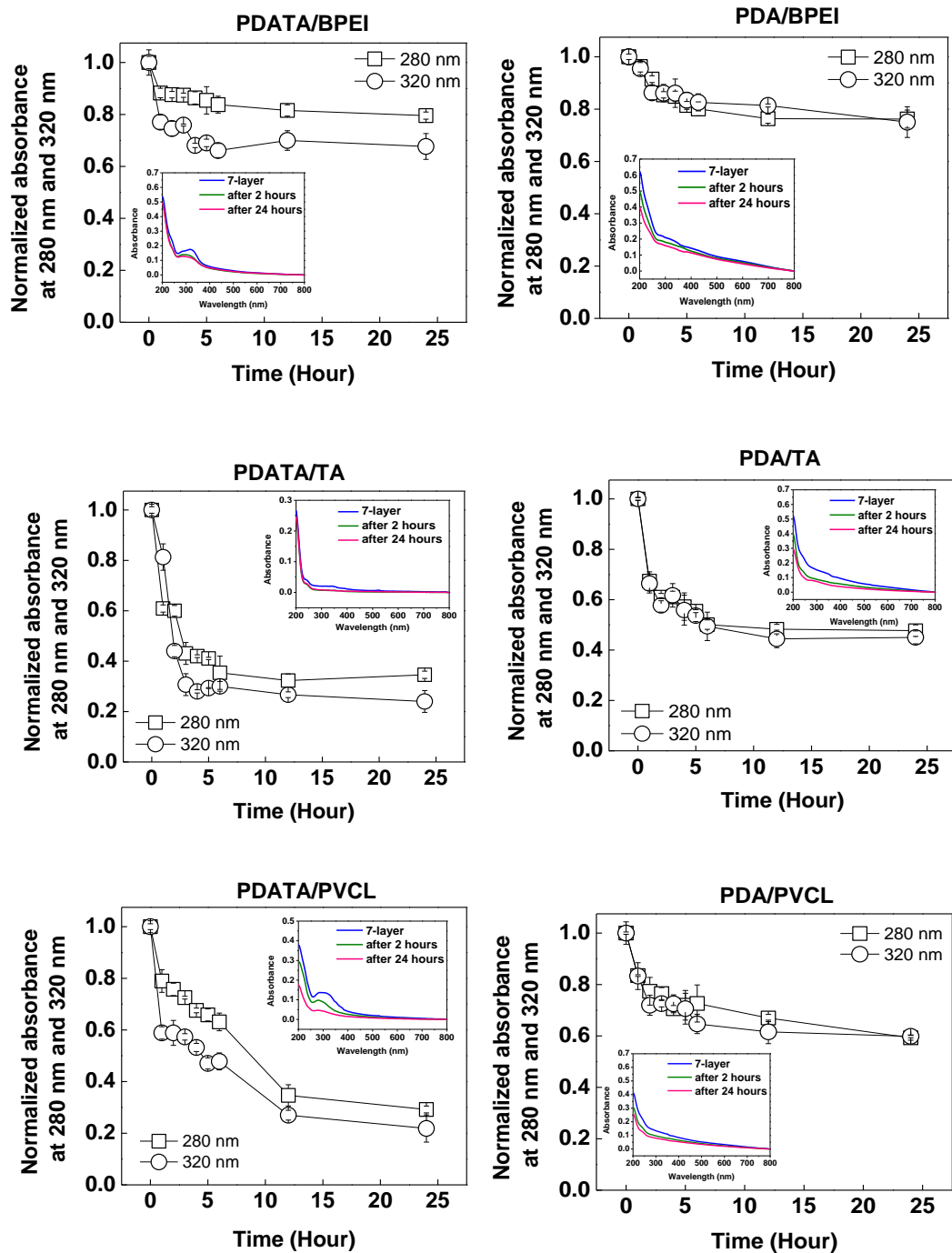


Figure 19. Evolution of normalized absorbance as a function of time for 7-layer A) PDATA/BPEI (left) and PDA/BPEI films (right); B) PDATA/TA (left) and PDA/TA films (right); C) PDATA/PVCL (left) and PDA/PVCL films (right). Insets show the

absorbance spectra of the films before and after 2 hours and 24 hours exposure to PBS at pH 7.4 and 37 °C. Multilayers were constructed onto quartz slides.

CHAPTER 4

CONCLUSION

This study aimed preparation of single-layer and multi-layer PDATA films and assessing their surface properties in comparison with PDA films. First, co-deposition PDA and TA (PDATA) was examined at pH 8.5 in 0.05 M Tris HCl at 25 °C through self-polymerization of DOP in the presence of TA. Increasing the concentration of DOP and TA as well as polymerization time led to formation of thicker films. The thickness of a single layer of PDATA was thinner than that of a PDA layer. However, this difference increased with increasing deposition time. The lower thickness of PDATA film was attributed to the formation of smaller particles and more network-like structure when self-polymerization of DOP proceeded in the presence of TA. In addition, PDA deposition occurs in the form of nanoparticles which imparts greater roughness to the films. The enhanced roughness might have provided additional site for chain-to-chain deposition of PDA, resulting in thicker films. Each PDATA or PDA layer was deposited for 4 hours in the preparation of multilayers composed solely of PDATA or PDA. Drying after each layer decreased the thickness due to ordering and rearrangement of the chains at the surface. Using the same polymerization solution also led to a decrease in film thickness due to increasing particle size with time and lower tendency of the larger particles towards deposition at the surface. Both single and multilayer films were found to be superhydrophilic except multilayers prepared using unrefreshed solutions. Surface roughness increased with increasing layer number due to irregular packing and deposition at the higher parts of the film. It was higher for PDA films because PDATA exhibits smaller nanoparticles, while PDA has larger nanoparticles which contributed to roughness with increasing layer number. The presence of TA was found to decrease the hydrodynamic size of PDATA particles due to a decrease in the extent of

intermolecular interactions among PDA oligomers. The greater hydrodynamic size of PDA particles was in good agreement with the higher roughness of PDA films.

The varying functional groups of PDATA and PDA provided LbL assembly through both electrostatic and hydrogen-bonding interactions. Self-assembly of PDATA or PDA with positively charged BPEI through electrostatic interactions provided the most stable films in PBS at pH 7.4 and 37 °C. On the other hand, PDATA and PDA co-assembled with TA through hydrogen bonding interactions exhibited the highest wettability due to higher amount of TA, rich with phenolic hydroxyl groups. Relatively smooth surfaces were obtained through co-assembly with PVCL and was attributed to the stronger association between the layers, provided by PVCL. The stability of hydrogen bonding driven films (TA and PVCL based) was lower than electrostatically driven films (BPEI based). Among hydrogen bonding driven films, PVCL-based films exhibited higher stability than TA-based films due to the stronger hydrogen accepting and hydrophobic character of PVCL. Overall, PDATA-based films were more prone to disintegration, attributed to the loss of TA from the surface. The presence of TA in PDATA layer contributed to the film thickness when co-assembly with BPEI and PVCL were in question. This can be explained by the additional interaction sites provided by TA molecules. In contrast, self-assembly of PDATA and TA displayed lower thickness probably due to higher hydrophilicity of TA and enhanced electrostatic repulsion between the layers.

In conclusion, this study demonstrates the versatility and tunable nature of PDATA- and PDA-based multilayers, offering valuable insights into their structural and functional properties. These findings highlight their potential for diverse applications in surface engineering.

OUTLOOK

The co-deposition of PDA and TA has been highlighted in several studies, as discussed in Section 1.7. These studies investigated surface properties of PDATA such as thickness and wettability; however, prepared surfaces were used in different applications areas. For example, PDATA has been used to provide the hydrophilicity to hydrophobic membranes, improve oil-repellent and dye rejection capabilities of membranes, create antifouling membranes, coat electrodes to increase capacitance, and functionalize silica nanoparticles for the removal of Cu^{+2} from aqueous solutions. However, the antibacterial properties of PDATA surfaces have not been thoroughly investigated.

The antibacterial properties of both PDA and TA were discussed in Section 1.4 and 1.6, respectively. This study aims to explore the antibacterial potentials of PDA/TA containing multilayer films as a future work. The results will be assessed in comparison with PDA based multilayers. Specifically, the effects of layer number, surface roughness and wettability on the antibacterial properties will be investigated.

In this regard, contact-killing experiments will be conducted to all multilayers presented in this thesis study.

REFERENCES

- [1] C.A. Marsden, Dopamine: the rewarding years, *Br J Pharmacol* 147 (2006). <https://doi.org/10.1038/sj.bjp.0706473>.
- [2] H. Lee, S.M. Dellatore, W.M. Miller, P.B. Messersmith, Mussel-Inspired Surface Chemistry for Multifunctional Coatings, *Science* (1979) 318 (2007) 426–430. <https://doi.org/10.1126/science.1147241>.
- [3] Y. Fu, L. Yang, J. Zhang, J. Hu, G. Duan, X. Liu, Y. Li, Z. Gu, Polydopamine antibacterial materials, *Mater Horiz* 8 (2021) 1618–1633. <https://doi.org/10.1039/D0MH01985B>.
- [4] B. Li, T. Gong, N. Xu, F. Cui, B. Yuan, Q. Yuan, H. Sun, L. Wang, J. Liu, Improved Stability and Photothermal Performance of Polydopamine-Modified Fe₃O₄ Nanocomposites for Highly Efficient Magnetic Resonance Imaging-Guided Photothermal Therapy, *Small* 16 (2020). <https://doi.org/10.1002/sml.202003969>.
- [5] Y. Liu, C. Su, Y. Zu, X. Chen, J. Sha, J. Dai, Ultrafast deposition of polydopamine for high-performance fiber-reinforced high-temperature ceramic composites, *Sci Rep* 12 (2022) 20489. <https://doi.org/10.1038/s41598-022-24971-3>.
- [6] Q. Lyu, N. Hsueh, C.L.L. Chai, The Chemistry of Bioinspired Catechol(amine)-Based Coatings, *ACS Biomater Sci Eng* 5 (2019) 2708–2724. <https://doi.org/10.1021/acsbiomaterials.9b00281>.
- [7] F. Wu, J. Li, K. Zhang, Z. He, P. Yang, D. Zou, N. Huang, Multifunctional Coating Based on Hyaluronic Acid and Dopamine Conjugate for Potential Application on Surface Modification of Cardiovascular Implanted Devices, *ACS Appl Mater Interfaces* 8 (2016) 109–121. <https://doi.org/10.1021/acsami.5b07427>.

- [8] Y. Wang, Q. Huang, X. He, H. Chen, Y. Zou, Y. Li, K. Lin, X. Cai, J. Xiao, Q. Zhang, Y. Cheng, Multifunctional melanin-like nanoparticles for bone-targeted chemo-photothermal therapy of malignant bone tumors and osteolysis, *Biomaterials* 183 (2018) 10–19. <https://doi.org/10.1016/j.biomaterials.2018.08.033>.
- [9] Z. Wang, Y. Zou, Y. Li, Y. Cheng, Metal-Containing Polydopamine Nanomaterials: Catalysis, Energy, and Theranostics, *Small* 16 (2020). <https://doi.org/10.1002/sml.201907042>.
- [10] L.C. Almeida, R.D. Correia, G. Squillaci, A. Morana, F. La Cara, J.P. Correia, A.S. Viana, Electrochemical deposition of bio-inspired laccase-polydopamine films for phenolic sensors, *Electrochim Acta* 319 (2019) 462–471. <https://doi.org/10.1016/j.electacta.2019.06.180>.
- [11] A. Prabhu, R.D. Crapnell, K. Eersels, B. van Grinsven, A.K. Kunhiraman, P. Singla, J. McClements, C.E. Banks, K. Novakovic, M. Peeters, Reviewing the use of chitosan and polydopamine for electrochemical sensing, *Curr Opin Electrochem* 32 (2022) 100885. <https://doi.org/10.1016/j.coelec.2021.100885>.
- [12] P. Yang, Z. Gu, F. Zhu, Y. Li, Structural and Functional Tailoring of Melanin-Like Polydopamine Radical Scavengers, *CCS Chemistry* 2 (2020) 128–138. <https://doi.org/10.31635/ccschem.020.201900077>.
- [13] Y. Liu, K. Ai, L. Lu, Polydopamine and Its Derivative Materials: Synthesis and Promising Applications in Energy, Environmental, and Biomedical Fields, *Chem Rev* 114 (2014) 5057–5115. <https://doi.org/10.1021/cr400407a>.
- [14] H. Li, J. Xi, A.G. Donaghue, J. Keum, Y. Zhao, K. An, E.R. McKenzie, F. Ren, Synthesis and catalytic performance of polydopamine supported metal nanoparticles, *Sci Rep* 10 (2020) 10416. <https://doi.org/10.1038/s41598-020-67458-9>.

- [15] N. Huang, S. Zhang, L. Yang, M. Liu, H. Li, Y. Zhang, S. Yao, Multifunctional Electrochemical Platforms Based on the Michael Addition/Schiff Base Reaction of Polydopamine Modified Reduced Graphene Oxide: Construction and Application, *ACS Appl Mater Interfaces* 7 (2015) 17935–17946. <https://doi.org/10.1021/acsami.5b04597>.
- [16] H.-W. Chien, T.-H. Chiu, Stable N-halamine on polydopamine coating for high antimicrobial efficiency, *Eur Polym J* 130 (2020) 109654. <https://doi.org/10.1016/j.eurpolymj.2020.109654>.
- [17] Z. Iqbal, E.P.C. Lai, T.J. Avis, Antimicrobial effect of polydopamine coating on *Escherichia coli*, *J Mater Chem* 22 (2012) 21608. <https://doi.org/10.1039/c2jm34825j>.
- [18] A. Cui, Y. Bao, H. Xu, X. Mu, X. Zhong, W. Wee, F. Wu, G. Shan, A dual-modal ROS generator based on multifunctional PDA–MnO₂@Ce6 nanozymes for synergistic chemo-photodynamic antibacterial therapy, *Biomater Sci* 11 (2023) 2243–2252. <https://doi.org/10.1039/D2BM01939F>.
- [19] L. Yang, X. Guo, Z. Jin, W. Guo, G. Duan, X. Liu, Y. Li, Emergence of melanin-inspired supercapacitors, *Nano Today* 37 (2021) 101075. <https://doi.org/10.1016/j.nantod.2020.101075>.
- [20] P. Yang, S. Zhang, X. Chen, X. Liu, Z. Wang, Y. Li, Recent developments in polydopamine fluorescent nanomaterials, *Mater Horiz* 7 (2020) 746–761. <https://doi.org/10.1039/C9MH01197H>.
- [21] S. Hong, Y. Wang, S.Y. Park, H. Lee, Progressive fuzzy cation- π assembly of biological catecholamines, *Sci Adv* 4 (2018). <https://doi.org/10.1126/sciadv.aat7457>.

- [22] P. Delparastan, K.G. Malollari, H. Lee, P.B. Messersmith, Direct Evidence for the Polymeric Nature of Polydopamine, *Angewandte Chemie International Edition* 58 (2019) 1077–1082. <https://doi.org/10.1002/anie.201811763>.
- [23] S. Hong, Y.S. Na, S. Choi, I.T. Song, W.Y. Kim, H. Lee, Non-Covalent Self-Assembly and Covalent Polymerization Co-Contribute to Polydopamine Formation, *Adv Funct Mater* 22 (2012) 4711–4717. <https://doi.org/10.1002/adfm.201201156>.
- [24] H. Hemmatpour, O. De Luca, D. Crestani, M.C.A. Stuart, A. Lasorsa, P.C.A. van der Wel, K. Loos, T. Giouisis, V. Haddadi-Asl, P. Rudolf, New insights in polydopamine formation via surface adsorption, *Nat Commun* 14 (2023) 664. <https://doi.org/10.1038/s41467-023-36303-8>.
- [25] J.-H. Jiang, L.-P. Zhu, X.-L. Li, Y.-Y. Xu, B.-K. Zhu, Surface modification of PE porous membranes based on the strong adhesion of polydopamine and covalent immobilization of heparin, *J Memb Sci* 364 (2010) 194–202. <https://doi.org/10.1016/j.memsci.2010.08.017>.
- [26] N.F. Della Vecchia, R. Avolio, M. Alfè, M.E. Errico, A. Napolitano, M. d'Ischia, Building-Block Diversity in Polydopamine Underpins a Multifunctional Eumelanin-Type Platform Tunable Through a Quinone Control Point, *Adv Funct Mater* 23 (2013) 1331–1340. <https://doi.org/10.1002/adfm.201202127>.
- [27] J. Liebscher, R. Mrówczyński, H.A. Scheidt, C. Filip, N.D. Hädade, R. Turcu, A. Bende, S. Beck, Structure of Polydopamine: A Never-Ending Story?, *Langmuir* 29 (2013) 10539–10548. <https://doi.org/10.1021/la4020288>.
- [28] D.R. Dreyer, D.J. Miller, B.D. Freeman, D.R. Paul, C.W. Bielawski, Elucidating the Structure of Poly(dopamine), *Langmuir* 28 (2012) 6428–6435. <https://doi.org/10.1021/la204831b>.

- [29] W. Chan, Investigation of the chemical structure and formation mechanism of polydopamine from self-assembly of dopamine by liquid chromatography/mass spectrometry coupled with isotope-labelling techniques, *Rapid Communications in Mass Spectrometry* 33 (2019) 429–436. <https://doi.org/10.1002/rcm.8373>.
- [30] Y. Ding, L.-T. Weng, M. Yang, Z. Yang, X. Lu, N. Huang, Y. Leng, Insights into the Aggregation/Deposition and Structure of a Polydopamine Film, *Langmuir* 30 (2014) 12258–12269. <https://doi.org/10.1021/la5026608>.
- [31] M.L. Alfieri, R. Micillo, L. Panzella, O. Crescenzi, S.L. Oscurato, P. Maddalena, A. Napolitano, V. Ball, M. d'Ischia, Structural Basis of Polydopamine Film Formation: Probing 5,6-Dihydroxyindole-Based Eumelanin Type Units and the Porphyrin Issue, *ACS Appl Mater Interfaces* 10 (2018) 7670–7680. <https://doi.org/10.1021/acsami.7b09662>.
- [32] Q. Lyu, N. Hsueh, C.L.L. Chai, Unravelling the polydopamine mystery: is the end in sight?, *Polym Chem* 10 (2019) 5771–5777. <https://doi.org/10.1039/C9PY01372E>.
- [33] H. Hemmatpour, O. De Luca, D. Crestani, M.C.A. Stuart, A. Lasorsa, P.C.A. van der Wel, K. Loos, T. Giouisis, V. Haddadi-Asl, P. Rudolf, New insights in polydopamine formation via surface adsorption, *Nat Commun* 14 (2023) 664. <https://doi.org/10.1038/s41467-023-36303-8>.
- [34] F. Bernsmann, A. Ponche, C. Ringwald, J. Hemmerlé, J. Raya, B. Bechinger, J.-C. Voegel, P. Schaaf, V. Ball, Characterization of Dopamine–Melanin Growth on Silicon Oxide, *The Journal of Physical Chemistry C* 113 (2009) 8234–8242. <https://doi.org/10.1021/jp901188h>.
- [35] J. Jiang, L. Zhu, L. Zhu, B. Zhu, Y. Xu, Surface Characteristics of a Self-Polymerized Dopamine Coating Deposited on Hydrophobic Polymer Films, *Langmuir* 27 (2011) 14180–14187. <https://doi.org/10.1021/la202877k>.

- [36] C. Zhang, Y. Lv, W.-Z. Qiu, A. He, Z.-K. Xu, Polydopamine Coatings with Nanopores for Versatile Molecular Separation, *ACS Appl Mater Interfaces* 9 (2017) 14437–14444. <https://doi.org/10.1021/acsami.7b03115>.
- [37] Y. Zou, Z. Wang, Z. Chen, Q.-P. Zhang, Q. Zhang, Y. Tian, S. Ren, Y. Li, Synthetic Melanin Hybrid Patchy Nanoparticle Photocatalysts, *The Journal of Physical Chemistry C* 123 (2019) 5345–5352. <https://doi.org/10.1021/acs.jpcc.8b10469>.
- [38] J. Jiang, L. Zhu, L. Zhu, H. Zhang, B. Zhu, Y. Xu, Antifouling and Antimicrobial Polymer Membranes Based on Bioinspired Polydopamine and Strong Hydrogen-Bonded Poly(*N*-vinyl pyrrolidone), *ACS Appl Mater Interfaces* 5 (2013) 12895–12904. <https://doi.org/10.1021/am403405c>.
- [39] Y. Cong, T. Xia, M. Zou, Z. Li, B. Peng, D. Guo, Z. Deng, Mussel-inspired polydopamine coating as a versatile platform for synthesizing polystyrene/Ag nanocomposite particles with enhanced antibacterial activities, *J. Mater. Chem. B* 2 (2014) 3450–3461. <https://doi.org/10.1039/C4TB00460D>.
- [40] J. Fu, Z. Chen, M. Wang, S. Liu, J. Zhang, J. Zhang, R. Han, Q. Xu, Adsorption of methylene blue by a high-efficiency adsorbent (polydopamine microspheres): Kinetics, isotherm, thermodynamics and mechanism analysis, *Chemical Engineering Journal* 259 (2015) 53–61. <https://doi.org/10.1016/j.cej.2014.07.101>.
- [41] V. Ball, D. Del Frari, V. Toniazzo, D. Ruch, Kinetics of polydopamine film deposition as a function of pH and dopamine concentration: Insights in the polydopamine deposition mechanism, *J Colloid Interface Sci* 386 (2012) 366–372. <https://doi.org/10.1016/j.jcis.2012.07.030>.
- [42] L.W. Teunissen, M.M.J. Smulders, H. Zuilhof, 19 nm-Thick Grafted-To Polymer Brushes onto Optimized Poly(Dopamine)-Coated Surfaces, *Adv Mater Interfaces* 10 (2023). <https://doi.org/10.1002/admi.202202503>.

- [43] J.C. García-Mayorga, H.-C. Rosu, A.B. Jasso-Salcedo, V.A. Escobar-Barrios, Kinetic study of polydopamine sphere synthesis using TRIS: relationship between synthesis conditions and final properties, *RSC Adv* 13 (2023) 5081–5095. <https://doi.org/10.1039/D2RA06669F>.
- [44] N.F. Della Vecchia, A. Luchini, A. Napolitano, G. D’Errico, G. Vitiello, N. Szekely, M. d’Ischia, L. Paduano, Tris Buffer Modulates Polydopamine Growth, Aggregation, and Paramagnetic Properties, *Langmuir* 30 (2014) 9811–9818. <https://doi.org/10.1021/la501560z>.
- [45] J.H. Ryu, P.B. Messersmith, H. Lee, Polydopamine Surface Chemistry: A Decade of Discovery, *ACS Appl Mater Interfaces* 10 (2018) 7523–7540. <https://doi.org/10.1021/acsami.7b19865>.
- [46] H.W. Kim, B.D. McCloskey, T.H. Choi, C. Lee, M.-J. Kim, B.D. Freeman, H.B. Park, Oxygen Concentration Control of Dopamine-Induced High Uniformity Surface Coating Chemistry, *ACS Appl Mater Interfaces* 5 (2013) 233–238. <https://doi.org/10.1021/am302439g>.
- [47] H.J. Cox, J. Li, P. Saini, J.R. Paterson, G.J. Sharples, J.P.S. Badyal, Bioinspired and eco-friendly high efficacy cinnamaldehyde antibacterial surfaces, *J Mater Chem B* 9 (2021) 2918–2930. <https://doi.org/10.1039/D0TB02379E>.
- [48] C. Mao, Y. Xiang, X. Liu, Y. Zheng, K.W.K. Yeung, Z. Cui, X. Yang, Z. Li, Y. Liang, S. Zhu, S. Wu, Local Photothermal/Photodynamic Synergistic Therapy by Disrupting Bacterial Membrane To Accelerate Reactive Oxygen Species Permeation and Protein Leakage, *ACS Appl Mater Interfaces* 11 (2019) 17902–17914. <https://doi.org/10.1021/acsami.9b05787>.
- [49] M.M. Cowan, Plant Products as Antimicrobial Agents, *Clin Microbiol Rev* 12 (1999) 564–582. <https://doi.org/10.1128/CMR.12.4.564>.

- [50] C. Papuc, G. V. Goran, C.N. Predescu, V. Nicorescu, G. Stefan, Plant Polyphenols as Antioxidant and Antibacterial Agents for Shelf-Life Extension of Meat and Meat Products: Classification, Structures, Sources, and Action Mechanisms, *Compr Rev Food Sci Food Saf* 16 (2017) 1243–1268. <https://doi.org/10.1111/1541-4337.12298>.
- [51] M. Salomäki, L. Marttila, H. Kivelä, T. Ouvinen, J. Lukkari, Effects of pH and Oxidants on the First Steps of Polydopamine Formation: A Thermodynamic Approach, *J Phys Chem B* 122 (2018) 6314–6327. <https://doi.org/10.1021/acs.jpcc.8b02304>.
- [52] P. Muñoz, S. Huenchuguala, I. Paris, J. Segura-Aguilar, Dopamine Oxidation and Autophagy, *Parkinsons Dis* 2012 (2012) 1–13. <https://doi.org/10.1155/2012/920953>.
- [53] S.-M. Chen, J.-Y. Chen, V.S. Vasantha, Electrochemical preparation of epinephrine/Nafion chemically modified electrodes and their electrocatalytic oxidation of ascorbic acid and dopamine, *Electrochim Acta* 52 (2006) 455–465. <https://doi.org/10.1016/j.electacta.2006.05.027>.
- [54] D.-Y. Lee, M. Park, N. Kim, M. Gu, H. Kim, B.-S. Kim, Sustainable hydrogen peroxide production based on dopamine through Janus-like mechanism transition from chemical to photocatalytic reactions, *J Catal* 411 (2022) 235–244. <https://doi.org/10.1016/j.jcat.2022.05.017>.
- [55] H. Liu, X. Qu, H. Tan, J. Song, M. Lei, E. Kim, G.F. Payne, C. Liu, Role of polydopamine's redox-activity on its pro-oxidant, radical-scavenging, and antimicrobial activities, *Acta Biomater* 88 (2019) 181–196. <https://doi.org/10.1016/j.actbio.2019.02.032>.
- [56] J. Li, M.A. Baird, M.A. Davis, W. Tai, L.S. Zweifel, K.M.A. Waldorf, M. Gale Jr, L. Rajagopal, R.H. Pierce, X. Gao, Dramatic enhancement of the

- detection limits of bioassays via ultrafast deposition of polydopamine, *Nat Biomed Eng* 1 (2017) 0082. <https://doi.org/10.1038/s41551-017-0082>.
- [57] M. Dai, T. Huang, L. Chao, Q. Xie, Y. Tan, C. Chen, W. Meng, Horseradish peroxidase-catalyzed polymerization of L-DOPA for mono-/bi-enzyme immobilization and amperometric biosensing of H₂O₂ and uric acid, *Talanta* 149 (2016) 117–123. <https://doi.org/10.1016/j.talanta.2015.11.047>.
- [58] X. Du, L. Li, J. Li, C. Yang, N. Frenkel, A. Welle, S. Heissler, A. Nefedov, M. Grunze, P.A. Levkin, UV-Triggered Dopamine Polymerization: Control of Polymerization, Surface Coating, and Photopatterning, *Advanced Materials* 26 (2014) 8029–8033. <https://doi.org/10.1002/adma.201403709>.
- [59] H. Feinberg, T.W. Hanks, Polydopamine: a bioinspired adhesive and surface modification platform, *Polym Int* 71 (2022) 578–582. <https://doi.org/10.1002/pi.6358>.
- [60] R. Ouyang, J. Lei, H. Ju, Surface molecularly imprinted nanowire for protein specific recognition, *Chemical Communications* (2008) 5761. <https://doi.org/10.1039/b810248a>.
- [61] S.H. Ku, C.B. Park, Human endothelial cell growth on mussel-inspired nanofiber scaffold for vascular tissue engineering, *Biomaterials* 31 (2010) 9431–9437. <https://doi.org/10.1016/j.biomaterials.2010.08.071>.
- [62] S. Huang, N. Liang, Y. Hu, X. Zhou, N. Abidi, Polydopamine-Assisted Surface Modification for Bone Biosubstitutes, *Biomed Res Int* 2016 (2016) 1–9. <https://doi.org/10.1155/2016/2389895>.
- [63] M. Suneetha, K.M. Rao, S.S. Han, Mussel-Inspired Cell/Tissue-Adhesive, Hemostatic Hydrogels for Tissue Engineering Applications, *ACS Omega* 4 (2019) 12647–12656. <https://doi.org/10.1021/acsomega.9b01302>.

- [64] M.E. Lyngé, R. Ogaki, A.O. Laursen, J. Lovmand, D.S. Sutherland, B. Städler, Polydopamine/Liposome Coatings and Their Interaction with Myoblast Cells, *ACS Appl Mater Interfaces* 3 (2011) 2142–2147. <https://doi.org/10.1021/am200358p>.
- [65] W. Cheng, J. Nie, L. Xu, C. Liang, Y. Peng, G. Liu, T. Wang, L. Mei, L. Huang, X. Zeng, pH-Sensitive Delivery Vehicle Based on Folic Acid-Conjugated Polydopamine-Modified Mesoporous Silica Nanoparticles for Targeted Cancer Therapy, *ACS Appl Mater Interfaces* 9 (2017) 18462–18473. <https://doi.org/10.1021/acsami.7b02457>.
- [66] L. Su, Y. Yu, Y. Zhao, F. Liang, X. Zhang, Strong Antibacterial Polydopamine Coatings Prepared by a Shaking-assisted Method, *Sci Rep* 6 (2016) 24420. <https://doi.org/10.1038/srep24420>.
- [67] K. Patel, N. Singh, J. Yadav, J.M. Nayak, S.K. Sahoo, J. Lata, D. Chand, S. Kumar, R. Kumar, Polydopamine films change their physicochemical and antimicrobial properties with a change in reaction conditions, *Physical Chemistry Chemical Physics* 20 (2018) 5744–5755. <https://doi.org/10.1039/C7CP08406D>.
- [68] H. Karkhanechi, R. Takagi, H. Matsuyama, Biofouling resistance of reverse osmosis membrane modified with polydopamine, *Desalination* 336 (2014) 87–96. <https://doi.org/10.1016/j.desal.2013.12.033>.
- [69] J. Song, H. Liu, M. Lei, H. Tan, Z. Chen, A. Antoshin, G.F. Payne, X. Qu, C. Liu, Redox-Channeling Polydopamine-Ferrocene (PDA-Fc) Coating To Confer Context-Dependent and Photothermal Antimicrobial Activities, *ACS Appl Mater Interfaces* 12 (2020) 8915–8928. <https://doi.org/10.1021/acsami.9b22339>.
- [70] Q. Huang, X. Liu, G. Zhao, T. Hu, Y. Wang, Potential and challenges of tannins as an alternative to in-feed antibiotics for farm animal production,

Animal Nutrition 4 (2018) 137–150.
<https://doi.org/10.1016/j.aninu.2017.09.004>.

- [71] A. Baldwin, B.W. Booth, Biomedical applications of tannic acid, *J Biomater Appl* 36 (2022) 1503–1523. <https://doi.org/10.1177/08853282211058099>.
- [72] A. Rahal, A. Kumar, V. Singh, B. Yadav, R. Tiwari, S. Chakraborty, K. Dhama, Oxidative Stress, Prooxidants, and Antioxidants: The Interplay, *Biomed Res Int* 2014 (2014) 1–19. <https://doi.org/10.1155/2014/761264>.
- [73] M. Farhan, M. Oves, S. Chibber, S. Hadi, A. Ahmad, Mobilization of Nuclear Copper by Green Tea Polyphenol Epicatechin-3-Gallate and Subsequent Prooxidant Breakage of Cellular DNA: Implications for Cancer Chemotherapy, *Int J Mol Sci* 18 (2016) 34. <https://doi.org/10.3390/ijms18010034>.
- [74] E. Bouki, V.K. Dimitriadis, M. Kaloyianni, S. Dailianis, Antioxidant and pro-oxidant challenge of tannic acid in mussel hemocytes exposed to cadmium, *Mar Environ Res* 85 (2013) 13–20. <https://doi.org/10.1016/j.marenvres.2012.12.005>.
- [75] L.L. Theisen, C.A.J. Erdelmeier, G.A. Spoden, F. Boukhallouk, A. Sausy, L. Florin, C.P. Muller, Tannins from *Hamamelis virginiana* Bark Extract: Characterization and Improvement of the Antiviral Efficacy against Influenza A Virus and Human Papillomavirus, *PLoS One* 9 (2014) e88062. <https://doi.org/10.1371/journal.pone.0088062>.
- [76] S. Priya, N.S. Kumar, S. Hemalatha, Antiviral phytochemicals target envelop protein to control Zika virus, *Comput Biol Chem* 77 (2018) 402–412. <https://doi.org/10.1016/j.compbiolchem.2018.08.008>.

- [77] B.W. Booth, B.D. Inskeep, H. Shah, J.P. Park, E.J. Hay, K.J.L. Burg, Tannic Acid Preferentially Targets Estrogen Receptor-Positive Breast Cancer, *Int J Breast Cancer* 2013 (2013) 1–9. <https://doi.org/10.1155/2013/369609>.
- [78] S. Karakurt, O. Adali, Tannic Acid Inhibits Proliferation, Migration, Invasion of Prostate Cancer and Modulates Drug Metabolizing and Antioxidant Enzymes, *Anticancer Agents Med Chem* 16 (2016) 781–789. <https://doi.org/10.2174/187152061666615111115809>.
- [79] N. Kakiuchi, M. Hattori, M. Nishizawa, T. Yamagushi, T. Okuda, T. Namba, Studies on dental caries prevention by traditional medicines. VIII. Inhibitory effect of various tannins on glucan synthesis by glucosyltransferase from *Streptococcus mutans*., *Chem Pharm Bull (Tokyo)* 34 (1986) 720–725. <https://doi.org/10.1248/cpb.34.720>.
- [80] V.N. Lima, C.D.M. Oliveira-Tintino, E.S. Santos, L.P. Morais, S.R. Tintino, T.S. Freitas, Y.S. Geraldo, R.L.S. Pereira, R.P. Cruz, I.R.A. Menezes, H.D.M. Coutinho, Antimicrobial and enhancement of the antibiotic activity by phenolic compounds: Gallic acid, caffeic acid and pyrogallol, *Microb Pathog* 99 (2016) 56–61. <https://doi.org/10.1016/j.micpath.2016.08.004>.
- [81] K.B. Myint, L.C. Sing, Z. Wei, Tannic Acid as Phytochemical Potentiator for Antibiotic Resistance Adaptation, *APCBEE Procedia* 7 (2013) 175–181. <https://doi.org/10.1016/j.apcbee.2013.08.030>.
- [82] N. Sahiner, S. Sagbas, N. Aktas, Single step natural poly(tannic acid) particle preparation as multitasking biomaterial, *Materials Science and Engineering: C* 49 (2015) 824–834. <https://doi.org/10.1016/j.msec.2015.01.076>.
- [83] Sardjiman, R. Rahardjoputro, J. Santoso, The Effect of Tannic Acid as Antimicrobial Agent on *Pseudomonas aeruginosa* Using In-vitro Diffusion Method, *J Pharm Res Int* 35 (2023) 24–29. <https://doi.org/10.9734/jpri/2023/v35i277442>.

- [84] J. Long, C. Yang, J. Liu, C. Ma, M. Jiao, H. Hu, J. Xiong, Y. Zhang, W. Wei, H. Yang, Y. He, M. Zhu, Y. Yu, L. Fu, H. Chen, Tannic acid inhibits *Escherichia coli* biofilm formation and underlying molecular mechanisms: Biofilm regulator CsgD, *Biomedicine & Pharmacotherapy* 175 (2024) 116716. <https://doi.org/10.1016/j.biopha.2024.116716>.
- [85] K. Nakamura, K. Ishiyama, H. Sheng, H. Ikai, T. Kanno, Y. Niwano, Bactericidal Activity and Mechanism of Photoirradiated Polyphenols against Gram-Positive and -Negative Bacteria, *J Agric Food Chem* 63 (2015) 7707–7713. <https://doi.org/10.1021/jf5058588>.
- [86] S.J. Lee, M.A. Gwak, K. Chathuranga, J.S. Lee, J. Koo, W.H. Park, Multifunctional chitosan/tannic acid composite films with improved anti-UV, antioxidant, and antimicrobial properties for active food packaging, *Food Hydrocoll* 136 (2023) 108249. <https://doi.org/10.1016/j.foodhyd.2022.108249>.
- [87] B. Kaczmarek, Tannic Acid with Antiviral and Antibacterial Activity as A Promising Component of Biomaterials—A Minireview, *Materials* 13 (2020) 3224. <https://doi.org/10.3390/ma13143224>.
- [88] M. Liu, M. Feng, K. Yang, Y. Cao, J. Zhang, J. Xu, S.H. Hernández, X. Wei, M. Fan, Transcriptomic and metabolomic analyses reveal antibacterial mechanism of astringent persimmon tannin against Methicillin-resistant *Staphylococcus aureus* isolated from pork, *Food Chem* 309 (2020) 125692. <https://doi.org/10.1016/j.foodchem.2019.125692>.
- [89] S.R. Tintino, C.D.M. Oliveira-Tintino, F.F. Campina, R.L.P. Silva, M. do S. Costa, I.R.A. Menezes, J.T. Calixto-Júnior, J.P. Siqueira-Junior, H.D.M. Coutinho, T.C. Leal-Balbino, V.Q. Balbino, Evaluation of the tannic acid inhibitory effect against the NorA efflux pump of *Staphylococcus aureus*,

- Microb Pathog 97 (2016) 9–13.
<https://doi.org/10.1016/j.micpath.2016.04.003>.
- [90] L. Boulekbache-Makhlouf, S. Slimani, K. Madani, Total phenolic content, antioxidant and antibacterial activities of fruits of *Eucalyptus globulus* cultivated in Algeria, *Ind Crops Prod* 41 (2013) 85–89.
<https://doi.org/10.1016/j.indcrop.2012.04.019>.
- [91] A. Pandey, P.S. Negi, Phytochemical composition, *in vitro* antioxidant activity and antibacterial mechanisms of *Neolamarckia cadamba* fruits extracts, *Nat Prod Res* 32 (2018) 1189–1192.
<https://doi.org/10.1080/14786419.2017.1323209>.
- [92] S.S. Costa, M. Viveiros, L. Amaral, I. Couto, Multidrug Efflux Pumps in *Staphylococcus aureus*: an Update, *Open Microbiol J* 7 (2013) 59–71.
<https://doi.org/10.2174/1874285801307010059>.
- [93] M. Haktaniyan, S. Atilla, E. Cagli, I. Erel-Goktepe, pH- and temperature-induced release of doxorubicin from multilayers of poly(2-isopropyl-2-oxazoline) and tannic acid, *Polym Int* 66 (2017) 1851–1863.
<https://doi.org/10.1002/pi.5458>.
- [94] I. Erel-Unal, S.A. Sukhishvili, Hydrogen-Bonded Multilayers of a Neutral Polymer and a Polyphenol, *Macromolecules* 41 (2008) 3962–3970.
<https://doi.org/10.1021/ma800186q>.
- [95] C. Chen, H. Yang, X. Yang, Q. Ma, Tannic acid: a crosslinker leading to versatile functional polymeric networks: a review, *RSC Adv* 12 (2022) 7689–7711. <https://doi.org/10.1039/D1RA07657D>.
- [96] Z. Guo, W. Xie, J. Lu, X. Guo, J. Xu, W. Xu, Y. Chi, N. Takuya, H. Wu, L. Zhao, Tannic acid-based metal phenolic networks for bio-applications: a

- review, *J Mater Chem B* 9 (2021) 4098–4110. <https://doi.org/10.1039/D1TB00383F>.
- [97] I. Zhuk, F. Jariwala, A.B. Attygalle, Y. Wu, M.R. Libera, S.A. Sukhishvili, Self-Defensive Layer-by-Layer Films with Bacteria-Triggered Antibiotic Release, *ACS Nano* 8 (2014) 7733–7745. <https://doi.org/10.1021/nn500674g>.
- [98] M.H. Iqbal, A. Schroder, H. Kerdjoudj, C. Njel, B. Senger, V. Ball, F. Meyer, F. Boulmedais, Effect of the Buffer on the Buildup and Stability of Tannic Acid/Collagen Multilayer Films Applied as Antibacterial Coatings, *ACS Appl Mater Interfaces* 12 (2020) 22601–22612. <https://doi.org/10.1021/acsami.0c04475>.
- [99] T.S. Sileika, D.G. Barrett, R. Zhang, K.H.A. Lau, P.B. Messersmith, Colorless Multifunctional Coatings Inspired by Polyphenols Found in Tea, Chocolate, and Wine, *Angewandte Chemie International Edition* 52 (2013) 10766–10770. <https://doi.org/10.1002/anie.201304922>.
- [100] A. V. Singhal, D. Malwal, S. Thiyagarajan, I. Lahiri, Antimicrobial and antibiofilm activity of GNP-Tannic Acid-Ag nanocomposite and their epoxy-based coatings, *Prog Org Coat* 159 (2021) 106421. <https://doi.org/10.1016/j.porgcoat.2021.106421>.
- [101] M. Haapakoski, A. Emelianov, D. Reshamwala, M. Laajala, J. Tienaho, P. Kilpeläinen, J. Liimatainen, T. Jyske, M. Pettersson, V. Marjomäki, Antiviral functionalization of cellulose using tannic acid and tannin-rich extracts, *Front Microbiol* 14 (2023). <https://doi.org/10.3389/fmicb.2023.1287167>.
- [102] X. Tan, H. Chen, X. Liu, Y. Liu, X. Jiang, Investigating the effect of tannin films prepared by low-energy electron beam deposition on the inhibition of bone tumors, *Appl Surf Sci* 657 (2024) 159811. <https://doi.org/10.1016/j.apsusc.2024.159811>.

- [103] S. Yang, Y. Wang, X. Wu, S. Sheng, T. Wang, X. Zan, Multifunctional Tannic Acid (TA) and Lysozyme (Lys) Films Built Layer by Layer for Potential Application on Implant Coating, *ACS Biomater Sci Eng* 5 (2019) 3582–3594. <https://doi.org/10.1021/acsbiomaterials.9b00717>.
- [104] X. Yang, L. Yan, Y. Wu, Y. Liu, L. Shao, Biomimetic hydrophilization engineering on membrane surface for highly-efficient water purification, *J Memb Sci* 589 (2019) 117223. <https://doi.org/10.1016/j.memsci.2019.117223>.
- [105] L. Xie, Y. Liu, W. Zhang, S. Xu, A Dopamine/Tannic-Acid-Based Co-Deposition Combined with Phytic Acid Modification to Enhance the Anti-Fouling Property of RO Membrane, *Membranes (Basel)* 11 (2021) 342. <https://doi.org/10.3390/membranes11050342>.
- [106] H. Zhang, X. Shen, Z. Fei, X. Fan, L. Ma, H. Wang, C. Tian, B. Zhang, R. Luo, Y. Wang, S. Huang, Ag-Incorporated Polydopamine/Tannic Acid Coating on Titanium With Enhanced Cytocompatible and Antibacterial Properties, *Front Bioeng Biotechnol* 10 (2022). <https://doi.org/10.3389/fbioe.2022.877738>.
- [107] Y.A. Lee, J. Lee, D.W. Kim, C.-Y. Yoo, S.H. Park, J.J. Yoo, S. Kim, B. Kim, W.K. Cho, H. Yoon, Mussel-inspired surface functionalization of porous carbon nanosheets using polydopamine and Fe³⁺/tannic acid layers for high-performance electrochemical capacitors, *J Mater Chem A Mater* 5 (2017) 25368–25377. <https://doi.org/10.1039/C7TA08010G>.
- [108] J. Gao, H. Lei, Z. Han, Q. Shi, Y. Chen, Y. Jiang, Dopamine functionalized tannic-acid-templated mesoporous silica nanoparticles as a new sorbent for the efficient removal of Cu²⁺ from aqueous solution, *Sci Rep* 7 (2017) 45215. <https://doi.org/10.1038/srep45215>.

- [109] A. Akbar Heidari, H. Mahdavi, P. Khodaei Kahriz, TFC solvent-resistant nanofiltration membrane prepared via a gyroid-like PE support coated with polydopamine/Tannic acid-Fe(III), *Journal of Industrial and Engineering Chemistry* 106 (2022) 400–410. <https://doi.org/10.1016/j.jiec.2021.11.017>.
- [110] J.J. Richardson, J. Cui, M. Björnmalm, J.A. Braunger, H. Ejima, F. Caruso, Innovation in Layer-by-Layer Assembly, *Chem Rev* 116 (2016) 14828–14867. <https://doi.org/10.1021/acs.chemrev.6b00627>.
- [111] N. Saracogullari, D. Gundogdu, F.N. Ozdemir, Y. Soyer, I. Erel-Goktepe, The effect of polyacid on the physical and biological properties of chitosan based layer-by-layer films, *Colloids Surf A Physicochem Eng Asp* 617 (2021) 126313. <https://doi.org/10.1016/j.colsurfa.2021.126313>.
- [112] C.-G. Wang, N.E.B. Surat'man, J.J.Q. Mah, C. Qu, Z. Li, Surface antimicrobial functionalization with polymers: fabrication, mechanisms and applications, *J Mater Chem B* 10 (2022) 9349–9368. <https://doi.org/10.1039/D2TB01555B>.
- [113] Y. Li, X. Wang, J. Sun, Layer-by-layer assembly for rapid fabrication of thick polymeric films, *Chem Soc Rev* 41 (2012) 5998. <https://doi.org/10.1039/c2cs35107b>.
- [114] H. Mitwalli, R. Alsahafi, A.A. Balhaddad, M.D. Weir, H.H.K. Xu, M.A.S. Melo, Emerging Contact-Killing Antibacterial Strategies for Developing Anti-Biofilm Dental Polymeric Restorative Materials, *Bioengineering* 7 (2020) 83. <https://doi.org/10.3390/bioengineering7030083>.
- [115] R. Kaur, S. Liu, Antibacterial surface design – Contact kill, *Prog Surf Sci* 91 (2016) 136–153. <https://doi.org/10.1016/j.progsurf.2016.09.001>.

- [116] J. Illergård, U. Römling, L. Wågberg, M. Ek, Biointeractive antibacterial fibres using polyelectrolyte multilayer modification, *Cellulose* 19 (2012) 1731–1741. <https://doi.org/10.1007/s10570-012-9742-0>.
- [117] J.A. Lichter, M.F. Rubner, Polyelectrolyte Multilayers with Intrinsic Antimicrobial Functionality: The Importance of Mobile Polycations, *Langmuir* 25 (2009) 7686–7694. <https://doi.org/10.1021/la900349c>.
- [118] A.P. Gomes, J.F. Mano, J.A. Queiroz, I.C. Gouveia, Layer-by-layer deposition of antimicrobial polymers on cellulosic fibers: a new strategy to develop bioactive textiles, *Polym Adv Technol* 24 (2013) 1005–1010. <https://doi.org/10.1002/pat.3176>.
- [119] W. Graisuwan, O. Wiarachai, C. Ananthanawat, S. Puthong, S. Soogarun, S. Kiatkamjornwong, V.P. Hoven, Multilayer film assembled from charged derivatives of chitosan: Physical characteristics and biological responses, *J Colloid Interface Sci* 376 (2012) 177–188. <https://doi.org/10.1016/j.jcis.2012.02.039>.
- [120] T.-D. Zhang, X. Deng, Y.-F. Wang, X.-T. Wang, X. Zhang, L.-L. Chen, X. Cao, Y.-Z. Zhang, C.-Y. Zhang, X. Zheng, D.-C. Yin, Layer-by-layer coating of polyvinylamine and dopamine-modified hyaluronic acid inhibits the growth of bacteria and tumor cell lines on the surface of materials, *Appl Surf Sci* 530 (2020) 147197. <https://doi.org/10.1016/j.apsusc.2020.147197>.
- [121] L. Séon, P. Lavalle, P. Schaaf, F. Boulmedais, Polyelectrolyte Multilayers: A Versatile Tool for Preparing Antimicrobial Coatings, *Langmuir* 31 (2015) 12856–12872. <https://doi.org/10.1021/acs.langmuir.5b02768>.
- [122] E. Guzmán, R.G. Rubio, F. Ortega, A closer physico-chemical look to the Layer-by-Layer electrostatic self-assembly of polyelectrolyte multilayers, *Adv Colloid Interface Sci* 282 (2020) 102197. <https://doi.org/10.1016/j.cis.2020.102197>.

- [123] J.-F. Briand, Marine antifouling laboratory bioassays: an overview of their diversity, *Biofouling* 25 (2009) 297–311. <https://doi.org/10.1080/08927010902745316>.
- [124] B. Liu, X. Liu, S. Shi, R. Huang, R. Su, W. Qi, Z. He, Design and mechanisms of antifouling materials for surface plasmon resonance sensors, *Acta Biomater* 40 (2016) 100–118. <https://doi.org/10.1016/j.actbio.2016.02.035>.
- [125] H. Schmolke, S. Demming, A. Edlich, V. Magdanz, S. Büttgenbach, E. Franco-Lara, R. Krull, C.-P. Klages, Polyelectrolyte multilayer surface functionalization of poly(dimethylsiloxane) (PDMS) for reduction of yeast cell adhesion in microfluidic devices, *Biomicrofluidics* 4 (2010). <https://doi.org/10.1063/1.3523059>.
- [126] Y. Xie, L. Chen, X. Zhang, S. Chen, M. Zhang, W. Zhao, S. Sun, C. Zhao, Integrating zwitterionic polymer and Ag nanoparticles on polymeric membrane surface to prepare antifouling and bactericidal surface via Schiff-based layer-by-layer assembly, *J Colloid Interface Sci* 510 (2018) 308–317. <https://doi.org/10.1016/j.jcis.2017.09.071>.
- [127] S. Park, H. Kim, S. Bin Yang, J.-H. Moon, H.-W. Ahn, J. Hong, A Polysaccharide-Based Antibacterial Coating with Improved Durability for Clear Overlay Appliances, *ACS Appl Mater Interfaces* 10 (2018) 17714–17721. <https://doi.org/10.1021/acsami.8b04433>.
- [128] S.Y. Wong, L. Han, K. Timachova, J. Veselinovic, M.N. Hyder, C. Ortiz, A.M. Klibanov, P.T. Hammond, Drastically Lowered Protein Adsorption on Microbicidal Hydrophobic/Hydrophilic Polyelectrolyte Multilayers, *Biomacromolecules* 13 (2012) 719–726. <https://doi.org/10.1021/bm201637e>.
- [129] H.F. Chuang, R.C. Smith, P.T. Hammond, Polyelectrolyte Multilayers for Tunable Release of Antibiotics, *Biomacromolecules* 9 (2008) 1660–1668. <https://doi.org/10.1021/bm800185h>.

- [130] A. Shukla, S. Puranam, P.T. Hammond, Vancomycin Storage Stability in Multilayer Thin Film Coatings for On-Demand Care, *J Biomater Sci Polym Ed* 23 (2012) 1895–1902. <https://doi.org/10.1163/156856211X598256>.
- [131] P. Gentile, M.E. Frongia, M. Cardellach, C.A. Miller, G.P. Stafford, G.J. Leggett, P. V. Hatton, Functionalised nanoscale coatings using layer-by-layer assembly for imparting antibacterial properties to polylactide-co-glycolide surfaces, *Acta Biomater* 21 (2015) 35–43. <https://doi.org/10.1016/j.actbio.2015.04.009>.
- [132] D.J. Schmidt, J.S. Moskowitz, P.T. Hammond, Electrically Triggered Release of a Small Molecule Drug from a Polyelectrolyte Multilayer Coating, *Chemistry of Materials* 22 (2010) 6416–6425. <https://doi.org/10.1021/cm102578j>.
- [133] Z. Hosseinidoust, A.L.J. Olsson, N. Tufenkji, Going viral: Designing bioactive surfaces with bacteriophage, *Colloids Surf B Biointerfaces* 124 (2014) 2–16. <https://doi.org/10.1016/j.colsurfb.2014.05.036>.
- [134] G. Tidim, M. Guzel, Y. Soyer, I. Erel-Goktepe, Layer-by-layer assembly of chitosan/alginate thin films containing *Salmonella enterica* bacteriophages for antibacterial applications, *Carbohydr Polym* 328 (2024) 121710. <https://doi.org/10.1016/j.carbpol.2023.121710>.
- [135] Z.-Y. Xi, Y.-Y. Xu, L.-P. Zhu, Y. Wang, B.-K. Zhu, A facile method of surface modification for hydrophobic polymer membranes based on the adhesive behavior of poly(DOPA) and poly(dopamine), *J Memb Sci* 327 (2009) 244–253. <https://doi.org/10.1016/j.memsci.2008.11.037>.
- [136] G. He, Y. Zhou, X. Chen, T. Ma, Y. Yin, Y. Chu, L. Fan, W. Cai, Preparation of poly (vinyl alcohol)/polydopamine/tannin acid composite hydrogels with dual adhesive, antioxidant and antibacterial properties, *Eur Polym J* 205 (2024) 112708. <https://doi.org/10.1016/j.eurpolymj.2023.112708>.

- [137] P. Schindler, H.R. Kamber, Die Acidität von Silanolgruppen. Vorläufige Mittheilung, *Helv Chim Acta* 51 (1968) 1781–1786. <https://doi.org/10.1002/hlca.19680510738>.
- [138] Z. Zhong, L. Jia, Room temperature preparation of water-soluble polydopamine-polyethyleneimine copolymer dots for selective detection of copper ions, *Talanta* 197 (2019) 584–591. <https://doi.org/10.1016/j.talanta.2019.01.070>.
- [139] S. Hong, J. Kim, Y.S. Na, J. Park, S. Kim, K. Singha, G. Im, D. Han, W.J. Kim, H. Lee, Poly(norepinephrine): Ultrasooth Material-Independent Surface Chemistry and Nanodepot for Nitric Oxide, *Angewandte Chemie International Edition* 52 (2013) 9187–9191. <https://doi.org/10.1002/anie.201301646>.
- [140] K.-Y. Ju, Y. Lee, S. Lee, S.B. Park, J.-K. Lee, Bioinspired Polymerization of Dopamine to Generate Melanin-Like Nanoparticles Having an Excellent Free-Radical-Scavenging Property, *Biomacromolecules* 12 (2011) 625–632. <https://doi.org/10.1021/bm101281b>.
- [141] C. Alonso, C. Nieto, J.C. Vargas, M.A. Vega, E.M. Martín del Valle, Understanding the growth kinetics of polydopamine nanoparticles as a function of the temperature and the type of alcohol used as solvent media in their polymerization, *Chemical Engineering Journal Advances* 20 (2024) 100638. <https://doi.org/10.1016/j.ceja.2024.100638>.
- [142] Z. Yang, Z. Zhou, H. Guo, Z. Yao, X. Ma, X. Song, S.-P. Feng, C.Y. Tang, Tannic Acid/Fe⁺³ Nanoscaffold for Interfacial Polymerization: Toward Enhanced Nanofiltration Performance, *Environ Sci Technol* 52 (2018) 9341–9349. <https://doi.org/10.1021/acs.est.8b02425>.
- [143] H.M. Hegab, A. ElMekawy, T.G. Barclay, A. Michelmore, L. Zou, C.P. Saint, M. Ginic-Markovic, Single-Step Assembly of Multifunctional Poly(tannic

- acid)–Graphene Oxide Coating To Reduce Biofouling of Forward Osmosis Membranes, *ACS Appl Mater Interfaces* 8 (2016) 17519–17528. <https://doi.org/10.1021/acsami.6b03719>.
- [144] J. Drelich, E. Chibowski, Superhydrophilic and Superwetting Surfaces: Definition and Mechanisms of Control, *Langmuir* 26 (2010) 18621–18623. <https://doi.org/10.1021/la1039893>.
- [145] L. Li, Y. Wang, K. Liu, L. Yang, B. Zhang, Q. Luo, R. Luo, Y. Wang, Nanoparticles-stacked superhydrophilic coating supported synergistic antimicrobial ability for enhanced wound healing, *Materials Science and Engineering: C* 132 (2022) 112535. <https://doi.org/10.1016/j.msec.2021.112535>.
- [146] R.N. Wenzel, Resistance of Solid Surfaces to Wetting by Water, *Ind Eng Chem* 28 (1936) 988–994. <https://doi.org/10.1021/ie50320a024>.
- [147] F.J. Dent, G. Tyagi, F. Esat, J.T. Cabral, S. Khodaparast, Tuneable Topography and Hydrophobicity Mode in Biomimetic Plant-Based Wax Coatings, *Adv Funct Mater* 34 (2024). <https://doi.org/10.1002/adfm.202307977>.
- [148] M.T. Rauter, S.K. Schnell, S. Kjelstrup, Cassie–Baxter and Wenzel States and the Effect of Interfaces on Transport Properties across Membranes, *J Phys Chem B* 125 (2021) 12730–12740. <https://doi.org/10.1021/acs.jpcc.1c07931>.
- [149] Z. Yan, Y. Zhang, H. Yang, G. Fan, A. Ding, H. Liang, G. Li, N. Ren, B. Van der Bruggen, Mussel-inspired polydopamine modification of polymeric membranes for the application of water and wastewater treatment: A review, *Chemical Engineering Research and Design* 157 (2020) 195–214. <https://doi.org/10.1016/j.cherd.2020.03.011>.

- [150] W.J. Barreto, S. Ponzoni, P. Sassi, A Raman and UV-Vis study of catecholamines oxidized with Mn(III), *Spectrochim Acta A Mol Biomol Spectrosc* 55 (1998) 65–72. [https://doi.org/10.1016/S1386-1425\(98\)00164-4](https://doi.org/10.1016/S1386-1425(98)00164-4).
- [151] E. Karabulut, T. Pettersson, M. Ankerfors, L. Wågberg, Adhesive Layer-by-Layer Films of Carboxymethylated Cellulose Nanofibril–Dopamine Covalent Bioconjugates Inspired by Marine Mussel Threads, *ACS Nano* 6 (2012) 4731–4739. <https://doi.org/10.1021/nn204620j>.
- [152] T. Shutava, M. Prouty, D. Kommireddy, Y. Lvov, pH Responsive Decomposable Layer-by-Layer Nanofilms and Capsules on the Basis of Tannic Acid, *Macromolecules* 38 (2005) 2850–2858. <https://doi.org/10.1021/ma047629x>.
- [153] A. Barbasz, M. Oćwieja, J. Barbasz, Cytotoxic Activity of Highly Purified Silver Nanoparticles Sol Against Cells of Human Immune System, *Appl Biochem Biotechnol* 176 (2015) 817–834. <https://doi.org/10.1007/s12010-015-1613-3>.
- [154] B. Szpoganicz, S. Gidanian, P. Kong, P. Farmer, Metal binding by melanins: studies of colloidal dihydroxyindole-melanin, and its complexation by Cu(II) and Zn(II) ions, *J Inorg Biochem* 89 (2002) 45–53. [https://doi.org/10.1016/S0162-0134\(01\)00406-8](https://doi.org/10.1016/S0162-0134(01)00406-8).
- [155] I. Erel, H.E. Karahan, C. Tuncer, V. Bütün, A.L. Demirel, Hydrogen-bonded multilayers of micelles of a dually responsive dicationic block copolymer, *Soft Matter* 8 (2012) 827–836. <https://doi.org/10.1039/C1SM06248D>.
- [156] X.-Q. Zhu, C.-H. Wang, H. Liang, J.-P. Cheng, Theoretical Prediction of the Hydride Affinities of Various p - and o-Quinones in DMSO, *J Org Chem* 72 (2007) 945–956. <https://doi.org/10.1021/jo0621928>.

- [157] K. Jodko-Piórecka, B. Sikora, M. Kluzek, P. Przybylski, G. Litwinienko, Antiradical Activity of Dopamine, L-DOPA, Adrenaline, and Noradrenaline in Water/Methanol and in Liposomal Systems, *J Org Chem* 87 (2022) 1791–1804. <https://doi.org/10.1021/acs.joc.1c02308>.
- [158] B. Yu, J. Liu, S. Liu, F. Zhou, Pdop layer exhibiting zwitterionicity: a simple electrochemical interface for governing ion permeability, *Chemical Communications* 46 (2010) 5900. <https://doi.org/10.1039/c0cc00596g>.
- [159] R. Tejido-Rastrilla, S. Ferraris, W.H. Goldmann, A. Grünewald, R. Detsch, G. Baldi, S. Spriano, A.R. Boccaccini, Studies on Cell Compatibility, Antibacterial Behavior, and Zeta Potential of Ag-Containing Polydopamine-Coated Bioactive Glass-Ceramic, *Materials* 12 (2019) 500. <https://doi.org/10.3390/ma12030500>.
- [160] D.R. Holycross, M. Chai, Comprehensive NMR Studies of the Structures and Properties of PEI Polymers, *Macromolecules* 46 (2013) 6891–6897. <https://doi.org/10.1021/ma4011796>.
- [161] M. Borkovec, G.J.M. Koper, Proton Binding Characteristics of Branched Polyelectrolytes, *Macromolecules* 30 (1997) 2151–2158. <https://doi.org/10.1021/ma961312i>.
- [162] V. Izumrudov, S.A. Sukhishvili, Ionization-Controlled Stability of Polyelectrolyte Multilayers in Salt Solutions, *Langmuir* 19 (2003) 5188–5191. <https://doi.org/10.1021/la034360m>.
- [163] Z. Sui, D. Salloum, J.B. Schlenoff, Effect of Molecular Weight on the Construction of Polyelectrolyte Multilayers: Stripping versus Sticking, *Langmuir* 19 (2003) 2491–2495. <https://doi.org/10.1021/la026531d>.
- [164] K.S. Shalini Devi, S. Jacob, A. Senthil Kumar, In Situ Structural Elucidation and Selective Pb²⁺ Ion Recognition of Polydopamine Film Formed by

- Controlled Electrochemical Oxidation of Dopamine, *Langmuir* 34 (2018) 7048–7058. <https://doi.org/10.1021/acs.langmuir.8b01209>.
- [165] H. Wei, J. Ren, B. Han, L. Xu, L. Han, L. Jia, Stability of polydopamine and poly(DOPA) melanin-like films on the surface of polymer membranes under strongly acidic and alkaline conditions, *Colloids Surf B Biointerfaces* 110 (2013) 22–28. <https://doi.org/10.1016/j.colsurfb.2013.04.008>.
- [166] Z.F. Gao, X.Y. Wang, J.B. Gao, F. Xia, Rapid preparation of polydopamine coating as a multifunctional hair dye, *RSC Adv* 9 (2019) 20492–20496. <https://doi.org/10.1039/C9RA03177D>.
- [167] W. Yang, C. Liu, Y. Chen, Stability of Polydopamine Coatings on Gold Substrates Inspected by Surface Plasmon Resonance Imaging, *Langmuir* 34 (2018) 3565–3571. <https://doi.org/10.1021/acs.langmuir.7b03143>.
- [168] S. Correa, N. Boehnke, E. Deiss-Yehiely, P.T. Hammond, Solution Conditions Tune and Optimize Loading of Therapeutic Polyelectrolytes into Layer-by-Layer Functionalized Liposomes, *ACS Nano* 13 (2019) 5623–5634. <https://doi.org/10.1021/acsnano.9b00792>.
- [169] E. Poptoshev, B. Schoeler, F. Caruso, Influence of Solvent Quality on the Growth of Polyelectrolyte Multilayers, *Langmuir* 20 (2004) 829–834. <https://doi.org/10.1021/la035485u>.
- [170] B.S. Gaylord, A.J. Heeger, G.C. Bazan, DNA Hybridization Detection with Water-Soluble Conjugated Polymers and Chromophore-Labeled Single-Stranded DNA, *J Am Chem Soc* 125 (2003) 896–900. <https://doi.org/10.1021/ja027152+>.
- [171] S. Boddohi, C.E. Killingsworth, M.J. Kipper, Polyelectrolyte Multilayer Assembly as a Function of pH and Ionic Strength Using the Polysaccharides

- Chitosan and Heparin, *Biomacromolecules* 9 (2008) 2021–2028.
<https://doi.org/10.1021/bm8002573>.
- [172] E. Kharlampieva, V. Kozlovskaya, S.A. Sukhishvili, Layer-by-Layer Hydrogen-Bonded Polymer Films: From Fundamentals to Applications, *Advanced Materials* 21 (2009) 3053–3065.
<https://doi.org/10.1002/adma.200803653>.
- [173] E. Kharlampieva, V. Kozlovskaya, J.F. Ankner, S.A. Sukhishvili, Hydrogen-Bonded Polymer Multilayers Probed by Neutron Reflectivity, *Langmuir* 24 (2008) 11346–11349. <https://doi.org/10.1021/la802502c>.
- [174] C.D. Bain, G.M. Whitesides, A Study by Contact Angle of the Acid-Base Behavior of Monolayers Containing ω -Mercaptocarboxylic Acids Adsorbed on Gold: An Example of Reactive Spreading, *Langmuir* 5 (1989) 1370–1378.
- [175] A. Mierczynska, A. Micheltore, A. Tripathi, R. V. Goreham, R. Sedev, K. Vasilev, pH-tunable gradients of wettability and surface potential, *Soft Matter* 8 (2012) 8399. <https://doi.org/10.1039/c2sm25221j>.
- [176] S.R. Holmes-Farley, C.D. Bain, G.M. Whitesides, Wetting of Functionalized Polyethylene Film Having Ionizable Organic Acids and Bases at the Polymer-Water Interface: Relations between Functional Group Polarity, Extent of Ionization, and Contact Angle with Water, *Langmuir* 4 (1988) 921–937.
- [177] B. Jiang, Y. Zhou, B. Ji, Y. Zheng, C.-F. Yu, J. Huang, X.-H. Wang, Investigation on the effect of functional groups on the wettability of coal dust: Experiments and theoretical validation, *Fuel* 351 (2023) 128987.
<https://doi.org/10.1016/j.fuel.2023.128987>.
- [178] S.T. Dubas, J.B. Schlenoff, Polyelectrolyte Multilayers Containing a Weak Polyacid: Construction and Deconstruction, *Macromolecules* 34 (2001) 3736–3740. <https://doi.org/10.1021/ma001720t>.

- [179] E. Kharlampieva, S.A. Sukhishvili, Hydrogen-Bonded Layer-by-Layer Polymer Films, *Journal of Macromolecular Science, Part C: Polymer Reviews* 46 (2006) 377–395. <https://doi.org/10.1080/15583720600945386>.
- [180] L. Zheng, J. Shi, Y. Chi, Tannic Acid Physically Cross-Linked Responsive Hydrogel, *Macromol Chem Phys* 219 (2018). <https://doi.org/10.1002/macp.201800234>.
- [181] W. Lin, Y. Guan, Y. Zhang, J. Xu, X.X. Zhu, Salt-induced erosion of hydrogen-bonded layer-by-layer assembled films, *Soft Matter* 5 (2009) 860–867. <https://doi.org/10.1039/B813614A>.
- [182] W. Xu, E. Ferain, S. Demoustier-Champagne, K. Glinel, A.M. Jonas, Hydrogen-Bonded Multilayers for the Release of Polyelectrolyte Nanotubes in Biocompatible Conditions, *ACS Appl Polym Mater* 1 (2019) 2407–2416. <https://doi.org/10.1021/acsapm.9b00529>.
- [183] C. Laurence, K.A. Brameld, J. Graton, J.-Y. Le Questel, E. Renault, The pKBHX Database: Toward a Better Understanding of Hydrogen-Bond Basicity for Medicinal Chemists, *J Med Chem* 52 (2009) 4073–4086. <https://doi.org/10.1021/jm801331y>.
- [184] C. Laurence, M. Berthelot, Observations on the strength of hydrogen bonding, *Perspectives in Drug Discovery and Design* 18 (2000) 39–60. <https://doi.org/10.1023/A:1008743229409>.